Holographic Instanton Calculations of Meson Decay

MACIEJ TADEUSZ MATUSZEWSKI

Holographic Instanton Calculations of Meson Decay

Maciej Tadeusz Matuszewski

A Thesis presented for the degree of
Doctor of Philosophy

Department of Mathematical Sciences
Durham University
United Kingdom

April 2019

Holographic Instanton Calculations of Meson Decay

Maciej Tadeusz Matuszewski

Submitted for the degree of Doctor of Philosophy

April 2019

Abstract: Calculations of decay rates for high spin mesons have proved difficult using traditional QCD methods. However holographic methods have recently shown great promise in modelling QCD systems. While previous such approaches have used string bit models, a worldline instanton approach also shows great promise. A simple toy example of a worldline instanton calculation for meson decay in a flat Euclidean background is shown to replicate the results of Casher, Neuberger, Nussinov calculation for meson decay. The AdS/CFT holographic method in general is then reviewed and assessed before showing that a holographic worldline instanton approach in the zero temperature Sakai Sugimoto background produced similar results. Approaches for expanding this to finite temperature are then discussed.

Contents

Declaration

The work in this thesis is based on research carried out in the Department of Mathematical Sciences at Durham University. The results, and (for sections 2.6 and 5) the text, are based on the following collaborative work:

- K. Peeters, M. Matuszewski and M. Zamaklar. 'Holographic meson decays via worldsheet instantons'. In: *JHEP* 83 (2018) arXiv:1803.06318

Appendix C is based on unpublished work with K. Peeters and M. Zamaklar.

No part of this thesis has been submitted elsewhere for any degree or qualification.

Acknowledgements

I would like to thank:

My parents, for always being there for me and offering me their unwavering help.

Rosemary, Sam M, Eth, Ben H, Amanda, Lizzie, Matthew, Ben A, Renju, Kirk, Hannah, Abi, Thom – and all my other dear friends who I don't have space to name here – for all their support and making my life that little bit brighter.

Vaios, Akash and Sam F, for their help with proofreading, printing, binding and other admin related to the submission of this thesis.

My supervisors Kasper and Marija, for their invaluable guidance.

This thesis is dedicated to

The Memory of George Walton

Chapter 1

Introduction

Mesons may be thought of as a quark-antiquark pair held together by the strong nuclear force, as shown in figure 1.1 [1]. Meson decay is an interesting process which has aroused a lot of theoretical and experimental interest over the past several decades. While it is a problem that has been heavily studied, several difficulties remain. Mesons, and other phenomena involving the strong nuclear force, are best understood using Quantum Chromodynamics (QCD), a gauge theory. QCD explains the running coupling of the strong nuclear force – that is, that the force is strong at low energies (and large distances) and weak at high energies (and small distances). This means that perturbative calculations – which depend on expanding the equations of the theory around small fluctuations – are possible in the latter case (for example when examining quarks within hadrons at high energies and over small distances) but not in the former. While lattice QCD [2], [3] (the process of discretising the QCD theory and solving problems numerically) has shown great success even at strong coupling it has struggled to successfully model many problems which involve time evolution. Therefore calculations of meson decay, a time dependent strong coupling problem, have often proved intractable.

Phenomenological models have been introduced to attempt to model meson decay. The most successful has been the Lund Model [4], [5] – which treats mesons as two massive particles (which represent quarks and antiquarks) connected by a string.

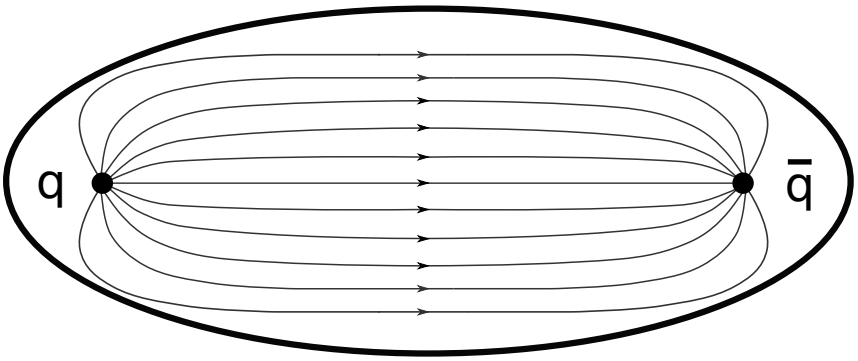

Figure 1.1: The structure of a meson as described by QCD. Bare quarks cannot be observed on their own due to confinement.

Baryons can also be modelled by having one of the massive particles within the model represent a diquark (that is a pair of quarks or antiquarks which are coupled to each other). The decay of these hadrons is then modelled by the string breaking, forming two new massive endpoints and therefore two daughter hadrons. This model has shown remarkable success in replicating and predicting experimental results. It is the basis of the PYTHIA event generator software which is widely used for modelling particle collisions in accelerators [6]. This model is attractive since it has the potential to replicate more features of QCD and is, in many cases, numerically simpler. However, it remains a phenomenological model which requires many parameters to be fine tuned by hand. So called 'top-down' [7] models, where the features of QCD appear more naturally and do not need to be put in by hand, are often considered preferable. One such model is holography.

The holographic Anti-de Sitter/Conformal Field Theory (AdS/CFT) correspondence is a development of string theory. First developed in the late '90s [8], [9], it posits that certain strongly coupled gauge theories may be seen as being equivalent, or dual, to certain weakly coupled string theories of gravity (thereby this is sometimes called a 'weak-strong' coupling duality). This is a holographic correspondence as the gauge theories exist in one dimension fewer than the string theories that they are said to be dual to – one may think of the string theory existing in a certain spacetime 'bulk' and the gauge theory existing on the 'boundary' of this bulk. This correspondence is very

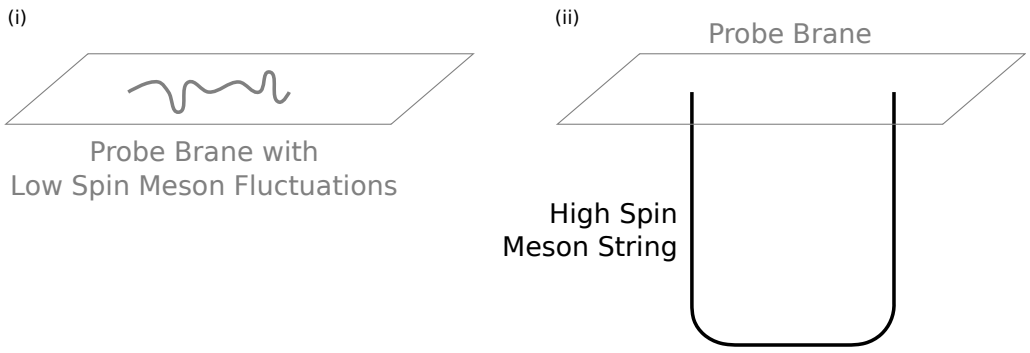

Figure 1.2: Diagram showing holographic picture representing (i) low spin mesons and (ii) high spin mesons.

useful as some problems are easier to solve in gauge theory while others are easier to solve in a string theory of gravity. If we have a 'dictionary' that translates problems from one framework to the other – which, in practice depends on showing how the source terms in the gauge theory Lagrangian are related to the string partition function – we can convert a difficult problem in one framework to an easier one in the other framework, solve it, and then translate the results back.

As the name suggests, the initial correspondence was found to be between string theory in Anti-de Sitter spacetime and Conformal Field Theory. Neither of these have direct relevance to the physical world around us – however, in recent years this theory has been significantly expanded. While an exact dual to QCD has not yet been found, several string systems have been shown to successfully model certain aspects of it. Several models have introduced mesons by considering multi-dimensional extended objects known as probe branes into AdS spacetime, with low spin mesons being modelled as fluctuations of these branes [10], [11] while high spin mesons being modelled as macroscopic strings extending between the branes [12]. This is illustrated in figure 1.2. These models have successfully been used to calculate the mass spectrum of mesons and the relationship between meson mass and angular momentum (the Regge behaviour).

A particularly interesting model was introduced by Kruczenski, Mateos, Myers and Winters [11] (building on the work of Witten [13]) which included $D6$ probe branes with a background including $D4$ branes which distorted spacetime. This could

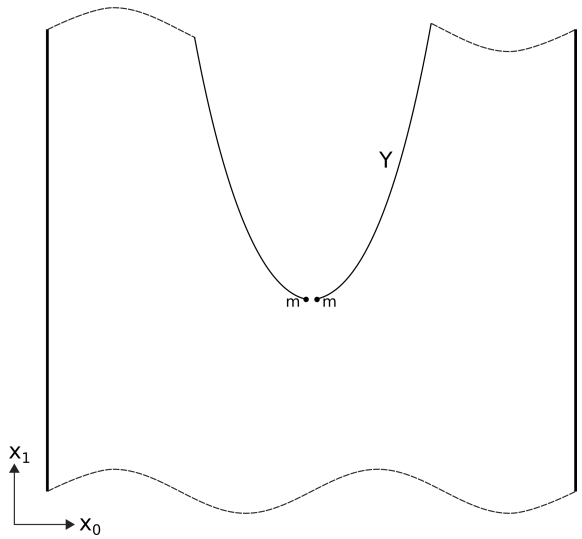

Figure 1.3: The decay of a holographic string (with massive end-points) representing a meson.

succesfully model the breaking of $U(1)_A$ Abelian chiral symmetry (the symmetry governing rotations of left and right handed fermions). However, the presence of supersymmetry meant that the model was not able to model the non-Abelian chiral symmetry breaking found in QCD. For this, a new non-supersymmetric model with $D8$ and $\bar{D}8$ probe branes had to be introduced, as was done by Sakai and Sugimoto [14], [15]. The presence of two different types of probe branes allowed $U(N)_L \times U(N)_R$ symmetry to be reproduced. This has been used to model meson decay already, however a novel approach is to do this modelling using the worldline instanton method. As an introductory exercise a novel string instanton approach in a flat Euclidean spacetime will be shown to successfully model the pair creation for a generic Abelian field [16], as in the Schwinger approach.

In this approach we consider the decay of a meson as the pair creation of a quark and antiquark from the energy in the colour field flux tube within an existing meson. The new quark and antiquark come into existence as virtual particles before moving apart from each other and gaining enough energy from the field to come on shell. This is essentially a quantum tunnelling process. The rate of pair production for an electric field was first calculated by Schwinger [17] in the '50s, with the work later being expanded to the QCD picture by Casher, Neuberger and Nussinov [18]. This

was a difficult and involved calculation. However, by Wick rotating all the timelike coordinates and parameters in the theory into the imaginary axis (thereby resulting in an Euclidean spacetime) all potentials are reversed. Therefore a potential barrier becomes a potential well and the problem can be solved semi-classically. Instantons are the solutions to the equations of motion of this Euclidean system.

The most appropriate string dual of a high spin meson for this approach in the Sakai-Sugimoto model is a U-shaped string with each endpoint hanging down from a 'flavour probe brane' into the bulk. The 'vertical' length of each leg of the string along the holographic direction is proportional to the mass of the quark it represents while the length of the 'horizontal' section of the string is proportional to the energy in the colour field between the quarks. The position of the 'flavour branes' therefore determines the masses, and flavours, of the quarks being considered. The meson decays by part of the string fluctuating to the flavour brane and splitting – creating two new vertical string segments (that is, a new quark antiquark pair) and therefore two U-shaped strings (that is, two daughter mesons). While this model does not replicate all of the meson's properties, this thesis will explain that by solving the equations of motion for this system and evaluating its action as a function of the mass of the newly created quarks (which, when exponentiated, will be shown to be proportional to the decay rate of the meson) it can be shown that this method can reproduce the traditional QCD pair production calculations done by Casher, Neuberger and Nussinov.

These calculations are simplest in the zero temperature case as we can impose cylindrical symmetry on the system – that is both the pre-existing quark and antiquark pair and the new quark antiquark pair trace out a circle in the plane defined by the Euclidean time direction and the spatial direction of their separation (a potential future expansion of this work being looking at the system without cylindrical symmetry – with potentially the most interesting system being the worldlines of the outer, pre-exisitng quarks being straight lines) . The calculations become more difficult in the finite temperature case, since in this situation in the holographic dual

the time direction is compactified with period inverse to the temperature. Therefore at high temperatures the instantons representing the mesons are distorted – resulting in a 'lemon' shape – as will be discussed at the end of this thesis [19]–[22].

*

In chapter 2 I will present an introductory look at QCD and meson decay, present the Casher, Neuberger, Nussinov method for calculating decay rates, and show how it can be reproduced using a novel simple toy string model in a flat Euclidean background. In chapter 3 I will introduce the AdS/CFT correspondence, including discussing a number of holographic backgrounds that have been used previously to model QCD, and why they are not appropriate in this case, as well as introducing the concept of Wilson loops and worldline instanton method in a toy AdS background. Side notes on other aspects of the AdS/CFT correspondence not directly applicable to meson decay will be presented in appendix B. In chapter 4 I will introduce the Sakai Sugimoto model. In chapter 5 I will present the main content of the work – a calculation of meson decay rates using holographic instanton methods in a Sakai Sugimoto background. In chapter 6 I will discuss the implications of my findings and suggest future work in a finite temperature Sakai Sugimoto background. The original results of this PhD project are primarily discussed in sections 2.6 and 5.

This thesis was created using the help of the Durham Mathematical Sciences Thesis Template [23].

Chapter 2

QCD and Old String Methods

2.1 Introduction to Models of the Strong Nuclear Force

The strong nuclear force is one of the four fundamental forces of nature. The gauge boson responsible for this force is the gluon and it acts to bind mesons together into hadrons (and, through the 'residual strong nuclear force' to mediate the interactions between hadrons) [1], [24]. The strong coupling for this force means that it is often very difficult to make calculations perturbatively, meaning that numerous different frameworks have been developed to study strong nuclear force interactions, including meson decay.

Section 2.2 will provide an introduction to Quantum Chromodynamics, our current best picture of the strong nuclear force. It will introduce the ideas of running coupling, asymptotic freedom and confinement – which will explain why we never see bare quarks, as well as why coupling is so strong for large scale processes. Section 2.3 will introduce Lattice QCD – our current best computational approach for making QCD calculations. Section 2.4 will detail the Casher, Neuberger and Nussinov calculation for pair production in the strong nuclear force – which may be seen as being part of the meson decay process. Section 2.5 will introduce the phenomenological Lund

Model for hadron decays and interactions, which has inspired holographic approaches to modelling meson decay. Finally section 2.6 will introduce the instanton method for flat spacetime – which will allow calculations to be done semiclassically. This section will also show how calculations for string setups can replicate point particle calculations.

2.2 QCD and Descriptions of Meson Decay

Our current best description of mesons and the strong nuclear force is quantum chromodynamics (QCD). The fundamental particles in this theory are quarks, which are found in six flavours and carry a quantum number we refer to as colour (there are three colour charges and three anti-colour charges). They transform under $SU(3)$ with the quarks transforming under the fundamental 3 representation, and the antiquarks transforming under the antifundamental $\bar{3}$ representation. The gauge bosons for the theory – the gluons – transform under the adjoint representation of $SU(3)$ so there are $3^2 - 1 = 8$ of them. We may therefore think of $SU(3)$ as the gauge group for QCD, with colour being the quantum number.

The QCD Lagrangian is given by [25]–[27]

$$\mathcal{L} = -\frac{1}{4}F^{\alpha}_{\mu\nu}F^{\mu\nu}_{\alpha} + \sum_i \bar{q}_i \left(i\gamma^\mu\partial_\mu - g\gamma^\mu A_\mu - m_i\right) q_i \tag{2.2.1}$$

where

$$A_\mu = \frac{\lambda_\alpha}{2}A^\alpha_\mu \tag{2.2.2}$$

$$F^\alpha_{\mu\nu} = \partial_\mu A^\alpha_\nu - \partial_\nu A^\alpha_\mu - g f^{\alpha\beta\gamma} A^\beta_\mu A^\gamma_\nu. \tag{2.2.3}$$

Here we note that q_i are the fields for the different flavour quarks (the flavour index i will be dropped for clarity apart from cases where it is relevant, such as transformation between different flavours), A^α_μ is the gluon field, g is the $SU(3)$ charge, $f^{\alpha\beta\gamma}$ are the $SU(3)$ structure constants, m_i is the mass associated with the field q_i (this mass is so small for up, down and strange quarks compared to the

others that it is often taken to be zero for these – this is called the chiral limit), λ_α are the Gell-Mann matrices, γ_μ are the Dirac matrices. The indices μ and ν are the standard Lorentz indices and the indices α, β and γ are related to $SU(3)$ and run from 1 to 8.

As can be inferred, the QCD Lagrangian is highly symmetric [28], [29]. There is of course global Poincare symmetry (rotations, translations and Lorentz boosts) such that

$$q \to q' = U_p q \tag{2.2.4}$$

where $U_p = e^{\frac{i}{2}\epsilon_{\mu\nu}M^{\mu\nu}+ia_\mu P^\mu}$ with $M^{\mu\nu}$ being the generator for rotations and boosts and P^μ being the generator for translations and $\epsilon_{\mu\nu}$ and a_μ are constants.

Global $SU(2)$ is related to isospin and acts only on the up and down quark fields

$$q_i \to q_i' = {U_I}^{ij} q_j \tag{2.2.5}$$

for constant U_I^{ij}, which is a unitary $SU(2)$ matrix. There is also a local $SU(N_C)$ colour symmetry. For $N_C = 3$ the $SU(3)$ gauge field transformations are as follows:

$$q \to q' = U\, q \tag{2.2.6}$$

$$A_\mu \to {A'}_\mu = U\, A_\mu\, U^\dagger + \frac{i}{g} U \partial_\mu U^\dagger \tag{2.2.7}$$

$$F_{\mu\nu} \to {F'}_{\mu\nu} = U\, F_{\mu\nu}\, U^\dagger \tag{2.2.8}$$

where $U \equiv U(x)$ are the transformation matrices for the $SU(3)$ group such that, for θ^a

$$U(x) = e^{\frac{i}{2}\theta_\alpha(x)\lambda^\alpha}. \tag{2.2.9}$$

We may naively think that the Lagrangian (2.2.1) would have approximate flavour symmetry $U(3)_L \times U(3)_R$ resulting from the lightest three quarks all having a very small mass. However $U(1)_A$ symmetry is broken by anomaly under quantisation, leaving us with $U(1)_V \times SU(3)_L \times SU(3)_R$ symmetry [30], [31]. The $U(1)_V$ symmetry

related is related to baryon number conservation and can be expressed as

$$q \to q' = e^{i\epsilon} q, \tag{2.2.10}$$

for constant ϵ. We have $SU(3)_L \times SU(3)_R$ symmetry rather than just $SU(3)$ as, in the chiral limit, we may split the q fields into left and right handed components

$$q_L = \frac{1}{2}(1 - \gamma_5)\, q \tag{2.2.11}$$

$$q_R = \frac{1}{2}(1 + \gamma_5)\, q \tag{2.2.12}$$

The Lagrangian for each is separately invariant under $SU(3)$. However this symmetry is spontaneously broken via the Goldstone-Nambu mechanism [32] – that is the fields may be expanded around a non-zero vacuum state expectation value χ such that the fields

$$q' = q - \chi \tag{2.2.13}$$

are no longer symmetric in $SU(3) \times SU(3)$ – generators G of the symmetry no longer annihilate them such that

$$G|q'\rangle \neq 0 \tag{2.2.14}$$

More specifically we find that the operator $\bar{q}_L q_R$ breaks the symmetry such that

$$\langle \bar{q}_L q_R \rangle \neq 0. \tag{2.2.15}$$

We are then left with eight Goldstone bosons which, in the chiral limit, are massless. We therefore say that the symmetry was broken

$$SU(3)_L \times SU(3)_R \to SU(3)_V \tag{2.2.16}$$

and that the new mesons are an adjoint representation of $SU(3)_V$. Indeed, we can observe eight mesons (in three categories η, $K^{\pm}$, $\bar{K}^0$, K^0, $\pi^{\pm}$ and π^0) which are much less massive than other mesons. In later sections we will see that the desire to replicate this property of QCD will determine which holographic background we

chose to use.

QCD exhibits confinement, which means that quarks must be grouped into objects with zero net colour charge – most commonly these are baryons (three quarks of different colour charge) and mesons (one quark one with a specific colour charge and an antiquark with the corresponding anticolour charge).

This may partially be explained by discussing running coupling. A single quark will interact with pairs of virtual quarks and antiquarks around it. These pairs will effectively form dipoles – with the particles of the opposite charge to the original quark moving closer to it. This cloud of virtual particles will therefore cause 'screening' at large distances, making the quark's coupling appear smaller. Interactions with virtual gluons cause 'antiscreening', meaning that they increase the quark's coupling at large distances. Together, these effects contribute to running coupling, meaning that the quark coupling changes with distance and energy scale [33], [34]. In QCD the antiscreening effect is stronger than the screening effect so, quark coupling is far stronger at large distances and small energy scales.

More precisely, we may consider this process as arising from the renormalization of loop divergences in QCD. As reviewed by [35]–[37] we may write the relationship between the renormalized QCD coupling g and the unrenormalized QCD coupling g_0 as

$$g^2 = \frac{{Z_2}^2 Z_3}{{Z_1}^2} {g_0}^2 \tag{2.2.17}$$

where Z_1 is the renormalization constant related to one-loop corrections of the quark-gluon vertex as shown in figure 2.2, Z_2 is the renormalization constant related to the one-loop correction of the quark self-energy as shown in figure 2.1, and Z_3 is the renormalization constant related to one-loop corrections of the gluon self-energy as shown in figure 2.3.

Considering these Feynmann diagrams, we find [37]:

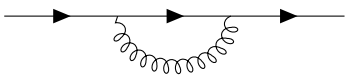

Figure 2.1: Feynmann diagram of one-loop quark self energy correction. Produced using [38] based on [35], [36].

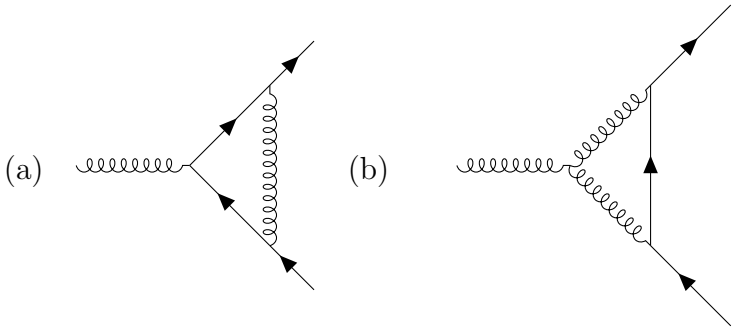

Figure 2.2: Feynmann diagrams of one-loop correction to the quark-antiquark-gluon vertex. Produced using [38] based on [35], [36].

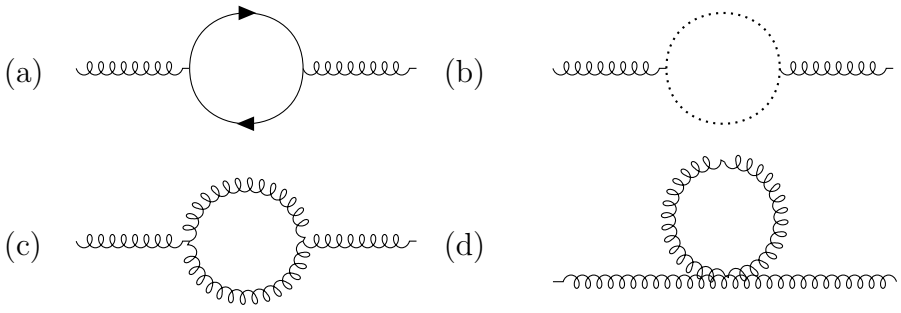

Figure 2.3: Feynmann diagram of one-loop correction to the gluon self energy with fermion loop (a), ghost loop (b), and gluon loops (c and d). Produced using [38] based on [35], [36].

$$Z_1 = 1 - \frac{\alpha_s}{4\pi}\frac{1}{\epsilon}(C_F + C_A) \tag{2.2.18}$$

$$Z_2 = 1 - \frac{\alpha_s}{4\pi}\frac{1}{\epsilon}C_F \tag{2.2.19}$$

$$Z_3 = 1 + \frac{\alpha_s}{4\pi}\frac{1}{\epsilon}\left(\frac{5}{3}C_A - \frac{2}{3}N_f\right) \tag{2.2.20}$$

where $\alpha_s = \frac{g^2}{4\pi}$, $C_F = \frac{{N_C}^2-1}{2N_c}$ is the Casimir operator in the fundamental representation, $C_A = N_c$ is the Casimir operator in the adjoint representation, N_c is the number of colours and N_f is the number of flavours [1], [24]. Additionally

$$\epsilon = \frac{\mu^{4-d}}{\pi^{\frac{d}{2}-2}\Gamma(2-\frac{d}{2})} \tag{2.2.21}$$

where μ is the energy scale and d is the number of spacetime dimensions. Considering (2.2.17) we find

$$\begin{aligned}
\frac{\mathrm{d}(g^2)}{\mathrm{d}(\mu^2)} &= \left(\frac{2Z_2Z_3}{{Z_1}^2}\frac{\mathrm{d}Z_2}{\mathrm{d}(\mu^2)} - \frac{2{Z_2}^2Z_3}{{Z_1}^3}\frac{\mathrm{d}Z_1}{\mathrm{d}(\mu^2)} + \frac{{Z_2}^2}{{Z_1}^2}\frac{\mathrm{d}Z_3}{\mathrm{d}(\mu^2)}\right) g_0 \\
&= \left(\frac{2}{Z_2}\frac{\mathrm{d}Z_2}{\mathrm{d}(\mu^2)} - \frac{2}{Z_1}\frac{\mathrm{d}Z_1}{\mathrm{d}(\mu^2)} + \frac{2}{Z_3}\frac{\mathrm{d}Z_3}{\mathrm{d}(\mu^2)}\right)\frac{{Z_2}^2Z_3}{{Z_1}^2}{g_0}^2 \\
&= \left(\frac{2}{Z_2}\frac{\mathrm{d}Z_2}{\mathrm{d}(\mu^2)} - \frac{2}{Z_1}\frac{\mathrm{d}Z_1}{\mathrm{d}(\mu^2)} + \frac{2}{Z_3}\frac{\mathrm{d}Z_3}{\mathrm{d}(\mu^2)}\right) g^2 \\
&= -\frac{\alpha_s}{12\pi\mu^2}\left(11N_c - 2N_f\right) g^2.
\end{aligned} \tag{2.2.22}$$

Finally, performing a change of coordinates, we find

$$\frac{\mathrm{d}g}{\mathrm{d}\log(\mu)} = -\frac{g^3}{48\pi^2}\left(11N_c - 2N_f\right). \tag{2.2.23}$$

Therefore, if we wish to consider the relation between coupling g_1 at energy scale μ_1 and coupling g_2 at energy scale μ_2 we may integrate to find

$$g^2(\mu_2) = \frac{g^2(\mu_1)}{1 + \frac{g^2(\mu_1)}{24\pi^2}\left(11N_c - 2N_f\right)\log\left(\frac{\mu_2}{\mu_1}\right)} \tag{2.2.24}$$

It is often useful to specify a specific reference energy scale μ_1 with which we compare any other scale. We call this Λ_{QCD}, the QCD scale [39]. This is defined such that

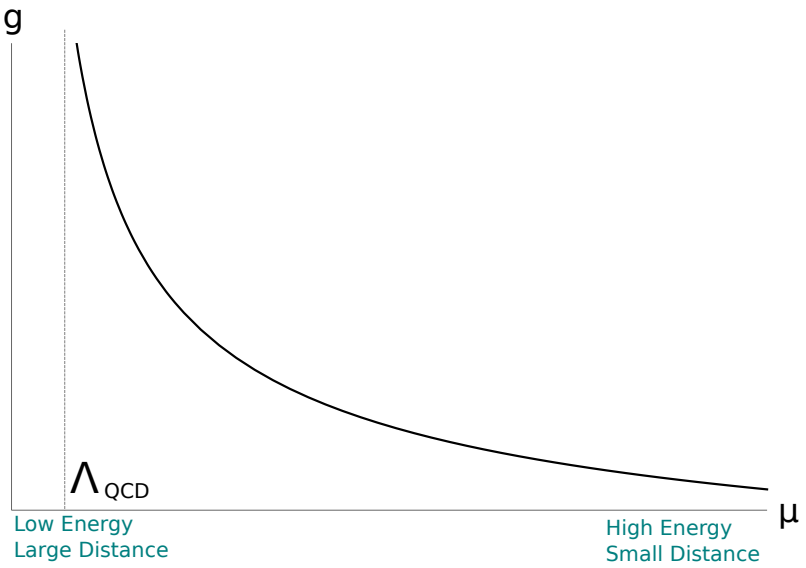

Figure 2.4: The running of the QCD coupling for $N_c = 3$ and $N_f = 6$. The position of the QCD scale Λ_{QCD} is marked with a dotted line.

$\frac{1}{g(\Lambda_{QCD})} = 0$ and therefore we may rewrite (2.2.24) as

$$g^2(\mu_2) = \frac{24\pi^2}{(11N_c - 2N_f)\log\left(\frac{\mu}{\Lambda_{QCD}}\right)} \tag{2.2.25}$$

Therefore the running of the coupling occurs as shown in figure 2.4. This means that at high energies or small distances (for example for quarks within hadrons) we get asymptotic freedom – in which quarks have low coupling and may be treated almost as free particles, allowing perturbative methods to be used. However, when quarks get far away from each other the coupling between them becomes so strong that it becomes energetically favourable to form a new quark-antiquark pair from the colour field flux tube between them – leading to confinement as no quark is able to get away from other quarks to be observed independently.

We may imagine the quark and antiquark in a meson to be connected to each other by a colour field flux tube. One possible mode of decay for the meson is for a new quark-antiquark pair to be created in the flux tube – breaking it in half – forming two new mesons. The Feynmann diagram for one such possible decay is shown in figure 2.6. Other channels are possible.

2.3 Lattice QCD

Such decays, and other properties of QCD, can be difficult or impossible to calculate using perturbative methods due to its strongly coupled nature. Therefore, the most common approach to strong nuclear force calculations is Lattice QCD [2], [3]. Lattice QCD works by transcribing QCD onto a Euclidean lattice – allowing calculations to be performed using Monte Carlo Methods, similar to problems in statistical mechanics. If the grid spacing is a and grid size L, and therefore momentum space quantisation is

$$k = \frac{2\pi n}{La}, n = 0, 1, 2, \ldots, L \tag{2.3.1}$$

we get a upper energy cutoff of $\frac{\pi}{a}$ – meaning that the theory has no infinities. The gauge action is given by [2]

$$S_G = \frac{6}{g^2} \sum_x \sum_{\mu<\nu} \mathrm{Re}\,\mathrm{Tr} \frac{1}{3} \left(1 - W_{\mu\nu}\right) \tag{2.3.2}$$

where

$$W_{\mu\nu} = U_\mu(x) U_\nu(x + \hat{\mu}) U_\mu^\dagger(x + \hat{\nu}) U_\nu^\dagger(x) \tag{2.3.3}$$

where $x + \hat{\mu}$ is the next grid point along from x in the μ direction and $U_\mu(x)$ is the operator that shifts the field A_μ in the μ direction. The operator $U_\mu^\dagger(x)$ shifts the field A_μ in the negative μ direction, so the repeated μ and ν indices do not indicate a contraction – just that the Wilson loop takes us back to the starting position in a rectangular path, as shown in figure (2.5). The fermion action may be given by

$$S_F = m_q \sum_x \bar{\psi}(x)\psi(x) + \frac{1}{2a} \sum_x \bar{\psi}(x)\gamma_\mu \left(U_\mu(x)\psi(x + \hat{\mu}) - U_\mu^\dagger(x - \hat{\mu})\psi(x - \hat{\mu})\right). \tag{2.3.4}$$

The usual next step is to write down an expression for an expectation value of an

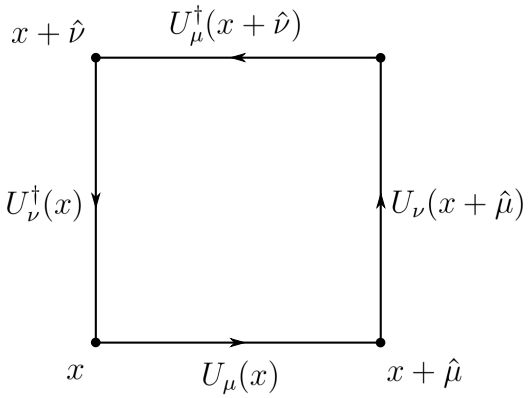

Figure 2.5: Diagram showing path represented by (2.3.3).

operator within the theory [40], for example

$$\langle \mathcal{O} \rangle = \frac{1}{\mathcal{Z}} \int \mathcal{D}U \mathcal{D}\psi \mathcal{D}\bar{\psi}\, \mathcal{O} e^{-S_F} \tag{2.3.5}$$

which can then be calculated using Monte Carlo methods. Quantities that are calculated can include interaction or decay matrix elements, or meson mass spectra [41].

Usually lattice QCD requires one to put in by hand the masses of the quarks and the QCD coupling scale Λ_{QCD} – but most other parameters can be obtained through calculation. Lattice QCD has proved successful in many such calculations [42], including that of hadron mass spectra and decay rates – many other promising methods have only recently begun to replicate the successful results of Lattice QCD [12]. Lattice QCD does not share perturbative QCD's problems with high coupling at low energies and large distances.

Despite these successes, in many situations QCD has proved difficult to use to make direct predictions for both decay rates and other properties described by QCD. Lattice methods have proved themselves very flexible but they do have some specific technical problem. The do not work well with time dependent problems [43] and are computationally very intensive. Workarounds are often required when the chemical potential is above zero as this makes the partition function for fermions complex, and therefore not possible to use with standard Monte Carlo Methods [44].

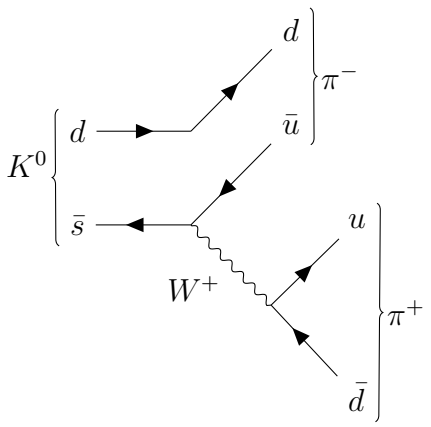

Figure 2.6: Feynmann diagram for K^0 decay. Other decay channels are also common. Produced using [38].

Finally, the discretisation used often leads to multiplying numbers of Weyl fermions, leading to chiral invariance not being upheld [45]. This latter problem can be easily demonstrated by attempting to discretise the derivative of a two component spinor $u(x)$. In the spatial domain we have no problems:

$$\frac{1}{i}\sigma^j \partial_j u(\mathbf{x}) \to \sum_{j=1}^{3} \frac{1}{2i}\sigma^j \Big(u(x_j + \mu_j) - u(x_j - \mu_j)\Big) \tag{2.3.6}$$

but when transforming to momentum space we get [45]

$$\sum_{j=1}^{3} \sigma^j \sin p_j \tilde{u}(\mathbf{p}). \tag{2.3.7}$$

Due to each sine having 2 zeros there are 8 overall zeros in the spectrum, each one acting as a particle.

Due to these problems, other methods, including holographic methods, have been developed. The key first step of the holographic method is to consider the type of decay shown in figure 2.6 to be instead a pair production of a new quark and antiquark from the colour field flux tube between the exisiting quark and antiquark – forming two daughter mesons. This probability for this process to occur was described by Casher, Neuberger and Nussinov [18].

2.4 Casher, Neuberger and Nussinov Model

In his famous paper Schwinger [17] showed that the pair production probability of an electron positron pair (each with charge magnitude e and mass m) from an electric field E is given by

$$\Gamma = \frac{\alpha^2}{\pi^2} E^2 \sum_{n=1}^{\infty} n^{-2} e^{-\frac{n\pi m^2}{eE}} \tag{2.4.1}$$

where $\alpha = \frac{e^2}{4\pi\hbar c}$.

Casher, Neuberger and Nussinov [18] expanded this work to consider the quark-antiquark pair production probability from a colour field, and in particular the colour field flux tube between another, pre-existing quark-antiquark pair.

Let us first consider the energy per unit length T within the flux tube – this is equivalent to the tension of the flux tube. We recall Gauss' Law

$$\nabla \cdot \boldsymbol{E}(x) = \frac{\rho(x)}{\epsilon_0} \qquad\qquad \boldsymbol{E}(x) = \int \mathrm{d}^d x \frac{\rho(x)}{\epsilon_0} \tag{2.4.2}$$

where $E(x)$ is the field strength, $\rho(x)$ is the charge distribution and ϵ_0 is the permittivity of free space. Then using the standard result for the energy of a charge distribution with a potential $V(x)$

$$\begin{aligned}
U &= \frac{1}{2} \int \mathrm{d}^d x \ \rho(x) V(x) \\
&= \frac{\epsilon_0}{2} \int \mathrm{d}^d x \ (\nabla \cdot \boldsymbol{E}(x)) V(x) \\
&= \frac{\epsilon_0}{2} \int \mathrm{d}^d x \ \Big(\nabla \cdot (\boldsymbol{E}(x) V(x)) - (\nabla V(x)) \cdot \boldsymbol{E}(x) \Big) \\
&= \frac{\epsilon_0}{2} \int V(x) \boldsymbol{E}(x) \cdot \mathrm{d}\boldsymbol{A} - \frac{\epsilon_0}{2} \int \mathrm{d}^d x \ (-\boldsymbol{E}(x)) \cdot \boldsymbol{E}(x) \qquad (2.4.3) \\
&= \frac{\epsilon_0}{2} \int \mathrm{d}^d x \ |\boldsymbol{E}(x)|^2 \qquad (2.4.4)
\end{aligned}$$

where $\boldsymbol{A}$ is the surface area of the region of space we are looking, we assume $V = 0$ at this boundary, and to get to (2.4.3) we used the divergence theorem and the relation

$$\nabla V(x) = -\boldsymbol{E}(x). \tag{2.4.5}$$

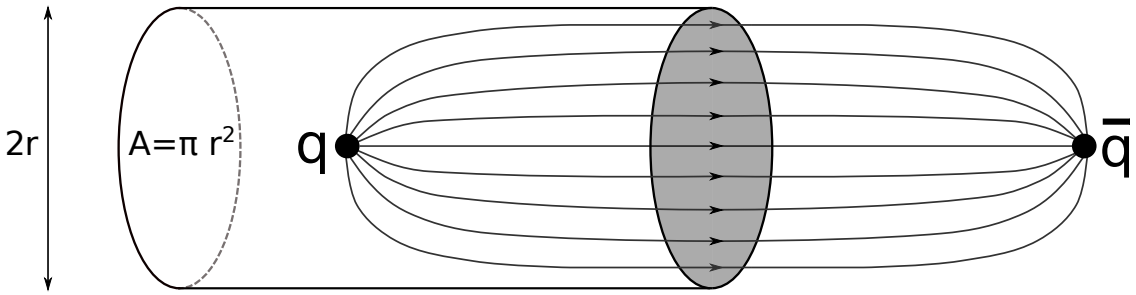

Figure 2.7: A cylindrical boundary around a quark, used to calculate the field strength via Gauss' Law. We only get flux going through the shaded face of the cylinder.

Considering a constant field E we therefore find the the energy per unit length (which, if the flux tube was modelled as a string, might be thought of as the string tension)

$$T = \frac{1}{2}E^2 A \tag{2.4.6}$$

where A is the area of a cylindrical flux tube of radius r such that

$$A = \pi r^2. \tag{2.4.7}$$

Now considering the field E in terms of quark charge g using Gauss' Law with the boundary shown in figure 2.7. We find

$$EA = \frac{1}{2}g \tag{2.4.8}$$

where the extra factor of $\frac{1}{2}$ is a result of the quark's coupling to the field through $SU(3)$. Then combining (2.4.6) and (2.4.8) we find

$$T = \frac{1}{4}gE. \tag{2.4.9}$$

When a quark-antiquark pair is created within the flux tube, they begin as virtual particles until they gain enough energy from the flux tube to come on shell. Each particle has mass m. Since we have

$$U^2 = p^2 + m^2 \tag{2.4.10}$$

and we require the particles to have 0 energy when created, they begin with imaginary momentum $p = im$. As they gain energy from the flux tube the momentum and potential for each one changes

$$p = i\sqrt{m^2 - \frac{1}{4}g^2E^2x^2} \tag{2.4.11}$$

$$V = m - \frac{1}{2}gEx \tag{2.4.12}$$

where x is the position of one of the particles from the point where it was created. When these reach zero the particles come on shell – this position is:

$$x_{os} = \frac{2m}{gE}. \tag{2.4.13}$$

The action for both particles is equal to twice the action for one particle and therefore given by

$$S_{2p} = 2S_{1p} = 2\int_0^{\tau(x_{os})} |p|\mathrm{d}\tau \tag{2.4.14}$$

$$= 2\int_0^{x_{os}} |p|\mathrm{d}x = \frac{\pi m^2}{gE}. \tag{2.4.15}$$

where we were able to take the step from (2.4.14) to (2.4.15) due to the circular symmetry of the problem and the fact that we are working in natural coordinates $c = 1$. Noting that the amplitude for the particle to come on shell is $\mathcal{A} = e^{-S_{2p}}$ [46], the probability for the particles to be created and come on shell is

$$\Gamma \propto e^{-2S_{2p}} \tag{2.4.16}$$

$$\propto e^{\frac{-2\pi m^2}{gE}} \tag{2.4.17}$$

which, using (2.4.9) becomes

$$\Gamma \propto e^{-\frac{\pi m^2}{2T}}. \tag{2.4.18}$$

2.5 Lund Model

The Lund Model has been a successful phenomenological model for meson behaviour [4], [5], which has been the basis of the very sucessful PYTHIA event generator software for simulating particle interactions [6]. It posits that mesons are made up of two partons (which can be identified with quarks) which collide elastically and are connected by a massless string (which may be thought of as the colour field flux tube) – in the simplest forms of the model the partons are massless themselves. It is reasonable to model the forces between the partons by using strings since, at large distances in QCD, the linear confining force dominates [47].

One useful introductory way of looking at the probability of meson decay in the Lund model is, as a toy model, to consider the unphysical system of a single quark jet – that is a quark q_0 with a colour field flux tube stretching off to infinity. At various points the flux tube can split, forming n quark-antiquark pairs – that is mesons – and a remenant q_n quark jet of lower energy. This is shown in figure 2.8.

We wish to consider the probability $D_q^{\mathfrak{m}}(z)$ that a specific meson $\mathfrak{m}$ of energy zE is found in the fragmentation products of a jet q of total energy E. In this case all the mesons in the fragmentation product have the same flavour. This is then given by the equation [5]

$$D^{\mathfrak{m}}(z)_q = f_q^{\mathfrak{m}}(z) + \int_z^1 \frac{\mathrm{d}z'}{z'} f_q^{\mathfrak{m}}(1-z') D_q^{\mathfrak{m}}\left(\frac{z}{z'}\right) \tag{2.5.1}$$

where $f(z)$ is the probability that the meson $\mathfrak{m}$ of energy zE (that is, z is the fraction of the total energy of the system that is held by $\mathfrak{m}$) is the first meson in the chain of fragmentation products (that is, that it is the meson $q_0\bar{q}_1$ as shown in 2.8). Then $f(1-z')$ is the probability that the first meson has instead energy $(1-z')E$ and therefore that the remainder of the chain energy $z'E$. Finally $D\left(\frac{z}{z'}\right)$ is the probability that the remainder chain contains the meson $\mathfrak{m}$ of energy $\frac{z}{z'}$ times the total energy of the remainder chain – that is that it contains the meson $\mathfrak{m}$ of energy $\frac{z}{z'}\, z'E = zE$. Therefore this can be thought of as an iterative equation.

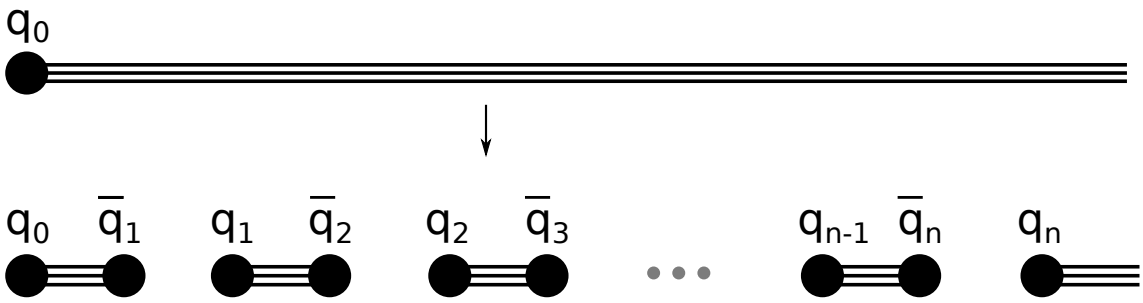

Figure 2.8: Diagram showing a single quark jet fragmenting to form multiple mesons.

When we are dealing with multiple flavours we must sum the second term over all the flavours, such that

$$D_q^{\mathfrak{m}} = f_q^{\mathfrak{m}}(z) + \int_z^1 \frac{\mathrm{d}z'}{z'} \sum_{q'} f_q^{q\bar{q}'}(1-z') D_{q'}^{\mathfrak{m}}\left(\frac{z}{z'}\right) \tag{2.5.2}$$

where $f_q^{q\bar{q}'}(1-z')$ is the probability that the first meson in the chain is $q\bar{q}'$ and has energy $(1-z')E$. We normalise it by the expression

$$\sum_{q'} \int_0^1 f_q^{q\bar{q}'}(z)\mathrm{d}z = 1. \tag{2.5.3}$$

We may now wish to study the dynamics of the quarks in this model, again following the explanation of [4], [5]. If we consider a model of massless quarks connected by a string representing the flux tube, we see that, in its simplest form, it has the Lagrangian

$$L = |p_1| + |p_2| - \gamma|x_1 - x_2| \tag{2.5.4}$$

where p_1 and p_2 are the momenta of each of the two quarks, x_1 and x_2 are their positions and γ is the tension in the string connecting them. This gives a 'yo-yo' type periodic motion, as seen in figure 2.9. The mass of the meson is then given by

$$M = L\gamma. \tag{2.5.5}$$

As in the preceding case, the string may split, forming a new quark and antiquark, which move away from each other. This may happen multiple times, as shown in

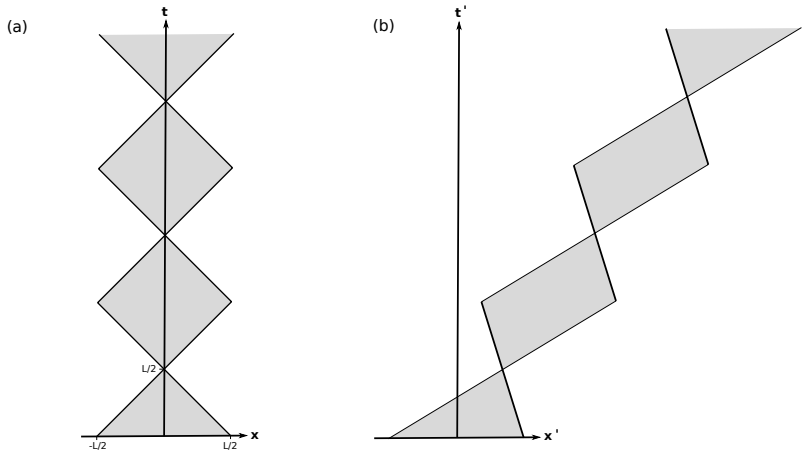

Figure 2.9: Diagram showing 'yo-yo' motion of string endpoints in (a) unboosted frame and (b) boosted frame.

figure 2.10. If a meson $q_1\bar{q}_2$ is formed by two such splits – one producing the pair $q_1\bar{q}_1$ at spacetime coordinates (x_1, t_1) and the other the pair $q_2\bar{q}_2$ at coordinates (x_2, t_2), then the meson energy will be $\gamma|x_2 - x_1|$ and momentum magnitude will be $\gamma|t_2 - t_1|$. Therefore the mass will be

$$M^2 = \gamma^2(x_2 - x_1)^2 - \gamma^2(t_2 - t_1)^2. \tag{2.5.6}$$

More generally, in the language of four momentum for a meson $q_{i-1}\bar{q}_i$, this may be referred to as

$$p_i^\mu = \gamma(x_{i-1}^\mu - x_i^\mu) \equiv \gamma\Delta x_i^\mu \tag{2.5.7}$$

$$p_i^\mu p_{i_\mu} = -\gamma^2 \Delta x_i^\mu \Delta x_{i_\mu} = {m_i}^2 \tag{2.5.8}$$

where we have used the mostly plus metric.

In lightcone coordinates ($x^\pm \equiv t \pm x$) we find that we may calculate the spacetime position $x_i^\pm$ at which a decay product of energy fraction z_i of its parent is produced as a function of the spacetime position $x_{i-1}^\pm$ at which said parent meson was produced. Recalling (2.5.7) we can see that

$$\Delta x_i^+ = z_i x_{i-1}^+ \tag{2.5.9}$$

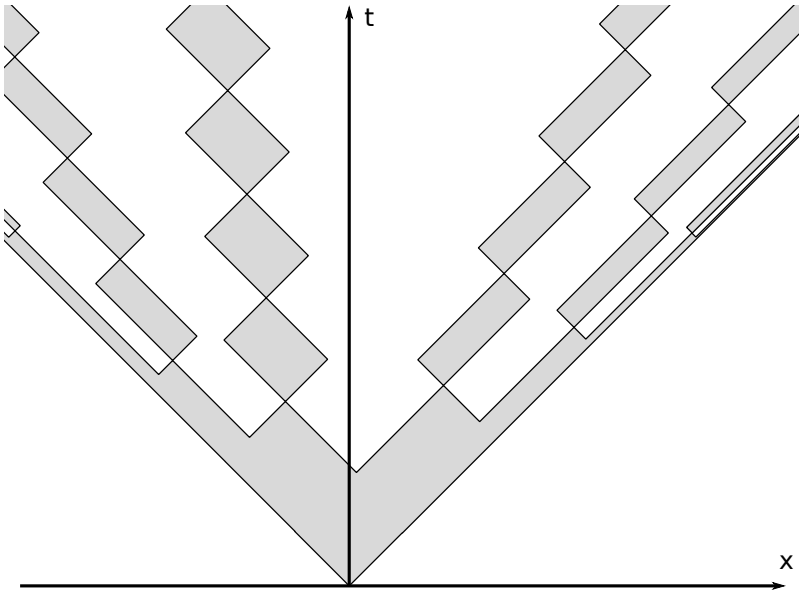

Figure 2.10: Diagram showing multiple fragmentation of Lund model string – representing multiple meson decays.

and Δx_i^- can be fixed by using (2.5.8), recalling that

$$-\Delta x_i^\mu \Delta x_{i\mu} = \Delta x_i^- \Delta x_i^+. \tag{2.5.10}$$

Then we find

$$x_i^+ = (1 - z_i) x_{i-1}^+ \tag{2.5.11}$$

$$x_i^- = x_{i-1}^- + \frac{m_i^2}{\gamma^2} \frac{1 - z_i^2}{z_i} \frac{1}{x_i^+}. \tag{2.5.12}$$

We can therefore come up with an iterative expression for the time it takes the string to break

$$\Gamma_i = (1 - z_i) \left(\Gamma_{i-1} + \left(\frac{m_i^2}{z_i} \right) \right) \tag{2.5.13}$$

and a corresponding probablity distribution for string splitting of

$$H(\Gamma) = \int \int \mathrm{d}z' \mathrm{d}\Gamma' f(z') \delta \Big(\Gamma - (1 - z')(\Gamma' + \frac{m^2}{z'}) \Big) H(\Gamma'). \tag{2.5.14}$$

Due to quantum fluctuations, all quarks will have some transverse (that is perpendicular to x as shown in 2.10) momentum $p_\perp$ and mass $m_\perp$. When calculating the dynamics of specific fragmentation possibilities, and then therefore the probability

distribution of the decay – we may start out by calculating the decay from either the left hand side (negative x as shown in 2.10) or from the right hand side (positive x). We want our result for H to be the same regardless of which side we start off with. This is not generally the case but, as shown by [5], it may be achieved if we choose the scaling function for the production of a meson with quark flavours labelled α and β

$$f_{\alpha\beta} = N_{\alpha\beta}\frac{z^{a_\alpha}}{z}\left(\frac{1-z}{z}\right)^{a_\beta} e^{-\frac{bm_\perp{}^2}{z}} \tag{2.5.15}$$

where $N_{\alpha\beta}$, a_α, a_β and b are free parameters. The exponential term reduces the probability for quarks with larger energy to be produced – this means that production of heavier quarks is suppressed so processes need to be modelled by perturbative methods [47].

If we consider mesons with more explicitly defined quarks of mass m we note that, similar to the original work by Schwinger [17] and the later CNN model [18] discussed in the previous section, if the quarks are produced at a point they must first move a certain distance d to gain enough energy to come on shell. This can be seen to be

$$d = \frac{m}{\gamma}. \tag{2.5.16}$$

If we know the wavefunction of the quark at this position to be Ψ_d we can calculate the wavefunction at a general position to be

$$\Psi(x) = \Psi_d e^{i\sqrt{(\gamma x)^2 - m^2}}. \tag{2.5.17}$$

We may find a specific solution

$$\Psi(0) = \Psi_d e^{-\frac{\pi m^2}{4\gamma}} \tag{2.5.18}$$

and therefore find the probability for decay to be

$$P \propto \Psi\bar{\Psi} \propto e^{-\frac{\pi m^2}{\gamma}} \tag{2.5.19}$$

We therefore see the repeated dependence of the decay probabilities in a number of

different models on the factor of $e^{-\frac{\pi m^2}{\gamma}}$.

Expansions to the model have allowed calculations of decay based on the mass of the mesons rather than just the quarks [48]. This proceeds in a similar way as described previously, but with the scaling function 2.5.15 replaced by

$$f_{\mathfrak{m}} = N\left(\frac{1-z}{z}\right)^{a} e^{-\frac{b(m_{\mathfrak{m}}{}^2+p_{\perp\mathfrak{m}}{}^2)}{z}} \tag{2.5.20}$$

where $\mathfrak{m}$ labels specific mesons, $m_{\mathfrak{m}}$ is the meson mass, $p_{\perp\mathfrak{m}}$ is the meson transverse momentum, z is the meson energy fraction, and N, a and b are constants. This is then normalised by the relation

$$N\sum_{\mathfrak{m}}\int\left(\frac{1-z}{z}\right)^{a} e^{-\frac{b(m_{\mathfrak{m}}{}^2+p_{\perp\mathfrak{m}}{}^2)}{z}}\mathrm{d}z\mathrm{d}p^2_{\perp\mathfrak{m}} \;=\; 1 \tag{2.5.21}$$

Baryon production in the Lund Model was intially modelled by specifying that string breaking could produce a diquark antidiquark ($qq\,\bar{q}\bar{q}$) pair rather than just a quark antiquark pair, and treating these diquarks as if they were just the same as other quark flavours [5]. However, an alternative 'popcorn model' [49], [50] has proved to give results more in accordance with experiment. In this model it is necessary to consider the colours of the individual quark pairs. Virtual quark-antiquark pairs can be produced 'within' a string between a quark-antiquark pair of different colour. Sometimes these just annihilate, but if the string breaks between this virtual quark-antiquark pair, a diquark-antiquark pair 'pops out', which can then form a baryon as in the earlier model. This is illustrated in figure 2.11.

By considering the collisions of endpoints of the string, a slight update to the Lund Model – the Linked Dipole Chain Model [4], [51] – can be used to make calculations for deep inelastic scattering (a process used to probe the interior of hadrons by sending high momentum particles and reconstructing said interior from the scatter pattern). This model may be though of [52] as a compromise between the DGLAP (Dokshitzer–Gribov–Lipatov–Altarelli–Parisi) Model which focuses on very high energy incident particles whose momentum dominates the result of the scattering and the BFKL (Balitsky, Fadin, Kuraev and Lipatov) Model which focuses

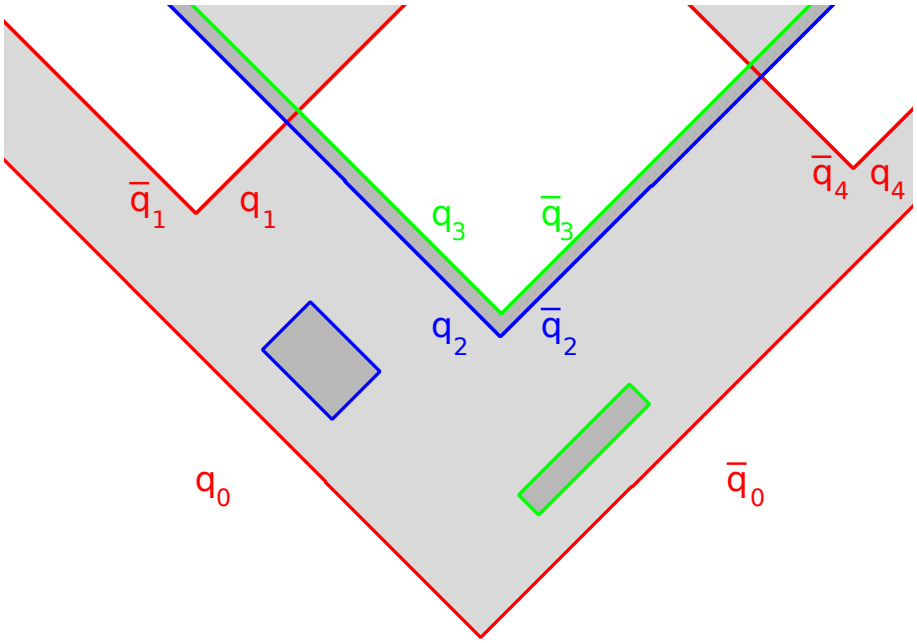

Figure 2.11: Diagram showing formation of both mesons ($q_0\bar{q}_1$, $q_4\bar{q}_0$) and baryons($q_1q_2q_3$, $\bar{q}_1\bar{q}_2\bar{q}_4$), as well as two virtual pairs which self-annihilate in popcorn model. Based on diagrams in [49], [50].

on lower energy incident particles which therefore have more time to be scattered.

These models, however, are all highly phenomenological, with many parameters that need to be fine tuned by hand. This motivates the introduction of holographic instanton model which – while not yet as successful as other models, offers the hope of being able to make predictions from first principles. This can first be motivated at looking at a toy instanton model in flat space, which will be introduced in the next section.

2.6 Comparison of Instanton Point Particles and String

It is now instructive to review the splitting of a single string with massive endpoints – forming two new massive endpoints, and see how this compares to the process that it is meant to model – the pair production of two massive point particles from a field.

In this simple example we will consider this field to be an Abelian field, such as an electric field, and we will work in flat spacetime. First, however, we must introduce Wick Rotation and instantons.

As explained previously, we may think of pair creation as the two particles starting out as virtual particles at a point, and then moving apart from one another, gaining enough energy from the colour field to come on shell. This may therefore be thought of as a tunnelling process, with the potential shown in figure 2.12(a). When we Wick rotate, however, we see the following change in action

$$S_M = \int \mathrm{d}t \left(\frac{m}{2} \left(\frac{\mathrm{d}x}{\mathrm{d}t} \right)^2 - V(x) \right) \qquad \rightarrow \qquad S_E = \int \mathrm{d}t \left(\frac{m}{2} \left(\frac{\mathrm{d}x}{\mathrm{d}t} \right)^2 + V(x) \right) \tag{2.6.1}$$

such that the potential is reversed in the new, Euclidean, set up – as shown in figure 2.12(b). This allows the calculation to be done semiclassically, which can be far easier.

A solution to a problem in such a Wick-rotated system is known as an instanton. Instantons have had a long a long track record of being used to help facilitate QCD calculations – one of their initial inspirations being to make calculations involving the evolution operator of a quantum system e^{-iHt} easier [53]. Since we will be using them to calculate the worldlines of particles we will refer to our solutions as worldline instantons. Since we are not working in Lorentzian spacetime, not all features of the mesons we are modelling will be accurately captured (for example the two daughter particles produced in the decay immediately come back together to form the parent particle) but it is a useful method for specifically calculating decays.

Reviewing the method for simple toy model will allow us to develop techniques which we will use when we move on to curved spacetime in later sections. We will see that the action of the system is proportional to $\frac{\pi m^2}{\gamma}$, leading to the same dependence of the decay probability on this factor as we saw in the previous sections. A detailed description of the calculation is presented in full in appendix A. The potential for pair creation is briefly analysed in more detail in appendix B.

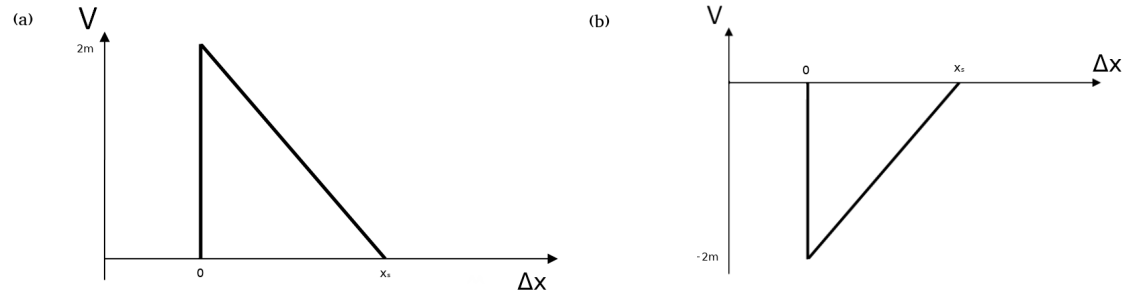

Figure 2.12: Pair production potential plotted against quark separation in (a) Minkowski spacetime and (b) Euclidean spacetime. In the Minkowski picture we visualise two virtual particles being created at 0 separation, and therefore with high potential in the field, and then having to gain energy from the field equivalent to their mass in order to be able to come on shell at separation x_s. This whole process may be visualised as tunnelling.

2.6.1 Point Particle Action

As discussed previously, the probability for the production of charged particle-antiparticle pairs was calculated by Schwinger [17]. This was done by perturbatively summing a class of one-loop diagrams in quantum field theory, the same result was later rederived in the worldline approach, by construction of a worldline instanton [54]. The same worldline instanton approach was also used to describe the production of monopole/anti-monopole pairs in an external magnetic field [55]. This section will review the worldline instanton method of calculating Schwinger-like pair production rates.

We assume that a non-vanishing electric field E is turned on in the X^1 direction. In order to construct the worldline instanton describing the production of a particle-antiparticle pair of masses m and charge q, one needs to consider the Wick rotated system obtained by $\tau \to -i\tau$, $A_0 \to iEX^1$ and solving the classical equations of motion of a particle in the Euclidean background. The action of the particle is given by

$$S_E = \int \mathrm{d}\tau \left(m\sqrt{\dot{X}^\nu \dot{X}_\nu} - iqA_\nu \dot{X}^\nu \right). \tag{2.6.2}$$

It is not hard to see that the solution for the particle worldline is given by

$$X^0(\tau) = R\cos(2\pi n\tau)\,, \quad X^1(\tau) = R\sin(2\pi n\tau)\,, \quad X^2 = 0\,, \quad X^3 = 0\,, \tag{2.6.3}$$

where X^0 is the Wick rotated target space time direction. We see that the worldline instanton looks like a loop of radius R. The parameter n labels different instantons, and describes how many times the particle 'winds' around the loop. As usual, the particle propagating 'backwards' in the (Euclidean) time X^0 is interpreted as an antiparticle. Hence, the left-hand side of the loop can be interpreted as the worldline of the antiparticle, while the right-hand side as the worldline of the particle, see figure 2.13.

We might think that we should only consider the motion of the particles up to $X_0 = 0$ on figure 2.13 since that is where they would come on shell in the Lorentzian picture. However, as we recall from (2.4.16), we would multiply the action of this system by two when exponentiating it and using it to calculate the probability. It is therefore equivalent, and often easier, to use the symmetery of the system and instead consider the action of the full circular path of the instanton.

Substituting the solution (2.6.3) into the particle action (2.6.2) and integrating over the worldline gives

$$S_{\text{class}} = 2\pi nRm - \pi nqER^2\,. \tag{2.6.4}$$

The extrema of the action will give classical solutions, and one finds that the radius of the loop is fixed to be $R = \frac{m}{qE}$ for which the action reduces to $S_{\text{class}} = \pi\frac{m^2}{qE}n$. So the full loop (2.6.3) describes a particle-antiparticle pair which is produced at the Euclidean time $X_0 = -\frac{m}{R}$, in which the particles move away from each other. Once the particle and antiparticle go on-shell, i.e. once they reach a distance $2\frac{m}{qE}$, one can analytically continue the solution (2.6.3) back to Lorentzian time. The Lorentzian solution describes a pair of produced particles accelerating away from each other with proper acceleration $a = \frac{m}{qE}$.

Exponentiation of this Euclidean action S_{class} with winding $n = 1$ gives the most

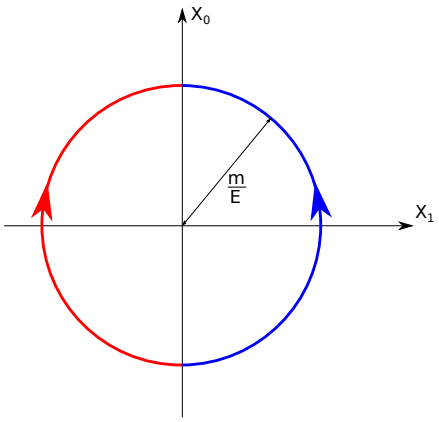

Figure 2.13: Worldline instanton for particle-antiparticle pair production in an external electric field E.

dominant contribution for the probability of particle production in the saddle point approximation. Looking at the fluctuations around this classical path (2.6.3), and summing over their contributions in the path integral [54], produces a pre-factor to the exponent $e^{-S_{\text{class}}}$, and one obtains the aforementioned Schwinger formula for the probability of production of particles. Therefore the probability for the pair production of charge q, per unit volume and per unit time, is given by [17]

$$P_{\text{pp}} = \frac{E^2}{8\pi^3} \sum_{n=1}^{\infty} \frac{1}{n^2} e^{-\frac{\pi m^2}{q|E|} n} . \tag{2.6.5}$$

In many calculations, we set $q = 1$ for simplicity and clarity.

2.6.2 String Action

In order to model mesons, including their flux tube as well as endpoint quarks, we can use an action for the relativistic string suplemented with two massive particles which are attached to the string endpoints. This is the "old" string model, as discussed and reviewed in [56]. We want to find the Euclidean worldsheet configuration which interpolates between the unsplit and split string with massive end points. After performing a Wick rotation in the target and worldsheet space-time, the string

action becomes.

$$S = \gamma \int_{\tau_1}^{\tau_2} \mathrm{d}\tau \int_0^{\pi} d\sigma \sqrt{-(\dot{X}\cdot X')^2 + \dot{X}^2 X'^2} + m \int_{\tau_1}^{\tau_2} \mathrm{d}\tau \left(\sqrt{\dot{X}^2(\tau, \sigma = 0)} + \sqrt{\dot{X}^2(\tau, \sigma = \pi)} \right) \tag{2.6.6}$$

$$\equiv S_{\text{bulk}} + S_{\partial,\sigma=0} + S_{\partial,\sigma=\pi} \,.$$

Here $X \cdot X \equiv X^\mu X^\nu g_{\mu\nu}(X)$ and $g_{\mu\nu}(X)$ denotes the Euclidean metric in the target space, which for us at this stage is just a flat metric, $g_{\mu\nu} = \delta_{\mu\nu}$. The tension of the string is denoted with $\gamma = \frac{1}{2\pi\alpha'}$ and m is the mass of the particles attached to the string endpoints.

We are interested in finding a Euclidean, two-dimensional string configuration which interpolates between a single and a double string. The initial string had only two quarks at its endpoints. In the fully dynamical string model, the position of these outer quarks is fixed by the total angular momentum of the meson, which prevents strings from collapsing, as discussed in [56]. To simplify the discussion, we will in this thesis take quarks in the original meson to satisfy Diriclet boundary conditions and confine them to move on a line in the Euclidean target space.

At some point in the Euclidean 'time', a pair of massive quarks is pair-produced in the interior of the string. These particles represent new 'internal' endpoints of the string, which can move freely, that is satisfy Neumann boundary conditions, see figure 2.14. In order to account for the pair-produced quarks, one needs to modify the action (2.6.6) by adding to it the worldline action of the pair-produced quarks. Adding this extra term in the action is in spirit the same as what one does in order to describe the pair-production of the charged particle-antiparticle pair in the external electric field using the instanton approach in the world-line formalism, see for example [16]. The main difference is that the role of the electric field is now played by the tension of the split string, which pulls apart the pair-produced particles. For simplicity, we will also assume that the particles have no transverse momentum, so that the whole process of string splitting is planar, that is that both

in- and outgoing strings are in the same two-dimensional plane.

As the variation of the action (2.6.6) leads to bulk and boundary equations of motion we have to make sure that both are satisfied. In the two-dimensional target space, the bulk equations of motion are always satisfied, thanks to reparametrisation invariance of the action. So we just need to make sure that the boundary equations of motion for the Neumann boundary conditions hold. Note that the boundary equations of motion receive nontrivial contribution from the surface terms of the bulk part of the action,

$$\frac{\partial}{\partial\tau}\left(\frac{\partial\mathcal{L}_{end}}{\partial\dot{X}^0}\right) - \left.\frac{\partial\mathcal{L}_{bulk}}{\partial X'^0}\right|_{\sigma_B} = 0\,, \tag{2.6.7}$$

where σ_B is the position of the boundary (or boundaries) of the string for which Neumann conditions are imposed.

Before the quarks were pair-produced, the string was straight and stretching between $(0, 2L)$ in the target space. To describe this string configuration we choose the parametrisation

$$X^0 = \tau\,, \qquad X^1 = 2L\frac{\sigma}{\pi}\,, \qquad \sigma \in [0, \pi\rangle\,. \tag{2.6.8}$$

The instanton configuration for a splittting string is plotted in figure 2.14, and is given by

$$\begin{aligned}
&X^0_L(\tau,\sigma) = X^0_R(\tau,\sigma) = \tau\,,\\
&X^1_L(\tau,\sigma) = x_L(\tau,\sigma) = -\frac{\sigma}{\pi}\left(\sqrt{-\tau^2+\kappa^2} - a\right)\,, && \sigma \in [0,\pi\rangle\,,\\
&X^1_R(\tau,\sigma) = x_R(\tau,\sigma) = \left(1-\frac{\sigma}{\pi}\right)\left(\sqrt{-\tau^2+\kappa^2} + a\right) + 2a\frac{\sigma}{\pi}\,, && \sigma \in [0,\pi\rangle\,,
\end{aligned} \tag{2.6.9}$$

where κ and a are arbitrary constants, and X_L and X_R describe left and right half of the instanton (the red and blue areas in figure 2.14). Note that while we have written the solution piece-wise, the two "sides" of the instanton, X_L and X_R are glued in a smooth way. The solution above is a Euclidean version of a solution found in [57].

It is easy to see that the ansatz (2.6.9) satisfies the Neumann boundary equations

of motions (2.6.7),

$$-m\frac{\partial}{\partial\tau}\left(\frac{\dot{X}_L^\mu(\tau,\sigma=\pi)}{\sqrt{1+\dot{x}_L^2(\tau,\sigma=\pi)}}\right)+\gamma\left(-\dot{x}_L\dot{X}_L^\mu+\left(\frac{1+\dot{x}_L^2}{x_L'}\right)X_L'^\mu\right)\Bigg|_{\sigma=\pi}=0\,, \quad (2.6.10)$$

(where $\mu=0,1$) provided that $\kappa=m/\gamma$. A similar expression holds for the right-hand piece X_R^μ. Note also that the solution (2.6.9), where the outer quarks are moving on straight lines, can be generalised to a solution for which the endpoints do not follow straight lines but move on arbitrary curves $f_L(\tau)$ and $f_R(\tau)$, see figure 2.14b.

$$\begin{aligned}
&X_L^0(\tau,\sigma)=X_R^0(\tau,\sigma)=\tau\,,\\
&X_L^1(\tau,\sigma)=x_L(\tau,\sigma)=-\frac{\sigma}{\pi}\left(\sqrt{-\tau^2+\kappa^2}-a\right)+f_L(\tau)\left(1-\frac{\sigma}{\pi}\right)\,, \qquad \sigma\in(0,\pi)\,,\\
&X_R^1(\tau,\sigma)=x_R(\tau,\sigma)=\left(1-\frac{\sigma}{\pi}\right)\left(\sqrt{-\tau^2+\kappa^2}+a\right)+f_R(\tau)\frac{\sigma}{\pi}\,, \qquad \sigma\in(0,\pi)\,,
\end{aligned} \quad (2.6.11)$$

with $\kappa=\frac{m}{\gamma}$ as above. We therefore see that in whichever way the outer quarks move, the dynamics of the inner free (Neumann) quarks is unaffected. The 'motion' of the inner quarks is always circular, with a radius of curvature which is determined by the ratio of the particle mass and the string tension which pulls the produced quarks.

In order to evaluate the probability for a single event of particle pair production, we need to evaluate the action of the instanton. The string configuration (2.6.9) describes the process of pair production inside the string, as well as the propagation of the outer, background quarks. Hence in order to isolate the part which describes particle production, we need to subtract the contribution corresponding to the background. In other words, the quantity of interest which gives us the probability for the particle production is

$$\begin{aligned}
S_{\rm pp}=S_{\rm full}-S_{\rm background}&=m(\text{Circumference of circle})-\gamma(\text{Area of circle})\\
&=m(2\pi\kappa)-\gamma(\pi\kappa^2)=\frac{\pi m^2}{\gamma}\,.
\end{aligned} \quad (2.6.12)$$

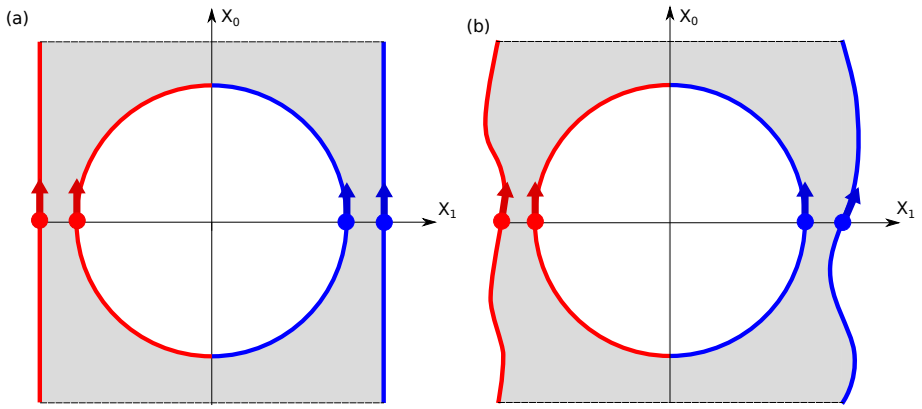

Figure 2.14: Flat space instantons, describing the breaking of the string flux tube. The instanton on the left describes breaking of the flux tube where the external quarks are at a fixed distance, while the instanton on the right depicts external quarks which 'move' on arbitrary paths.

Here $S_{\text{background}}$ is the action of the background configuration with no particle production (2.6.8), S_{full} is the action of the instanton configuration (2.6.10) and γ is the string tension. It is easy to see that the same result is obtained with the more general solution (2.6.11), where the outer quarks move on arbitrary, non-straight paths. In other words, the dynamics of the external quarks is fully decoupled from the production process inside the flux tube.

We thus find that the probability for a single pair production event to happen is given by

$$P_{\text{PP}} = e^{-S_{\text{PP}}} = e^{-\frac{\pi m_q^2}{\gamma}}, \tag{2.6.13}$$

We see that this is the same as the contribution of a single instanton in the CNN formula (2.4.18), up to a numerical factor of a half. So we see that in the process of string splitting, the string tension has the same role as the electric field in the Schwinger process, that is, it pulls the produced particles away from each other.

The position of the instanton can be at any arbitrary point on the string worlsheet, as long as the instanton is not too close to the boundary of the string worldsheet, so that size of the instanton circle "fits" into the string worldsheet. One can therefore compute the probability per unit time Γ from the the probability per unit volume

and unit time (2.6.13) as $\Gamma = P_{\rm pp} L$ where L is the string length. On the other hand, the mass of the initial mesonic "particle" is $M = \gamma L + 2m$, where m is the mass of the initial quark pairs. In the limit of long strings ($L \gg m/\gamma$) one can approximate $M \approx \gamma L$ and also ignore subtleties related to whether the instanton fits into the worldsheet or not. In this limit one recovers the results that Γ/M is a constant for all mesonic particles, as seen in, for example, [58].

Chapter 3

Outline of Holography

3.1 Introduction to AdS/CFT Correspondence

The concept of dualities – parameters or entire theories which have been shown to be equivalent under certain transformations – has long been important in physics. A duality between a gauge theory and a gravity theory seems to be of great interest, and was suggested early on by 't Hooft [59]. A weakly coupled theory of gravity can be numerically more tractable and could be used to solve difficult problems in the equivalent strongly coupled gauge theory. However, the two theories long seemed irreconcilable. However, there have long been clues that these might be overcome with the help of string theory. This was originally developed as a model for phenomena involving the strong nuclear force and the discovery that it contained gravitons resulted in a rush of excitement and speculation that it might be the long awaited grand unified theory. While work in that direction is still proceeding, the late 90's brought a new exciting development in the shape of the AdS/CFT correspondence [9]. This section and section 3.2 will provide an introduction to the correspondence, section 3.3 will outline how to introduce temperature, section 3.4 will provide background on methods that have previously been used to model QCD and mesons holographically, while section 3.5 will introduce the basic methods for using worldline instantons in AdS/CFT – which will later be expanded more fully for

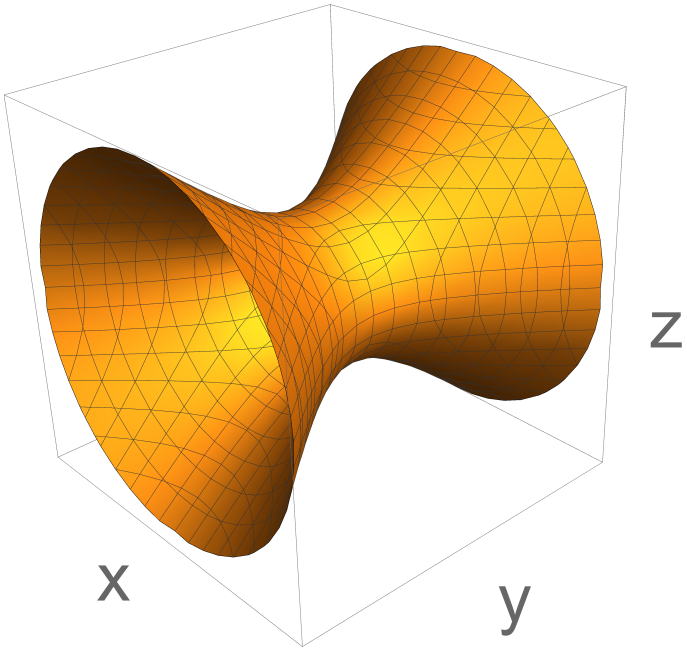

Figure 3.1: An AdS_2 spacetimetime embedded in $\mathbb{R}^3$ according to the relation $x^2 - y^2 + z^2 = 1$

confining backgrounds in chapter 5. This is a rich topic and comprehensive reviews include [8], [60]–[63].

Anti de Sitter is a simple spacetime which may be described as a d dimensional plane embedded in an $d+1$ dimensional $M^{d-1,2}$ Minkowski spacetime (or, after Wick rotation, in Euclidean spacetime) [64], [65] according to the relation

$$(X^0)^2 - X_i X^i + (X^d)^2 = R^2, \tag{3.1.1}$$

where i runs from 1 to $d-1$ and the metric is given by

$$\mathrm{d}s^2 = -\left(dX^0\right)^2 + \left(\mathrm{d}X^i \mathrm{d}X_j\right) - \left(dX^d\right)^2. \tag{3.1.2}$$

From this, it is clear the spacetime has $SO(d-1,2)$ symmetry. An example of such an AdS embedding can be seen in figure 3.1.

It is often useful to re-write this in so-called Poincaré coordinates. We begin by

redefining the AdS condition (3.1.1) such that

$$T^2 - \boldsymbol{X}^2 + Z^2 - Y^2 = R^2 \tag{3.1.3}$$

where

$$T \equiv X^0 \qquad \boldsymbol{X} = X^j \qquad Y = X^{d-1} \qquad Z = X^d \tag{3.1.4}$$

where j runs from 1 to $d-2$. Then we transform the coordinates such that

$$T = R\frac{t}{z} \tag{3.1.5}$$

$$\boldsymbol{X} = R\frac{\boldsymbol{x}}{z} \tag{3.1.6}$$

$$Y = \frac{1}{2z}\left(\boldsymbol{x}^2 - t^2 + z^2 + R^2\right) \tag{3.1.7}$$

$$Z = \frac{1}{2z}\left(\boldsymbol{x}^2 - t^2 + z^2 + R^2\right) \tag{3.1.8}$$

such that the metric (3.1.2) becomes

$$\mathrm{d}s^2 = \frac{1}{z^2}\left(-\mathrm{d}t^2 + \mathrm{d}\boldsymbol{x}^2 + \mathrm{d}z^2\right). \tag{3.1.9}$$

From this formulation it is clear that at a constant z slice AdS^d reduces to $M^{d-2,1}$, as shown in figure 3.2.

It is also common to redefine

$$u \equiv \frac{1}{z} \tag{3.1.10}$$

such that we get

$$\mathrm{d}s^2 = u^2\left(-\mathrm{d}t^2 + \mathrm{d}\boldsymbol{x}^2\right) + \frac{1}{u^2}\mathrm{d}u^2. \tag{3.1.11}$$

The idea of the AdS/CFT correspondence was introduced by Maldacena in [9], where he found that the boundary of a type IIB string theory of gravity in AdS crossed with a compact space (in his example the five sphere S^5) was dual to a conformal field theory.

More specifically, he considered a spacetime deformed by a stack of N parallel $D3$

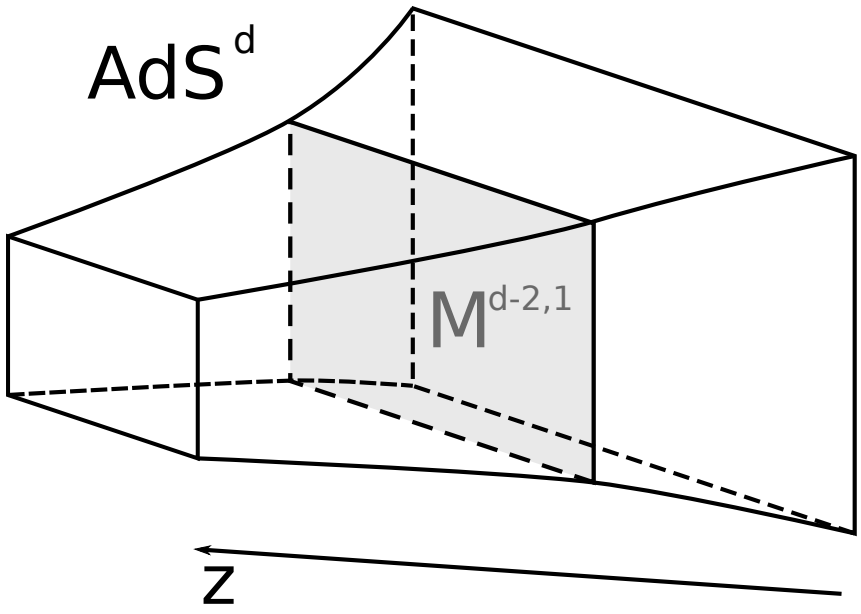

Figure 3.2: Slices of AdS^d at constant z are just Minkowski $M^{d-2,1}$ slices. Image based on diagram from [65].

branes and string coupling g_S. D-branes, or Dirchlet branes, were first introduced by Polchinski [66] as objects which provide the necessary Ramond-Ramond charges for string duality (the phenomenon where a strongly coupled string theory may be shown to be equivalent to a weakly coupled string theory). A Dp brane extends in p spatial dimensions, plus the time dimension.

There may be seen to be two regimes in this set up. For weak string coupling $g_S N \ll 1$ the branes have no impact on the geometry and the spacetime remains flat. In this regime the branes may act as endpoints for open strings – with Dirchlet boundary conditions for their spatial dimensions, explaining their name. Massive string states decouple and we are just left with a theory of supergravity. For strong string coupling $g_S N \gg 1$ the branes begin to curve the spacetime, resulting in a metric:

$$\mathrm{d}s^2 = \frac{\left(\alpha'\right)^2 u^2}{R_{sph}^2}\Big(- f(u)\mathrm{d}t^2 + \mathrm{d}x_i \mathrm{d}x_j \delta^{ij}\Big) + \frac{R_{sph}^2}{f(u)\, u^2}\mathrm{d}u^2 + R_{sph}^2 \mathrm{d}{\Omega_5}^2 \tag{3.1.12}$$

where

$$f(u) = 1 - \frac{{u_\Lambda}^4}{u^4} \tag{3.1.13}$$

$$u_\Lambda{}^4 = \frac{2^7}{3}\pi^4 {g_S}^2 \mu, \tag{3.1.14}$$

μ is the energy density of the system, $R_{sph} = \left(\alpha'\right)^{\frac{1}{2}}\left(4\pi g_S N\right)^{\frac{1}{4}}$ is the radius of S^5 and $\sqrt{\alpha'} = l$ is the string length [60]. At large u this metric reduces to flat spacetime while at small u it reduces to pure AdS of the form (3.1.11).

We will work in the low energy limit to simplify calculations and require that the size of strings is small compared to the curvature of the spacetime. This is equivalent to saying

$$\alpha' \to 0 \qquad\qquad l \to 0 \tag{3.1.15}$$

and is called the Maldacena Limit.

In this regime, for the $g_S N \ll 1$ limit open strings on the $D3$ branes give an $\mathcal{N} = 4$ super Yang-Mills theory with $SU(N)$ symmetry. In the $g_S N \gg 1$ limit, and near the horizon as $u \to \infty$, the spacetime metric simplifies to

$$\mathrm{d}s^2 = \frac{\left(\alpha'\right)^2 u^2}{R_{sph}^2}\mathrm{d}x_\mu \mathrm{d}x_\nu \eta^{\mu\nu} + \frac{R_{sph}^2}{u^2}\mathrm{d}u^2 + R_{sph}^2 \mathrm{d}{\Omega_5}^2 \tag{3.1.16}$$

which is just $AdS_5 \times S^5$ (the first two terms representing AdS_5 and the last term S^5). The AdS_5 metric given here is the Poincaré AdS metric [67]– which is a subset of the global AdS metric in the region $u > 0$. The full global AdS_5 metric may be written as

$$\mathrm{d}s^2 = -\left(\frac{\rho^2}{{R_{sph}}^2} + 1\right)\mathrm{d}\tau^2 + \left(\frac{\rho^2}{{R_{sph}}^2} + 1\right)^{-1}\mathrm{d}\rho^2 + \rho^2 \mathrm{d}{\Omega_3}^2 + R_{sph}^2 \mathrm{d}{\Omega_5}^2 \tag{3.1.17}$$

Since the field theory could be extended to any g_S Maldacena conjectured a duality between the two regimes. Specifically that a string theory of gravity in $AdS_5 \times S^5$ was dual to an $\mathcal{N} = 4$ $SU(N)$ super Yang-Mills; identifying the couplings ${g_{YM}}^2 = 2\pi g_S$.

There has been much early discussion as to which regions of the parameter space this duality is valid [63]. For this it is useful to consider the ratio $\frac{R_{sph}}{l}$ – which needs to remain large in order to eliminate corrections to the geometry from string effects that would no longer make it a useful theory of gravity. Then defining the 't Hooft

coupling $\lambda \equiv {g_{YM}}^2 N$ and noting that

$$\frac{R_{sph}}{l} = \left(4\pi g_S N\right)^{\frac{1}{4}} \sim \lambda^{\frac{1}{4}} \tag{3.1.18}$$

we see that we require $\lambda \gg 1$ and $N \gg 1$ – this is called the 't Hooft limit. The 't Hooft limit has been explained as being necessary to give the gauge theory a sufficiently large SU(N) group to have sufficient degrees of freedoms to match with the excitations in the additional dimension in the gravity theory. In this case we say that we have the gauge gravity correspondence in the 'weak form' – in this case the IIB string theory can be expressed as a supergravity theory (that is the low energy limit of the full theory) with $g_s N \ll 1$.

However, more recent work has investigated the duality and lower values of N and λ. In the strongest form of the theory all our parameters (such as λ, N, and g_S) may take values of arbitary size and on the gravity side we get a full theory quantum string theory [60], [63].

The AdS/CFT correspondence is known as a holographic principle as a lower dimensional gauge theory is seen to be dual to a higher dimensional string gravity theory. We say that the gauge theory lives on the boundary of its dual bulk string theory of gravity. This gets around the Weinberg Witten no go theorem – which states that theories with a Lorentz covariant energy momentum tensor cannot have massless particles with spin of greater that 1 and theories with Lorentz covariant currents cannot have massless particles with spin of greater than $\frac{1}{2}$ [68]. This is circumvented in framework by having the gravity live in a higher dimension.

The dimensions of the two theories can easily be matched. The flat dimensions x_μ in the AdS part of the string theory are indentified directly with the spacetime dimensions of the gauge theory. The additional dimension in the holographic gravity picture can be thought to correspond to the energy scale of the field theory picture (with low values of u corresponding to the IR and high values of u corresponding to the UV). The S^5 dimensions can be thought to correspond to φ^i scalars in the

gauge theory. This can be seen when considering how the symmetries of the two theories match up. The gauge symmetry group of the φ^i scalars is $SU(4) \backsimeq SO(6)$ which matches up with the $SO(6)$ global symmetry of the S^5 sphere. The $SO(4,2)$ conformal group for four dimensions then matches up with the $SO(4,2)$ group for AdS_5.

It is even possible to find a gauge dual of M-Theory [9], [69]. In this case we need an $AdS_4 \times S^7$ spacetime – which in its most general form is given by

$$\mathrm{d}s^2 = f^{-\frac{2}{3}}(u)\left(-\mathrm{d}{x_0}^2 + \mathrm{d}{x_1}^2\right) + f^{\frac{1}{3}}(u)\left((\alpha')^2\,\mathrm{d}u^2 + (\alpha')^2\,u^2\mathrm{d}{\Omega_7}^2\right) \tag{3.1.19}$$

where

$$f(u) = 1 + \frac{{R_{sph}}^6}{(\alpha')^2\,u^6} \tag{3.1.20}$$

This is found to be dual to ABJM, a type of Chern Simons theory. More recent work, which will be discussed in later sections, has explored yet more general gauge/gravity correspondences – moving away from $AdS_5 \times S^5$ and $\mathcal{N} = 4$ $SU(N)$ super Yang-Mills to explore different geometries that are dual to different field theories – with very broad applications.

This is also known as a 'weak-strong coupling' duality as the gauge theory coupling is strong but is dual to a string theory with weak coupling. The theory has proved useful in modelling entanglement entropy [70] and condensed matter systems (both modelling specific condensed matter systems directly [71], [72] or used together with approaches such as optical lattices [73], [74] – specific condensed matter systems which can model other, related systems). A good introductory review of AdS/CFT from the latter viewpoint is presented in [75]. A discussion of how holography is applicable to the study of quark jet quenching, which is tangentially related to the main focus of this work, is presented in appendix C. We will, however, focus on its applications to QCD.

3.2 Matching Operators and Fields

It is instructive to explore more formally which elements of the string theory are dual to which elements of the gauge. After a generic explanation, it is particularly useful to study the example of Weyl tensors in the gravity theory and conformal operators in the gauge theory as it can be easily shown how the mass of the fields in the former case can be related to the dimension of the latter.

As suggested earlier, operators (that is, observable quantities) in the gauge theory correspond to fields and string states in the string bulk [63]. More specifically, a source term in the gauge theory Lagrangian

$$\mathcal{L}_s = \phi_0(x)\mathcal{O}(x), \tag{3.2.1}$$

where $\phi_0(x)$ specifies the conditions of a bulk field on the boundary and $\mathcal{O}$ is a gauge theory operator, can be seen to be related to the string partition function

$$\mathcal{Z}_{\text{string}}[\phi_0] = \left\langle e^{\int \mathrm{d}^4x \phi_0 \mathcal{O}} \right\rangle. \tag{3.2.2}$$

An example of this particular duality is that between bulk string theory gravitons and the boundary gauge theory energy momentum tensor. This is a particularly useful aspect of the correspondence as it allows for a direct 'dictionary' to be written between the two theories, allowing us to translate a problem or quantity in one theory to an equivalent one in the other theory, where it might be easier to to solve or calculate.

One also finds that the rank k of the Weyl tensors in the gravity theory is dual to the dimension of the conformal operators Δ in the gauge theory. Under this duality we may [60] re-write the Klein-Gordon equation for the fields in the gravity theory from

$$\Box_{AdS}\phi = \frac{1}{{R_{sph}}^2} k(k-d)\phi \tag{3.2.3}$$

where d is the number of dimensions of the gauge theory, to

$$\Box_{AdS}\phi = \frac{1}{{R_{sph}}^2}\Delta(\Delta-1)\phi \tag{3.2.4}$$

and therefore

$$m^2 R_{sph}^2 = \Delta(\Delta-1) \tag{3.2.5}$$

giving a relationship between masses of fields m in the gravity theory and the conformal dimension Δ of the gauge theory. To understand this relationship better we may Fourier decompose the fields ϕ such that

$$\phi(z,x) = e^{ip^\mu x_\mu}\phi_p(z) \tag{3.2.6}$$

allowing the Klein-Gordon equation to be re-written as

$$z^2 \mathrm{d}_z^2\phi_p(z) - (d-1)z\partial_z\phi_p(z) - ({m^2{R_{sph}}^2} + p^2z^2)\phi_p(z) = 0 \tag{3.2.7}$$

giving us two modes at $z \to 0$:

$$\phi_+ \equiv \phi_{p+} = z^{\Delta_+} \tag{3.2.8}$$

$$\phi_- \equiv \phi_{p-} = z^{\Delta_-} \tag{3.2.9}$$

where

$$\Delta_\pm = \frac{d}{2} \pm \sqrt{\frac{d^2}{4} + {m^2{R_{sph}}^2}}. \tag{3.2.10}$$

Therefore

$$\phi(z,x) \sim \phi_-(x)z^{\Delta_-} + \phi_+(x)z^{\Delta_+} + \dots \tag{3.2.11}$$

We note that we require $\Delta > \frac{d-2}{2}$ for the action to remain finite and therefore re-normalisable. We require $\Delta < d$ as the conformal dimension must be less than the number of dimensions in the theory. Therefore we see that we have two regions.

For

$$\frac{d-2}{2} < \Delta < \frac{d}{2} \tag{3.2.12}$$

we have $\Delta = \Delta_-$ and we therefore identify ϕ_- as the vacuum expectation value of the dual operator in the gauge theory and ϕ_+ as its source.

For

$$\frac{d}{2} < \Delta < d \tag{3.2.13}$$

we have $\Delta = \Delta_+$ and we therefore identify ϕ_+ as the vacuum expectation value of the dual operator in the gauge theory and ϕ_- as its source.

We note that, in the gravity theory region of

$$-\frac{d^2}{4} < m^2 {R_{sph}}^2 < -\frac{d^2}{4} + 1 \tag{3.2.14}$$

we may have both of these regimes. This is demonstrated in figure 3.3.

The minimum mass condition

$$m^2 {R_{sph}}^2 \gg -\frac{d^2}{4} \tag{3.2.15}$$

is known as the Breitenlohner-Freedman bound – the system is still stable in this region since, despite the mass square being negative the total energy remains positive due to additional energy contributions from the spacetime [60], [69], [76], [77].

3.3 Temperature and Black Holes

A particularly useful system to study is that of the bulk with a black hole put in by hand. Black holes have been considered as a useful tool in gauge string duality since the very start of the development of the field [9], [13], [64]. Doing this will allow us to study finite temperature states in the gauge dual, and will allow us to find further examples of properties that are equivalent in the gauge and gravity systems –

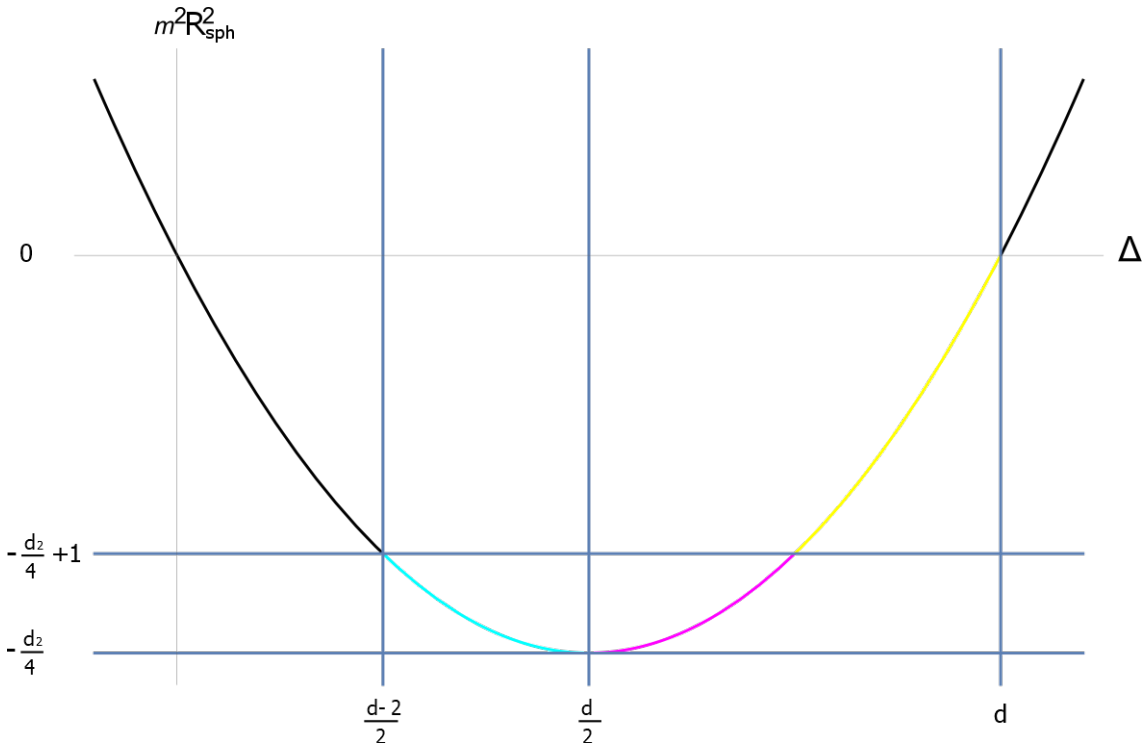

Figure 3.3: A graph of ${m^2R_{sph}}^2$ with the coloured areas showing the allowed regions. In the cyan region we have a low mass in the gravity theory and $\Delta = \Delta_-$ in the gauge theory. In the magenta region we have a low mass in the gravity theory and $\Delta = \Delta_+$ in the gauge theory. In the yellow region we have a high mass in the gravity theory and $\Delta = \Delta_+$ in the gauge theory.

giving further evidence for the correspondence. A readable review of this procedure is provided in [63].

In the gauge dual systems with black holes will correspond to some thermal states – for example a hot plasma. If we insert a black hole into $AdS_5 \times S^5$ the global metric (3.1.17) becomes the Schwarzschild-$AdS_5 \times S^5$:

$$\mathrm{d}s^2 = -g(\rho)\mathrm{d}\tau^2 + g^{-1}(r)\mathrm{d}\rho^2 + \rho^2\mathrm{d}{\Omega_3}^2 + {R_{sph}}^2\mathrm{d}{\Omega_5}^2 \tag{3.3.1}$$

where

$$g(r) = 1 + \frac{\rho^2}{{R_{sph}}^2} - \frac{{\rho_0}^2}{\rho^2} \tag{3.3.2}$$

and

$$r_0{}^2 \equiv \frac{8GM}{3\pi} = \rho_{BH}{}^2 \left(\frac{\rho_{BH}{}^2}{R_{sph}{}^2} + 1 \right) \tag{3.3.3}$$

with G being Newton's constant, M being the black hole mass, ρ_{BH} being interpreted as a measure of the black hole size and the Hawking Temperature being given by

$$T = \frac{2\rho_{BH}{}^2 + R_{sph}{}^2}{2\pi\rho_{BH}R_{sph}{}^2}. \tag{3.3.4}$$

For large M and ρ_{BH} this simplifies to

$$\mathrm{d}s^2 = \frac{\rho^2}{R_{sph}{}^2}\left(-f(\rho)\mathrm{d}\tau^2 + \mathrm{d}x_i\mathrm{d}x_j\delta^{ij}\right) + \frac{\rho^2}{R_{sph}{}^2}f^{-1}(\rho)\mathrm{d}\rho^2 + R_{sph}{}^2\mathrm{d}\Omega_5{}^2 \tag{3.3.5}$$

where

$$f(\rho) = 1 - \frac{\rho_{BH}{}^4}{\rho^4} \tag{3.3.6}$$

and we find

$$T = \frac{\rho_{BH}}{\pi R_{sph}^2}. \tag{3.3.7}$$

In this set up the entropy of the system is given by

$$s = \frac{\pi^2}{2}N^2T^3 = \frac{A}{4G}, \tag{3.3.8}$$

where A is the surface area of the black hole and G is Newton's constant.

The entropy per unit volume of the hot plasma the gauge system is roughly

$$\frac{s_{YM}}{V} \sim N^2T^3 \tag{3.3.9}$$

which is of the same order as the entropy per unit volume of the black hole system

$$\frac{s_{BH}}{V} \sim \frac{R_{sph}{}^2\rho_{BH}{}^3}{g_S{}^2R_{sph}{}^8} \sim \frac{N^2\rho_{BH}{}^3}{l^6} \sim N^2T^3 \tag{3.3.10}$$

where in the intermediate step we used (3.1.18). This suggests that this model is valid.

By looking at different types of black holes it is possible to model various interesting

quantum mechanical systems. This setup, in particular, can also elucidate interesting phenomena about black holes. The black hole Information Paradox arises from consideration of how when black holes evaporate by Hawking Radiation the information contained within the matter it had absorbed has been destroyed – something that should not be possible. However, such system of an evaporating black hole would be dual to a gauge theory with unitary operators, which do not allow for information loss. This provides interesting leads in avoiding the paradox [78]. Similar set ups have successfully modelled viscosities of quark gluon plasmas [79]–[81].

We will use a similar set-up in chapter 4 to discuss the system dual to mesons. This is because at finite temperature the supersymmetry and conformal invariance of the AdS/CFT system is lost, suggesting that this system might be useful in studying certain aspects of high temperature QCD [80].

3.4 Introducing Mesons and Aspects of QCD

There is much to suggest that a string theory of gravity should be, in some way, successful in modelling QCD. String theory was originally developed to describe hadrons – only losing favour when it was discovered that it contained non physical elements such as tachyons [10]. Later work tied strings more directly to QCD. 't Hooft showed that, for large N, $SU(N)$ theories – such as QCD with a large number of colours – begin to look like string theories [59]. In particular, the path of mesons propagating in time in this picture look like a thin dense sheet of gluons – a structure which could also be identified with a string worldsheet.

While QCD is, of course, not a CFT, clever choices of gravity dual allow us to be able to model gauge systems which are either very similar to QCD or replicate certain of its features [82]–[84]. The geometry of these spacetimes, and how they incorporate D branes, will be discussed in section 3.4.1. Section 3.4.2 will discuss how they can be used to model mesons through either probe brane fluctuations (for low spin mesons) or by using strings attached to the probe branes (for large spin mesons).

			0	1	2	3	4	5	6	7	8	9
D3/D7	N_c :	D3	•	•	•	•	-	-	-	-	-	-
	N_f :	D7	•	•	•	•	•	•	•	•	-	-
D4/D6	N_c :	D4	•	•	•	•	•	-	-	-	-	-
	N_f :	D6	•	•	•	•	-	•	•	•	-	-
D4/D8	N_c :	D4	•	•	•	•	•	-	-	-	-	-
	N_f :	D8	•	•	•	•	-	•	•	•	•	•

Figure 3.4: Table showing embedding in spacetime of different brane setups. The full black dots represent the brane fully filling that spacetime dimension. The dimension x_0 is the timelike dimension. In each case the setup consists of a stack of a large number (N_c) of branes which determine the number of colours in the system plus a smaller number (N_f) of probe branes which determine the number of flavours in the system.

3.4.1 Brane Embedding

As discussed by Karch and Katz [85], flavour may be added by considering different arrangements of D branes. A large number of 'colour' branes will warp the spacetime of the system such that fermions in the theory will begin to have mass spectra somewhat reminiscent to those seen in quantum field theories – as in the Witten $D4$ model sketched below. Flavour can be added more explicitly by including a small number of probe flavour branes. As will be discussed below, low spin mesons can be seen as fluctuations of these branes while high spin mesons can be seen as macroscopic strings connecting these branes. As the holographic dimension u determines the energy scale of the dual gauge theory, the positioning of these branes will help determine the mass of the corresponding mesons. Negative mass fluctuations are allowed as long as they are above the Breitenlohner-Freedman bound discussed in section 3.2, in which case the shape of the spacetime is sufficient to prevent instabilities. A number of different brane arrangements will be considered and their embedding in the 10 dimensional spacetime is summarised in table 3.4.

D3/D7 System

If one adds probe branes (that is branes that do not backreact and alter the geometry of the spacetime) that are seperated from the $D3$ branes by dimensions orthogonal to both of them, then strings stretched between these branes will have a mass (since mass can be thought of as the length of the string multiplied by its tension) [10]. By altering the position of the branes we alter the mass of the string states – we can therefore say that we have introduced flavour. The need for the new flavour branes to be orthogonally separated from the $D3$ branes means that they may not be $D9$ branes. The simplest system to consider is that of $D7$ probe branes. While the $D7$ branes are larger dimensional objects than the $D3$ branes we may say that they are probes since we are working in the limit of a large number N of $D3$ branes so their effects dominate.

The general Dirac-Born-Infield action for the D7 brane is given by

$$S \propto \int \mathrm{d}^8x \sqrt{-\det\left(G_{ab} + F_{ab}\right)} \tag{3.4.1}$$

where G_{ab} is the induced metric on the brane while F_{ab} is the field strength on the brane [10], [86]. However, there are more immediately useful formulations of the action. Following the example of [10] it is simplest to consider the supersymmetric theory that arises from the embedding of the $D7$ branes by rewriting the $AdS_5 \times S^5$ metric in the form

$$\mathrm{d}s^2 = \frac{r^2}{{R_{sph}}^2}\eta_{\mu\nu}x^\mu x^\nu + \frac{{R_{sph}}^2}{r^2}(\mathrm{d}\rho^2 + \rho^2\mathrm{d}{\Omega_3}^2 + \mathrm{d}{x_8}^2 + \mathrm{d}{x_9}^2) \tag{3.4.2}$$

where μ and ν run from 0 to 3 and

$$\rho^2 = {x_4}^2 + {x_5}^2 + {x_6}^2 + {x_7}^2 \qquad\qquad r^2 = \rho^2 + {x_8}^2 + {x_9}^2 \tag{3.4.3}$$

and therefore $r = u$. The action for the D7 brane is given by

$$S \propto \int \mathrm{d}^8x\rho^3 \sqrt{1 + \left(\frac{\partial x_8}{\partial \rho}\right)^2 + \left(\frac{\partial x_9}{\partial \rho}\right)^2} \tag{3.4.4}$$

giving equations of motion

$$\frac{\partial}{\partial\rho}\left(\frac{\rho^3}{\sqrt{1+\left(\frac{\partial x_8}{\partial\rho}\right)^2+\left(\frac{\partial x_9}{\partial\rho}\right)^2}}\frac{\partial x_8}{\partial\rho}\right)=0 \tag{3.4.5}$$

$$\frac{\partial}{\partial\rho}\left(\frac{\rho^3}{\sqrt{1+\left(\frac{\partial x_8}{\partial\rho}\right)^2+\left(\frac{\partial x_9}{\partial\rho}\right)^2}}\frac{\partial x_9}{\partial\rho}\right)=0. \tag{3.4.6}$$

The solution to these equations is given by constant values of x_8 and x_9, which may [87], for simplicities' sake, be chosen to be

$$x_8=0 \qquad x_9=L \tag{3.4.7}$$

where L is a constant distance between the $D3$ branes and $D7$ brane and is therefore proportional to the mass of the quarks represented by strings attached to the $D7$ brane. We may therefore think of the $D7$ probe as filling AdS_5 and wrapping around S^3. The metric on the $D7$ is given by

$$\mathrm{d}s^2=\frac{r^2}{{R_{sph}}^2}\eta_{\mu\nu}x^\mu x^\nu+\frac{{R_{sph}}^2}{r^2}+\frac{{R_{sph}}^2\rho^2}{r^2}\mathrm{d}{\Omega_3}^2. \tag{3.4.8}$$

Since $r^2=\rho^2+L^2$ we see that the radius of S^3 must fall to 0 at $\rho=0$, $r=L$. The geometry of the system is illustrated in by figure 3.5.

As will be discussed in section 3.4.2, fluctuations of the branes will be seen to represent particles. The action for these fluctuations includes a Yukawa term $\bar{\psi}_i A\psi_i$ representing interactions between the fermionic field ψ_i, often thought to represent quarks, and scalar field A. This term is the reason why we only have $U(1)_A$ symmetry rather than $U(N)_A$ symmetry in this theory. Spontaneous symmetry breaking turns this into a mass term $A_0\bar{\psi}_i\psi_i$ for the fermions, where A_0 is the vacuum expectation value of the field A.

D7 Embedding in Constable-Myers Background

A very similar model has also been shown to replicate Abelian $U(1)_A$ chiral symmetry breaking [10], [87]–[91]. In this model we consider $D7$ branes embedded in the non-

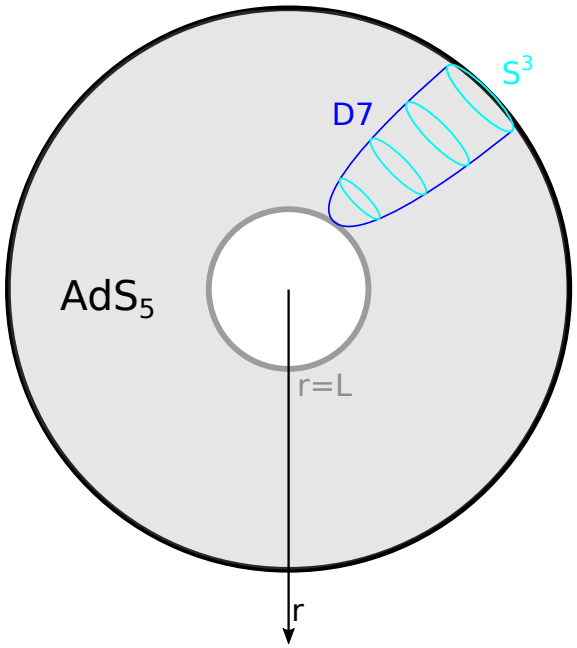

Figure 3.5: A graph of $AdS_5 \times S^5$ showing the embedding of a $D7$ brane (in blue). AdS_5 is shown in blue and S^3 is shown at 4 different radii r in cyan. Based on figures in [10] and [87].

supersymmetric Constable-Myers background [92].

$$\mathrm{d}s^2 = H(r)^{-\frac{1}{2}} \left(\frac{r^4+b^4}{r^4-b^4}\right)^{\frac{\delta}{4}} \sum_{i=0}^{3} \mathrm{d}x_i \mathrm{d}x^i + H(r)^{\frac{1}{2}} \left(\frac{r^4+b^4}{r^4-b^4}\right)^{\frac{2-\delta}{4}} \frac{r^4-b^4}{r^4} \sum_{j=4}^{9} \mathrm{d}x_j \mathrm{d}x^j \tag{3.4.9}$$

where the deformation of the spacetime is due to a dilaton

$$e^{2\phi} = e^{2\phi_0} \left(\frac{r^4+b^4}{r^4-b^4}\right)^{\Delta} \tag{3.4.10}$$

where

$$H(r) = \left(\frac{r^4+b^4}{r^4-b^4}\right)^{\delta} - 1 \qquad \delta = \frac{{R_{sph}}^4}{2b^4} \qquad \Delta^2 + \delta^2 = 10 \tag{3.4.11}$$

and b and ϕ_0 are constants.

Even without the $D7$ embedding we may observe confinement by considering the Nambu-Goto action for a string embedded in this background [92], which may be considered to represent a quark-antiquark pair with separation d, we find a linear

potential

$$V(d) = \frac{C^{\frac{\delta-|\Delta|}{4\delta}}}{2\pi\alpha'\sqrt{1-C}}d \tag{3.4.12}$$

where

$$C = \frac{|\Delta| - \delta}{|\Delta| + \delta}. \tag{3.4.13}$$

The linear potential indicates confinement. This is because it means that the energy in the field between the pair increases as they get further apart, meaning that eventually a point will be reached when it is energetically more favourable to form a new pair.

Returning to the case of the $D7$ embedding [10], [87]–[91], we find the action of the brane to be

$$S = -\frac{2\lambda N}{(2\pi)^4}\int \mathrm{d}\rho\, e^{\phi}\mathcal{G}(\rho, x_8, x_9)\sqrt{1 + g^{ab}g_{88}\partial_a x_8\partial_b x_8 + g^{ab}g_{99}\partial_a x_9\partial_b x_9} \tag{3.4.14}$$

where λ is a constant, g refers to the Constable-Myers metric and

$$\mathcal{G}(\rho, x_8, x_9) = \rho^3\frac{\Big((\rho^2 + {x_8}^2 + {x_9}^2) + b^4\Big)\Big((\rho^2 + {x_8}^2 + {x_9}^2) - b^4\Big)}{(\rho^2 + {x_8}^2 + {x_9}^2)^4}. \tag{3.4.15}$$

Then, if we choose $x_8 = 0$ we find the equation of motion

$$\frac{\mathrm{d}}{\mathrm{d}\rho}\left(\frac{e^{\phi}\mathcal{G}(\rho, x_9)}{\sqrt{1 + (\partial_\rho x_9)^2}}\partial_\rho x_6\right) - \sqrt{1 + (\partial_\rho x_9)^2}\frac{\mathrm{d}}{\mathrm{d}x_9}\Big(e^{\phi}\mathcal{G}(\rho, x_9)\Big) = 0 \tag{3.4.16}$$

We can find numerical solutions of this equation such that

$$x_9 \sim m + \frac{c}{\rho^2} \tag{3.4.17}$$

where $c \equiv \langle\psi\bar{\psi}\rangle$, the vacuum expectation value of a quark condensate, and m is the equivalent quark mass. Since solutions exist where c is non-zero (as $m \to \infty$) the $U(1)_A$ symmetry that normally rotates between x_8 an x_9 is broken. This symmetry may be identified with the axial symmetry of the gauge dual by matching symmetries. After the symmetry is broken an attempt to rotate between x_8 and x_9 by a small amount results in normalisable fluctuations $x_5 = f(\rho)\sin(k_\mu x^\mu)$ where f is a function,

μ runs between 0 and 3 and $k^2 = -M^2$. M is the mass of the particle associated with the fluctuations, which may be considered a meson. When m tends to zero so does M so the meson may be identified with the Goldstone boson for the symmetry breaking. By following the same procedure for fluctuations in the x_9 direction, we find a spectrum of mesons with a mass gap [93].

However, non-Abelian chiral symmetry breaking, that is the breaking of a $U(N)_L \times U(N)_R$ symmetry that is not present this model, requires the Sakai Sugimoto model, which will be discussed in chapter 4.

Witten's D4 system

An early model – but one which leads directly to the more recent Kruczenski-Mateos-Myers-Winters $D4/D6$ and Sakai-Sugimoto $D4/D8$ models, was put forward by Witten [13]. Witten began by considering $M5$ branes giving a supergravity solution on $AdS_7 \times S^4$ and then compactifing two directions to give a superstring theory with a $D4$ brane background – this was found to be dual to four dimensional $SU(N)$ super Yang-Mills. By taking $N \to \infty$ the size of one of the compactified dimensions shrinks to zero and one is left. Therefore the background metric is given by

$$\mathrm{d}s^2 = \frac{u^{\frac{3}{2}}}{{R_{D4}}^{\frac{3}{2}}}\left(\eta^{\mu\nu}\mathrm{d}x_\nu\mathrm{d}x_\nu + f(u)\mathrm{d}{x_4}^2\right) + \frac{{R_{D4}}^{\frac{3}{2}}}{u^{\frac{3}{2}}}\left(f^{-1}(u)\mathrm{d}u^2 + u^2\mathrm{d}{\Omega_4}^2\right) \tag{3.4.18}$$

where μ and ν run over $0, 1, 2, 3$; x_4 is the remaining compactified periodic dimension around which the $D4$ branes are wrapped; $\mathrm{d}\Omega_4$ is a line element for an S^4 sphere, R_{D4} is the radius of said S^4 sphere which can further be defined in terms of the string length ${l_s}^2 = \alpha'$, string coupling g_s and number of colours N_C as

$${R_{D4}}^3 = \pi g_s N_C {l_S}^3, \tag{3.4.19}$$

and

$$f(u) = 1 - \frac{{u_\Lambda}^3}{u^3}. \tag{3.4.20}$$

The theory also features a dilaton

$$e^{\phi} = g_s \left(\frac{u}{R_{D4}} \right)^{\frac{3}{4}} \tag{3.4.21}$$

where g_s is the string coupling. Initially, this theory is supersymmetric (as in the previous model that was discussed). However, in addition to compactifying the $D4$ branes, one can impose anti-periodic boundary conditions on all the fermions in the theory, which breaks the supersymmetry.

The period of x_4 is required to be

$$\delta x_4 = \frac{4\pi}{3} \sqrt{\frac{{R_{D4}}^3}{u_\Lambda}}. \tag{3.4.22}$$

The size of the x_4 circle increases with u, from a size of 0 at u_Λ, which is sometimes referred to as an IR wall (the periodicity given above may be thought of as being an angular distance). This gives a shape that is often referred to as a 'cigar', which is illustrated in figure 3.6. The geometry model may be modified by adding $D6$ flavour branes, as shown in figure 3.7. It may also be modified, as done by Sakai and Sugimoto, by adding $D8$ flavour branes – this is illustrated, for the case of different temperatures, in figure 4.1, and for the specific case of the worldline instanton approach, in figure 5.1.

When the scale of the fields exceeds that of the size of the compactified dimension, which may also be though of as masses exceeding the Kaluza Klein mass,

$$m_{KK} = \frac{2\pi}{\delta x_4} = \frac{3}{2} \sqrt{\frac{u_\Lambda}{{R_{D4}}^3}} \tag{3.4.23}$$

the dual theory becomes five dimensional SU(N) Yang-Mills.

This original Witten model may be used to consider quarks and mesons by using Wilson loops, in the same way as will be discussed in section 3.5.1. We can see confinement appear by how the expectation value of the Wilson loops falls exponentially with their area – meaning large loops, representing systems with quarks far away from each other, are suppressed.

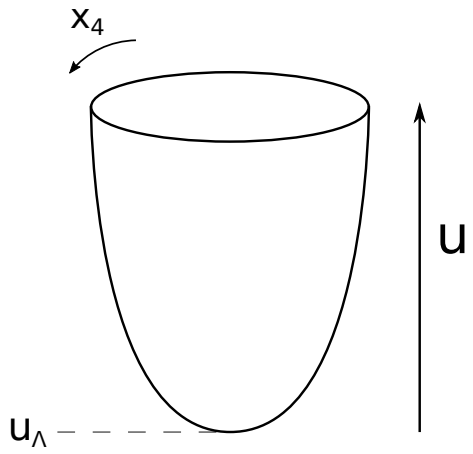

Figure 3.6: A graph showing the change of the shape of the x_4 circle with u.

The theory also exhibits a mass gap and a discrete mass spectrum. This arises from the requirement on any field to end smoothly at the wall at u_Λ in the radial u direction, and to fall off to zero at infinity. Only a discrete set of fields with $m > 0$ fulfils these conditions. Brower, Mathur and Tan [94] calculated a glueball spectrum for this theory that showed reasonable agreement with lattice QCD results.

D4/D6 System

Kruczenski, Mateos, Myers, and Winters [11] expanded on the work of Witten by introducing flavour through the introduction of $D6$ branes. Strings stretching between the $D4$ and $D6$ branes lead to N_f hypermultiplets containing two fermions and two scalars, which all get mass from the chiral symmetry breaking. It is the appearance of these particles naturally in the theory that makes it particularly attractive. The spectra of some of these will be explored in the next section.

The $D6$ branes fill all dimensions apart from x_4, x_8 and x_9 and the $D4$ and $D6$ branes may be seperated in the x_8 and x_9 dimensions. We introduce new polar coordinates for the space spanned by x_5 to x_9 such that

$$u = \left(\rho^{\frac{3}{2}} + \frac{{u_\Lambda}^{\frac{3}{2}}}{4\rho^{\frac{3}{2}}}\right)^{\frac{2}{3}}$$

$$r^2 = {x_8}^2 + {x_9}^2$$

$$\begin{aligned}\tan(\phi) =& \frac{x_8}{x_9} \\ \lambda^2 =& {x_5}^2 + {x_6}^2 + {x_7}^2\end{aligned} \tag{3.4.24}$$

and Ω_2 is the solid angle associate with spherical polar coordinates in x_5, x_6 and x_7.

We therefore find the metric to be

$$\mathrm{d}s^2 = \frac{u^{\frac{3}{2}}}{{R_{D4}}^{\frac{3}{2}}}\left(\eta^{\mu\nu}\mathrm{d}x_\nu\mathrm{d}x_\nu + f(u)\mathrm{d}{x_4}^2\right) + K(\rho)(\mathrm{d}\lambda^2 + \lambda^2 + \mathrm{d}{\Omega_2}^2 + \mathrm{d}r + r^2\mathrm{d}\phi^2) \tag{3.4.25}$$

such that

$$K(\rho) \equiv \frac{{R_{D4}}^{\frac{3}{2}}u}{\rho^2}. \tag{3.4.26}$$

If we specify that the position of the $D6$ brane must satisfy

$$r = r(\lambda) \qquad\qquad \phi = \phi_0 \tag{3.4.27}$$

we find the metric g on the $D6$ brane as

$$\mathrm{d}{s_g}^2 = \eta^{\mu\nu}\mathrm{d}x_\nu\mathrm{d}x_\nu + K(\rho)\left(\left(1 + \left(\frac{\mathrm{d}r}{\mathrm{d}\lambda}\right)^2\right)\mathrm{d}\lambda^2 + \lambda^2\mathrm{d}{\Omega_2}^2\right). \tag{3.4.28}$$

We therefore get the action

$$S_{D6} = -\frac{1}{(2\pi)^6{l_S}^7}\int \mathrm{d}^7x e^{-\phi}\sqrt{-\det g} \tag{3.4.29}$$

which gives the equation of motion

$$\frac{\mathrm{d}}{\mathrm{d}\lambda}\left(\left(1 + \frac{{u_\Lambda}^3}{4\rho^3}\right)^2\lambda^2\frac{\left(\frac{\mathrm{d}r}{\mathrm{d}\lambda}\right)^2}{\sqrt{1 + \left(\frac{\mathrm{d}r}{\mathrm{d}\lambda}\right)^2}}\right) = -\frac{3}{2}\frac{{u_\Lambda}^3}{\rho^5}\left(1 + \frac{{u_\Lambda}^3}{4\rho^3}\right)\lambda^2 r\sqrt{1 + \left(\frac{\mathrm{d}r}{\mathrm{d}\lambda}\right)^2}. \tag{3.4.30}$$

In the limit of large λ this gives the solution

$$r(\lambda) = \frac{2^{\frac{1}{2}}3^{-\frac{1}{3}}{u_\Lambda}^2}{\lambda^2}\left(aJ_{-\frac{1}{3}} + bJ_{\frac{1}{3}}\right) \tag{3.4.31}$$

where $J_{-\frac{1}{3}}$ and $J_{\frac{1}{3}}$ are Bessel functions and a and b are constants.

A major problem faced by this model in simulating QCD is that it lacks chiral

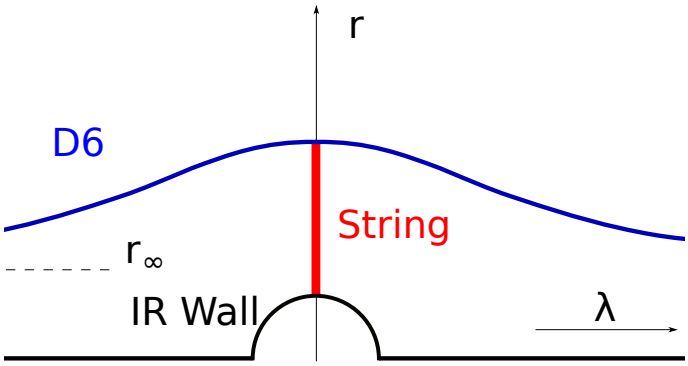

Figure 3.7: A graph showing a string (in red) hanging off a $D6$ brane in a $D4/D6$ system. Based on diagram from [58].

fermions [95] due to the lack of non-Abelian chiral symmetry breaking – as in the case of the $D7$ model in the Constable-Myers background, this model only exhibits Abelian chiral symmetry breaking. As mentioned previously, a similar $D4/D8$ system, the Sakai Sugimoto model, overcomes this problem and will be used in our modelling of mesons. It achieves this since it has both $D8$ and $\bar{D}8$ branes, meaning we have a $U(N)_L \times U(N)_R$ symmetry before breaking. This theory is described in chapter 4. The techniques explored in chapter 4 will then, in chapter 5, be used to calculate the action of the decay of mesons in the $D4/D8$ Sakai-Sugimoto model using the worldline instanton method.

3.4.2 Mesons from Flavour Branes

Including probe flavour branes – which are called 'probe' branes since they do not deform the spacetime, and 'flavour' branes since their position determines the flavour of the particles in the theory – can explicitly add mesons to the model being studied.

In the case of low spin, we can model a meson as a fluctuation of the probe brane. However, above spin 2, this is no longer possible [96] so we must instead consider a macroscopic open string with its two endpoints attached to probe branes – this will be the main focus of this work.

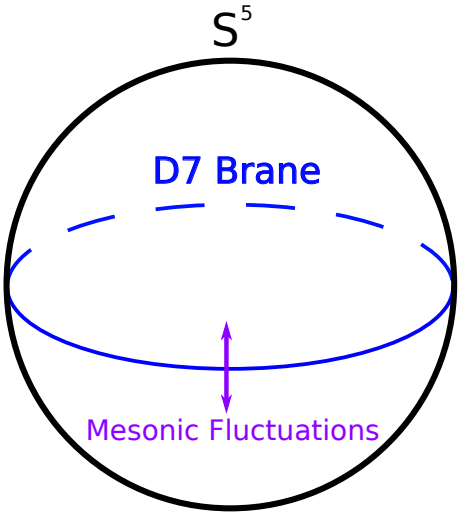

Figure 3.8: An alternative picture of the setup presented in figure 3.5. The mesons are represented as fluctuations of the $D7$ brane along the S^5 sphere. Based on a diagram from [10].

Low Spin Mesons – Probe Brane Fluctuations

The first, probe brane fluctuation, picture showed promise in the $D3/D7$ model described in section 3.4.1. In this picture, we consider scalar mesons to be fluctuations of the $D7$ probe brane in directions perpendicular to it along the S^5 sphere [10], [97] – this is illustrated in figure 3.8. As reviewed by Erdmenger et al. [10], in this situation the Lagrangian for the fluctuations Φ is given by

$$\mathcal{L} \propto \sqrt{-\det\, g}\left(1+\frac{1}{2}\frac{R_{sph}^2}{r^2}g^{ab}\partial\Phi_a\partial\Phi_b\right) \tag{3.4.32}$$

where g is the $AdS_5 \times S^5$ metric and the other symbols are as defined in section 3.4.1. This gives the equation of motion

$$\frac{R_{sph}^4}{(\rho^2+L^2)^2}\partial^\mu\partial_\mu\Phi+\frac{1}{\rho^3}\partial_\rho\left(\rho^3\partial_\rho\Phi\right)+\frac{1}{\rho^2}\nabla^i\nabla_i\Phi=0 \tag{3.4.33}$$

where the radial coordinate has been shifted such that $r^2 \equiv \rho^2 + L^2$. The trial solution suggested by Erdmenger et al. [10]

$$\Phi = \phi(\rho)e^{ik\cdot x}\mathcal{Y}^l\left(S^3\right), \tag{3.4.34}$$

$$\nabla^i\nabla_i\mathcal{Y}^l = -l(l+2)\mathcal{Y}^l, \tag{3.4.35}$$

is found to work only for certain values of k. Noting that the square of the meson mass is given by

$$M^2 = -k^2 \tag{3.4.36}$$

we find the mass spectrum of the scalar mesonic fluctuations to be given by

$$M = \frac{2L}{R^2_{sph}}\sqrt{(n+l+1)(n+l+2)} \qquad n,\, l \in \mathbb{Z}. \tag{3.4.37}$$

Vector mesons can also be found. Considering spin one half fluctuations using the same method gives the mass spectrum of the supersymmetric, fermionic partners of the mesons – often referred to as the mesions. The fluctuations form $\mathcal{N} = 2$ supersymmetry supermultiplets with $16(l+1)$ states, half bosonic and half fermionic. By comparing quantum numbers, these fluctuations can be shown to match operators, and therefore particles, in the gauge dual. Detailed tables of the quantum numbers are presented by Erdmenger et al [10]. The interaction of these mesons can be described by the term [10], [98], [99]

$$S_{int} \sim \int \mathrm{d}^8x\sqrt{-g}g^{\alpha\beta}g^{\mu\nu}f^{abc}A^a_\mu A^b_\alpha \partial A^c_\beta \tag{3.4.38}$$

where the fields A describe the mesons and f^{abc} are constants.

We may consider similar fluctuations for the $D4/D6$ system, again as described in section 3.4.1. Using the coordinate system detailed in (3.4.24) we consider, following the example of Kruczenski et al [11] the following fluctuations around the vacuum:

$$\phi = 0 + \delta\phi \qquad\qquad r = r_{vac}(\lambda) + \delta r. \tag{3.4.39}$$

That is, we say that the vacuum for ϕ is 0 and the vacuum for r is the function $r_{vac}(\lambda)$. Varying the action results in complicated expressions but one can, in analogy to (3.4.34), come up with the following solutions

$$\begin{aligned}\delta\phi &= \mathcal{P}(\lambda)e^{ik_\phi\cdot x}\mathcal{Y}_{l_\phi m_\phi}\left(S^2\right)\\ \delta r &= \mathcal{R}(\lambda)e^{ik_r\cdot x}\mathcal{Y}_{l_\phi m_\phi}\left(S^2\right)\end{aligned} \tag{3.4.40}$$

and therefore, in analogy to (3.4.36), the mass is given by

$$M_{\phi,r}^2 = -k_{\phi,r}^2. \tag{3.4.41}$$

Again following the example of Kruczenski et al [11] we see that it is simplest to find the mass in the special asymptotic case of $\lambda \to \infty$ in which we may write $r_{vac} \sim r_\infty + \frac{c}{\lambda}$ where r_∞ and c are constants. The constant r_∞ is proportional to the bare quark mass in the system, as it determines the distance between the $D4$ and $D6$ branes.

We then find the equations of motion

$$\begin{aligned} \frac{9M_\phi^2}{4M_{KK}^2}\frac{r_{vac}^2}{\lambda}(\delta\phi) + \partial_\lambda\left(\lambda^2 r_{vac}^2 \partial_\lambda(\delta\phi)\right) &= 0 \\ \frac{9M_r^2}{4M_{KK}^2}\frac{1}{\lambda}(\delta r) + \partial_\lambda\left(\lambda^2 \partial_\lambda(\delta r)\right) &= 0 \end{aligned} \tag{3.4.42}$$

where $M_{KK} \equiv \frac{3}{2}\sqrt{\frac{u_\Lambda}{R_{D4}^3}}$ is the Kaluza-Klein mass, effectively an upper limit of the mass of the system. By considering different values of r_∞ we can find the solutions for the lowest mass modes of δr and $\delta\sigma$ such that

$$\mathbf{r_\infty = 0}: \qquad \delta\phi = 1 \to M_\phi = 0 \qquad \delta r = \frac{1}{\lambda} \to M_r = 0 \tag{3.4.43}$$

$$\mathbf{r_\infty \neq 0}: \qquad \delta\phi = \frac{1}{\lambda} \to M_\phi \neq 0 \qquad \delta r = \frac{1}{\lambda} \to M_r = 0 \tag{3.4.44}$$

We therefore see that the zero mass ϕ direction fluctuation may be considered to be a Goldstone boson related to the chiral symmetry breaking, as in the example of $D7$ branes in the Constable-Myers background. The remaining modes may be calculated numerically. One finds that, for larger r_∞, and therefore larger distance between the $D4$ and $D6$ branes and larger bare quark masses, the meson masses become degenerate. This is because the different masses are caused by the shape of the $D6$ branes being distorted by the $D4$ branes. However, the further the $D6$ and $D4$ branes are from each other, the less this matters.

The probe brane fluctuation method for the Sakai-Sugimoto model will be briefly discussed in section 4.3.

High Spin Mesons – Strings

In the second, high spin, picture two 'vertical' sections of the string, which may roughly be thought of as the constituent quarks of the meson, have endpoints attached to a 'flavour brane' and a bulk extending down to an 'infra-red wall'. The mass of the constituent quarks will be proportional to the the distance between the flavour brane and the IR wall. For the meson to decay, the string will have to fluctuate from the IR wall to the flavour brane and then split – the probability of meson decay is therefore the probability of this happening. This is demonstrated in figure 3.9.

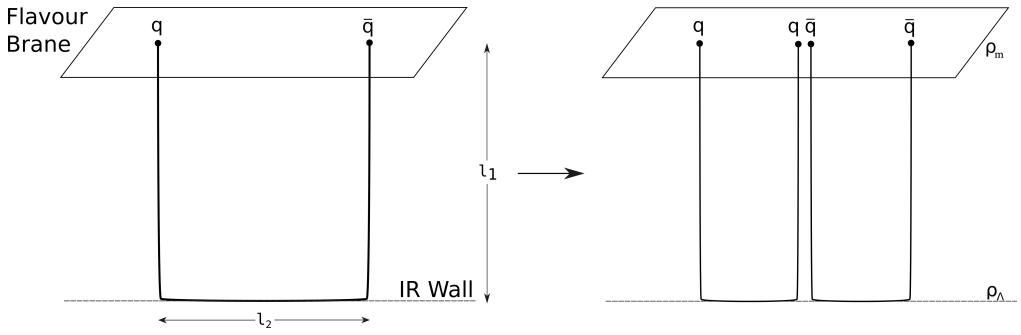

Figure 3.9: Modelling meson decay using strings. The length l_1 is proportional to the mass of the constituent quarks while the length l_2 is proportional to the energy of the flux tube connecting the quarks.

As shown in the figure the string profile may, to a large degree of accuracy, be described as three straight segments joined together – two of them vertical and one of them horizontal. One may model mesons consisting of quarks of different masses by including more than one flavour brane and having each endpoint attached to a different one.

As discussed, the most successful dual geometry to QCD, and therefore the most promising for modelling mesons, is Sakai-Sugimoto. However, the calculations for large spin mesons are similar in all geometries [12], it is instructive to consider a different model first.

A particularly interesting example is the that of the $D4/D6$ system described in the previous section [12], [96], [100]. Mesons are modelled in the exact same way

as depicted in figure 3.9, with the $D6$ brane acting as the flavour brane. Using the notation presented in equation 3.4.25 we find we may immediately place a condition on the motion of the string by requiring that, as it rotates, the 'vertical' segments have same linear velocity as the outermost parts of the 'horizontal' parts of the string. Therefore, following the example of Peeters, Zamaklar and Sonnenschein [12], we find

$$1 - \omega^2 {l_2}^2 = \omega^2 l_2 \frac{m}{T_{ef}} \tag{3.4.45}$$

where the left hand side relates to the horizontal segment of the string, the right hand side the vertical segments, ω is the angular velocity,

$$m = \frac{1}{2\pi\alpha'} \int_{\rho_\Lambda}^{\rho_m} \sqrt{g_{00} g_{\rho\rho}} \tag{3.4.46}$$

is the quark mass and

$$T_{ef} = \frac{1}{2\pi\alpha'} \sqrt{g_{00} g_{xx}}|_{\rho=\rho_\Lambda} \tag{3.4.47}$$

is the effective tension of the string. We will see mass and tension calculated in the same way for Wilson loops in section 3.5.1.

We can consider the energy E and angular momentum J of the two parts of the string. For the horizontal section we find

$$E_H = T_{ef} \frac{2}{\omega} \arcsin(\omega l_2) \qquad J_H = T_{ef} \frac{1}{\omega^2} \left(\arcsin(\omega l_2) - \omega l_2 \sqrt{1 - \omega^2 {l_2}^2} \right) \tag{3.4.48}$$

and for the vertical section we find

$$E_V = \frac{2m}{\sqrt{1 - \omega^2 {l_2}^2}} \qquad J_V = \frac{2m\omega {l_2}^2}{\sqrt{1 - \omega^2 {l_2}^2}}. \tag{3.4.49}$$

If we compare the total energy and total momentum we find two different results depending on the circumstances. If the quark mass is low (compared to the energy

in the colour flux tube – that is $m_q \ll T_{ef} l_2$) we find

$$E_T = \pi T_{ef} l_2 \qquad J = \frac{\pi}{2} T_{ef} {l_2}^2. \tag{3.4.50}$$

Combining them leads to the well known Regge relationship between angular momentum and energy (though it could also be reformulated to involve mass):

$$J_T = \frac{1}{2\pi T_{ef}} {E_T}^2 \tag{3.4.51}$$

which indicates that this can replicate physical phenomena. For $m_q \gg T_{ef} l_2$ the quantities T and E tend towards infinity as it takes a lot more angular momentum and energy to get moving.

Peeters, Zamaklar and Sonnenschein [58] considered meson decay in this framework by considering quantum fluctuations of the string. One can define a quantity

$$\mathcal{P}_{\text{split}} \equiv \frac{1}{T} \frac{\Gamma_{\text{open}}}{L} \tag{3.4.52}$$

where T is the tension of the string, L is the length of the horizontal section of the string along the IR wall and Γ_{open} is the decay width of a string which has different form for different situations but which had previously been calculated for an open string in four dimensions with large N as [101]–[103] as

$$\Gamma_{\text{open}} \approx \frac{1}{E_{\text{ext}}} \frac{0.448 g^2}{16\pi} \tag{3.4.53}$$

where E_{ext} is the energy of the external states and g is a coefficient related to the tachyon vertex operator. Then the total decay width for the string can then be approximated by

$$\Gamma = T\, \mathcal{P}_{\text{split}}\, L\, \kappa_{\text{max}}\, \mathcal{P}_{\text{fluc}} \tag{3.4.54}$$

where κ_{max} is a measure of the maximum proportion of the string intersecting the flavour brane and $\mathcal{P}_{\text{flux}}$ is the probability of the quantum fluctuation, which is to be calculated.

Using the coordinate transform

$$\eta^2 = \frac{u - u_\Lambda}{u_\Lambda} \tag{3.4.55}$$

$$\zeta = \sqrt{\frac{4}{3}} u_\Lambda^{-\frac{1}{2}} R_{D4}^{\frac{3}{2}} \eta \tag{3.4.56}$$

and assuming that we are working close to the IR wall where the spacetime can be approximated to be flat, we may assume the metric to reduce to

$$\mathrm{d}s^2 \sim \left(\frac{u_\Lambda}{R}\right)^{\frac{3}{2}} \left(\mathrm{d}x^\mu \mathrm{d}x_\mu + \mathrm{d}z^2\right) + \sqrt{R_{D4}^3 u_\Lambda}\ \mathrm{d}\Omega_4^2. \tag{3.4.57}$$

Furthermore, assuming that the string, with worldsheet parametrised by τ and σ is rigid and rotating, that is

$$T = L\tau \qquad x_1 = L\sin\tau\ \sin(\sigma) \qquad x_1 = L\cos\tau\ \sin(\sigma) \tag{3.4.58}$$

the action of the fluctuations becomes

$$S_{\text{flux}} = \frac{L}{2\pi\alpha'} \int \mathrm{d}T \mathrm{d}\sigma \left(-(\partial_T \zeta)^2 + \frac{1}{L^2}(\partial_\sigma \zeta)^2\right) \tag{3.4.59}$$

which can be solved to give modes

$$\Phi(\zeta_n) = \left(\frac{n}{\pi\alpha'}\right)^{\frac{1}{4}} \exp\left(-\frac{n}{2\alpha'}\zeta_n^2\right). \tag{3.4.60}$$

Integrating over all such modes where the maximum fluctuation does not reach the position of the flavour brane ζ_B – that is, integrating over all the modes where the string does not cross or touch the flavour brane – and subtracting this from 1 results in the lower bound for the probability of fluctuating up to the flavour brane (this is only the lower bound since some individual modes may add up with others to reach the brane) which is

$$\mathcal{P}_{\text{fluc}}^{\min} \approx \exp\left(-1.3\frac{\zeta_B^2}{\alpha'}\right) \tag{3.4.61}$$

An alternative method attempted by Peeters, Zamaklar and Sonnenschein [58], in

which the string is discretised, gives

$$\mathcal{P}_{\text{fluc}} \approx \exp\left(-1.0\frac{\zeta_B^2}{\alpha'}\right). \tag{3.4.62}$$

Noting that ζ_B is related to the mass of the constituent quarks of the meson, we see that these results agree qualitatively with the CNN calculation as discussed in section 2.4.

A somewhat different approach will be taken in the main body of the work, considering meson decay using the worldline instanton approach with Wilson loops. The worldline instanton method was introduced in section 2.6 while Wilson loops more specifically will be introduced in the next section.

3.5 Wilson Loops

3.5.1 Theory of Wilson Loops

Wilson initially introduced his eponymous loops as a means to investigate quark confinment [3]. Wilson loops can be thought of as the phase factors of a gauge theory evaluated along a closed loop in Euclidean spacetime – which can, for example, represent the path taken by a quark-antiquark pair – that is, a meson. The operator for such loops is given by

$$\langle W \rangle = e^{ig \oint A_\mu \mathrm{d}x^\mu} \sim e^{ic\mathbb{A}} \tag{3.5.1}$$

where A_μ is the quark field, g is the coupling, c is a constant and A is the area of the loop. Therefore large loops have a larger imaginary factor in the exponential and are therefore suppressed (since we may think of (3.5.1) as weighting factors for a path integral [3], and a large imaginary exponential corresponds to high frequency oscillations which cancel out in the path integral) – potentially offering one explanation for confinement.

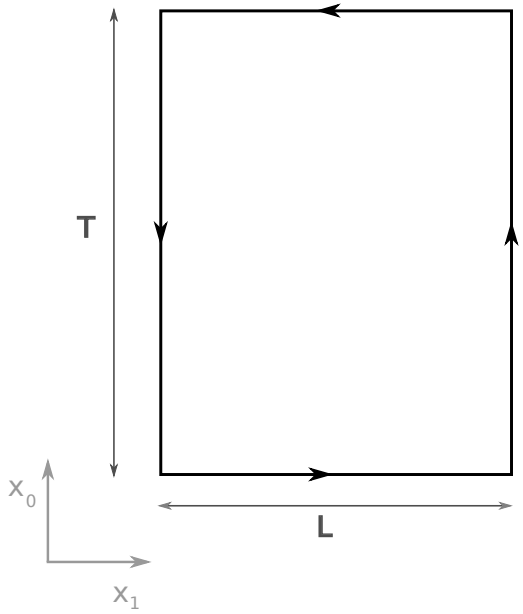

Figure 3.10: A rectangular Wilson loop, based on diagram in [105].

In the holographic picture, we may calculate these operators by evaluating the area of a macroscopic string worldsheet which streaches into the bulk direction u and whose boundary is the Wilson loop in the gauge theory [104]–[107]. It is often simplest to consider a rectangular loop, as depicted in figure 3.10.

In this picture we may also think of the quarks as W bosons of mass m. They gain a mass m by the $U(N+1) \to U(N) \times U(1)$ symmetry breaking of the Higgs field. This leads to the operator

$$\langle W \rangle \sim e^{-S-lm} \tag{3.5.2}$$

where S is the action of the system, $l = 2T + 2L$ and the second term in the exponent is required to remove infinities arising from the mass of the W bosons.

We may then look at the action and the mass in this system more closely – allowing us to see more explicitly how confinement arises from the potential of the system. Kinar et al [104] calculate the action for said string in a generic background as

$$S = T \int \mathrm{d}x \sqrt{f^2(u) + g^2(u)(u')^2} \tag{3.5.3}$$

where $x \equiv X_1$ and

$$f^2(u) = g_{00}\Big(u(x)\Big)g_{xx}\Big(u(x)\Big)$$
$$g^2(u) = g_{00}\Big(u(x)\Big)g_{uu}\Big(u(x)\Big) \tag{3.5.4}$$

If the horizon is located at u_m and the loop stretches down to u_B then, similar to the mass calculation we saw in previous sections,

$$m = \int_0^{u_m} g(u)\mathrm{d}u \tag{3.5.5}$$

and also

$$L = \int \mathrm{d}x = 2\int_{u_B}^{u_m} \mathrm{d}u \ \frac{g(u)}{f(u)}\frac{f(u_B)}{\sqrt{f^2(u) - f^2(u_B)}}, \tag{3.5.6}$$

where the latter direction is taken by integrating in the x direction along the string that results from the equations of motion

$$\frac{\mathrm{d}x}{\mathrm{d}u} = \frac{g(u)}{f(u)}\frac{f(u_B)}{\sqrt{f^2(u) - f^2(u_B)}}. \tag{3.5.7}$$

Then, putting everything together, the potential of the system is

$$V = \int \mathrm{d}\, x\mathcal{L} - 2m \tag{3.5.8}$$
$$= f(u_B)L - 2K(u_B) \tag{3.5.9}$$

where in (3.5.8) we subtract the quark mass to regulate singluarities as before (getting rid of the integral over $g(u)$ in the region between u_B and u_m), and then $K(u_B)$ is a constant defined by Kinar et al [104] as

$$K(u_B) \equiv \int_{u_B}^{u_m} \mathrm{d}u \ \frac{g(u)}{f(u)}\left(f(u) - \sqrt{f^2(u) - f^2(u_B)}\right) + \int_0^{u_B} \mathrm{d}u \ g(u). \tag{3.5.10}$$

We want the potential along the bottom of the loop, which represents the colour field, to be linear for the theory to be confining. This is, as before, because the energy in the field between the pair increases as they get further apart, eventually to the point where it is favourable to form a new pair. Therefore, the theory is confining

if $f(u_B) \neq 0$. By dimensional analysis we see that, in this case, $f(u_B)$ is the string tension.

The original holographic Wilson loop calculation was done by Maldacena in $AdS_5 \times S^5$ [105]. In this geometry, if $u_m = \infty$ and the two string endpoints are at $x = \pm\frac{L}{2}$ we may solve the equations of motion related to the action (3.5.6) to give,

$$x = \frac{R^2}{u_B} \int_1^{\frac{u}{u_B}} \mathrm{d}U \; \frac{1}{U^2\sqrt{U^4 - 1}}. \tag{3.5.11}$$

We know the shape of the Wilson loop at the boundary, that is that at $u = \infty$ we have $x = \frac{L}{2}$, so, by plugging this into equation (3.5.11), we find

$$u_B = \frac{2\sqrt{2}\pi^{\frac{3}{2}}}{\Gamma(\frac{1}{4})^2}\frac{R^2}{L}. \tag{3.5.12}$$

This gives a potential of

$$E = -\frac{4\pi^2\sqrt{2N}g}{\Gamma(\frac{1}{4})^4 L}. \tag{3.5.13}$$

with the factor of $\frac{1}{L}$ being a result of the theory being conformal. However, Wilson loops can also be used in non-conformal backgrounds. For example, Dp branes in a model with 16 supersymmetries [108] can break the conformal symmetry and result in a potential of the order $E \sim L^{\frac{-2}{5-p}}$.

In the finite temperature case the calculations are broadly similar however, as was discussed briefly in section 3.3, there is now a wall – a lower bound u_Λ on the value of the u. The larger the separation between the quarks, the lower down the bottom of the loop reaches, therefore there is a critical separation L_c above which this calculation no longer applies. Above this critical value it is energetically more favourable for two lines to streak vertically down to the wall, rather than form a joined-up loop. The cross sections of the system in these two regimes is shown in figure 3.11.

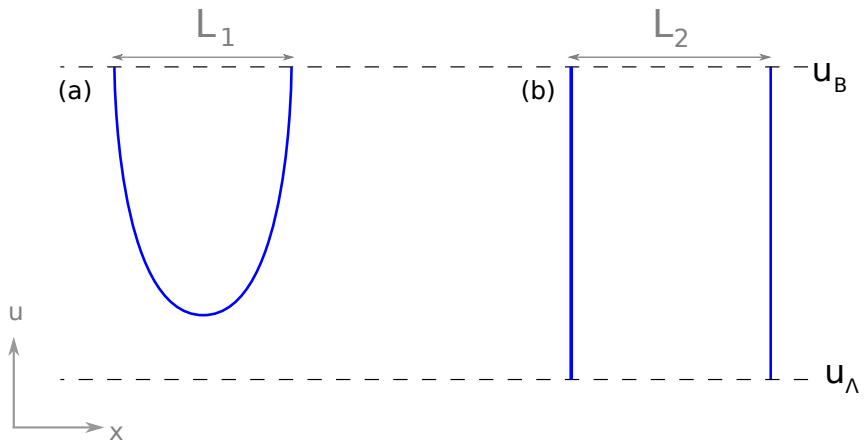

Figure 3.11: Rough sketches of the system represting the a quark-antiquark pair in the case (a) of zero temperature and finite temperature where $L_1 < L_C$ and (b) of finite temperature where $L_2 > L_C$. Based on a figure in [106].

3.5.2 Circular Wilson Loops

Due to the additional symmetry, it is often more useful to consider circular Wilson loops. This is a very specific geometry, corresponding in the Lorentzian frame to two quarks accelerating away from each other, but it will be shown in later chapters to be sufficient to model meson decay. The techniques for calculating the shapes of these loops in AdS will be introduced here before similar techniques are used for more complicated backgrounds in future chapters. The form of the AdS_5 metric that is easiest to use for calculations may be given by:

$$\mathrm{d}s^2_{AdS} = \frac{R^2}{z^2}\left(\mathrm{d}z^2 + \mathrm{d}t^2 + \mathrm{d}r^2 + r^2\mathrm{d}\theta^2 + r^2\sin^2\theta\mathrm{d}\phi^2\right) \tag{3.5.14}$$

where R is the curvature of the spacetime and z is the inverse of the radial AdS direction such that $z \equiv \frac{1}{\rho} \equiv \frac{1}{u\alpha'}$. We have Wick rotated the time coordinate, as discussed in section 2.6.

We wish to study a similar problem to the one described by Zarembo [109] and more recently Armoni et al [110] – that of a string hanging down in the AdS bulk from two endpoints which move along concentric circles with radii a and b ($a > b$) on the plane $z = 0$, with calculations using the cut-off $z = z_\Lambda$ to avoid the coordinate

singularity at $z = 0$.

The action that we wish to evaluate is

$$S = S_{split} - S_{background} \tag{3.5.15}$$

where S_{split} is the action for the split double loop and $S_{background}$ is the action of a loop hanging in a bulk from a single circle in the $z = 0$ plane. This circle must have a radius equal to the largest radius of the two concentric loops used to calculate $S_{string\ in\ bulk}$, as shown in figure 3.12.

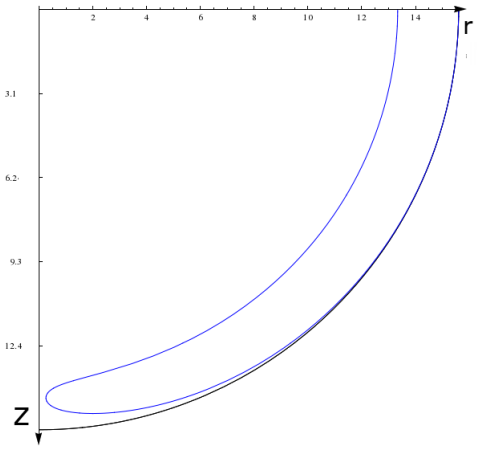

Figure 3.12: Cross section of the solution loop, in blue, and the background loop, in black.

In the calculations, we will use the same parametrisation suggested by Armoni et al

$$\theta = \frac{\pi}{2} \quad \mathrm{d}\theta = 0 \tag{3.5.16}$$

$$t = 0 \quad \mathrm{d}t = 0 \tag{3.5.17}$$

$$\theta = \tau \quad \mathrm{d}\theta = \mathrm{d}\tau \tag{3.5.18}$$

$$z = \sigma \quad \mathrm{d}z = \mathrm{d}\sigma \tag{3.5.19}$$

$$r = r(\sigma) = r(z) \tag{3.5.20}$$

We therefore find the equation of motion

$$(2r(z)r'(z) + z)(r'(z)^2 + 1) - zr(z)r''(z) = 0. \tag{3.5.21}$$

Solving numerically for the solution loop, we must apply the following conditions

$$r(z_{IR}) = r_{IR} \tag{3.5.22}$$

$$r'(z_{IR}) = \pm\infty \tag{3.5.23}$$

where (z_{IR}, r_{IR}) are the coordinates of the lowest point the loop goes in the bulk. The numerical calculation starts at this point and shoots off in both the $r'(z_{IR}) = +\infty$ and $r'(z_{IR}) = -\infty$ directions, until the $z_\wedge$ is reached. The two parts are then added to give a full solution.

We choose $r_{IR} = 2$ and vary z_{IR}, obtaining solutions as shown in figure 3.13

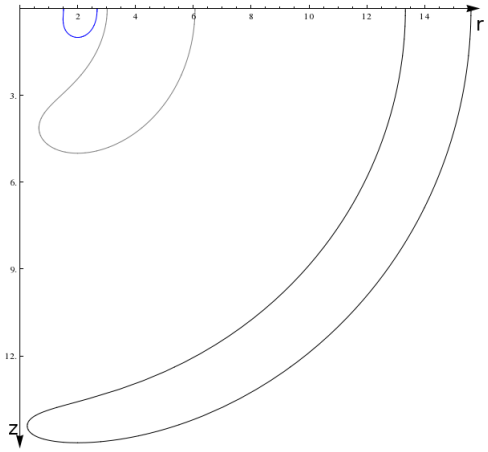

Figure 3.13: Different solution loops for $z_{IR} = 1$ (blue), $z_{IR} = 5$ (grey) and $z_{IR} = 15$ (black).

To find the background loop we set $r_{IR} = 0.001$ and $r'(z_{IR}) = \pm\infty$. This gives a quarter circle solution, as shown in figure 3.12, so all that we need to do to ensure that the end of the background loop corresponds with the end of the solution loop is to set $z_{IR,\, background} = r_{maximum,\, solution}$.

We may then calculate (3.5.15), as shown in figure 3.14. As we are dealing with strings, the easiest way to explicitly do this calculation, for both single and double loops, is the Nambu-Goto action (which has been Wick rotated in this case)

$$S \propto \int \mathrm{d}\tau \mathrm{d}\sigma \sqrt{\left(\dot{X}\right)^2 \left(X'\right)^2 - \left(\dot{X} \cdot X'\right)^2} \tag{3.5.24}$$

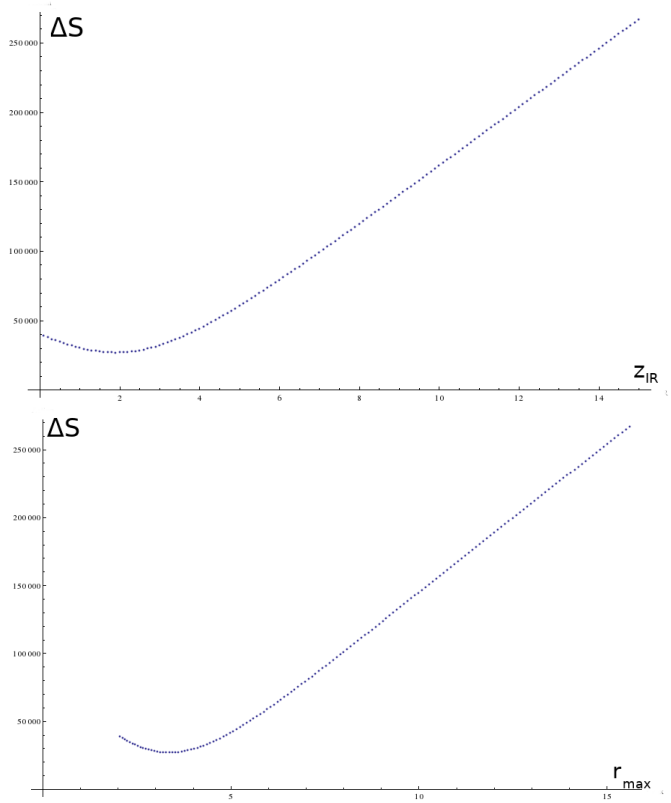

Figure 3.14: The action for the solution with the background subtracted plotted against z_{IR} (top) and r_{max} (bottom).

which, for this specific parametrisation, may be expressed as

$$S \propto \int \mathrm{d}z \frac{r(z)}{z^2} \sqrt{1 + \left(\frac{\mathrm{d}r}{\mathrm{d}z}\right)^2} \tag{3.5.25}$$

These techniques will be applicable when calculating action for systems modelling mesons in confining bakgrounds in chapter 5.

Chapter 4

Holographic Sakai Sugimoto Model

4.1 Introduction to Sakai Sugimoto

Ordinary Anti-de Sitter is not a confining background and so cannot be used as even an approximate dual to QCD. The other models described in the previous chapter introduced confinement but continued to have problems, in particular they lacked the non-Abelian chiral symmetry breaking that is seen in QCD. An alternative, background which has shown a lot of promise in this area, including being able to replicate many results from lattice QCD [111], was introduced by Sakai and Sugimoto in [14] and [15]. This is an adaptation of the standard AdS string model with colour $D4$ branes and probe flavour $D8$ branes. Indeed it is very similar to the $D4/D6$ Kruczenski-Mateos-Myers-Winters model described in the previous chapter, but with $D8$ and $\bar{D}8$ probe branes (which now intersect the $D4$ branes) rather than $D6$ probe branes. This section will provide an introduction to the Sakai Sugimoto model, in particular at zero temperature. Section 4.2 will discuss the extensions that need to be made at finite temperature. Section 4.3 will discuss how this method can be used to calculate the spectrum of low spin mesons. Finally, section 4.4 will discuss how to use a worldline instanton method to calculate the dynamics of large

spin mesons – the method that will be used in subsquent chapters of this thesis.

The model depends on using the probe brane approximation, which is equivalent to quenched approximation in earlier QCD methods [10], [112]. On the QCD side this requires that the number of colours (N_C) is infinite while the number of flavours (N_F) remains finite, that is, we consider only the effect of gluons rather than also that of the quarks – the so called 't Hooft limit [59]. In the holographic picture this translates to us having to take the flavour branes to be probe branes – this follows the earlier work of Karch and Katz [85]. This means that their positioning does not affect the spacetime and we are left with a simpler metric.

The theory is interesting even in the low coupling limit $g_S N \ll 1$ [14]. In this limit none of the branes have a large effect on the spacetime and strings can attach to $D4$, $D8$ or $\bar{D}8$ branes. One may consider open strings with both ends on a $D4$ brane, the fluctuations of which give vector and scalar modes in the adjoint of $U(N_C)$. One may also consider open strings with one end on a $D4$ brane and one end on a $D8$ or $\bar{D}8$ brane – these are fermions in the fundamental representation of $U(N_C)$. These strings carry a colour and a flavour index and so we may consider these fermions to be quarks.

However, more interesting is the higher coupling system where the $D4$ branes do warp the spacetime and can no longer be attached to strings. As reviewed by Sato and Yoshida [113] the background metric for the zero temperature version of this may be expressed, as in Witten's $D4$ model, as

$$\mathrm{d}s^2 = \frac{u^{\frac{3}{2}}}{{R_{D4}}^{\frac{3}{2}}}\left(\mathrm{d}{x_0}^2 + \delta^{ij}\mathrm{d}x_i\mathrm{d}x_j + f(u)\mathrm{d}{x_4}^2\right) + \frac{{R_{D4}}^{\frac{3}{2}}}{u^{\frac{3}{2}}}\left(f^{-1}(u)\mathrm{d}u^2 + u^2\mathrm{d}{\Omega_4}^2\right) \tag{4.1.1}$$

where $i = 1, 2, 3$; x_4 is a compactified periodic dimension; $\mathrm{d}\Omega_4$ is a line element for an S^4 sphere, R_{D4} is the radius of said S^4 sphere which can further be defined in terms of the string length ${l_s}^2 = \alpha'$, string coupling g_s and number of colours N_C as

$${R_{D4}}^3 = \pi g_s N_C {l_S}^3, \tag{4.1.2}$$

and

$$f(u) = 1 - \frac{{u_\Lambda}^3}{u^3}. \tag{4.1.3}$$

The period of x_4 is required to be

$$\delta x_4 = \frac{4\pi}{3}\sqrt{\frac{{R_{D4}}^3}{u_\Lambda}} \tag{4.1.4}$$

in order to avoid a singularity at $u = u_\Lambda$ – this means x_4 is effectively a polar coordinate. Sakai and Sugimoto explain that the Kaluza-Klein mass is

$$m_{KK} = \frac{2\pi}{\delta x_4} = \frac{3}{2}\sqrt{\frac{u_\Lambda}{{R_{D4}}^3}}. \tag{4.1.5}$$

Above this mass scale this set-up no longer effectively models QCD since, as in Witten's model, we begin to see five dimensional effects. The theory also contains a dilaton

$$e^\phi = g_s\left(\frac{u}{R_{D4}}\right)^{\frac{3}{4}} \tag{4.1.6}$$

and a four-form field

$$F_4 = \frac{2\pi N_C}{V_4}\epsilon_4 \tag{4.1.7}$$

where ϵ_4 is the volume form and V_4 is the volume of the S^4 sphere such that

$$V_4 = \frac{8\pi^2}{3}, \tag{4.1.8}$$

which will not further impact the work [15].

We can see that this metric describes a stack of N_C $D4$ branes which fill the dimensions x_0 through to x_4 and pairs of probe D8 and $\overline{D8}$ branes which fill all dimensions apart from x_4. As explained by Peeters, Zamaklar and Sonnenschein [12], and Erdmenger and Ammon [60] these pairs of branes can be either disconnected or connected, the latter breaking chiral symmetry. We will primarily look at the connected configuration.

As discussed by Peeters and Zamaklar [95] the action for the $D8$ branes in the

$D4/D8$ system is given by

$$S_{D8} = \int \mathrm{d}^4x \mathrm{d}x_4 u^4 \sqrt{f(u) + \left(\frac{R_{D4}}{u}\right)^3 \frac{1}{f(u)} \left(\frac{\partial u}{\partial x_4}\right)^2} \tag{4.1.9}$$

which gives the equation of motion

$${u_0}^4 \sqrt{f(u_0)} \frac{\partial u}{\partial x_4} = \left(\frac{u}{R_{D4}}\right)^{\frac{3}{2}} f(u) \sqrt{u^8 f(u) - {u_0}^8 f(u_0)} \tag{4.1.10}$$

where u_0 is the position of the bottom of the $D8$ brane. This can be solved numerically to give the shape of the brane.

We can see that u stretches from infinity to an IR wall at $u = u_\Lambda$. As explained by Erdmenger and Ammon [60] it is the presence of this wall that makes this background confining. When working in the string worldline model – which will be discussed in section 4.4 – the string configurations which represent mesons extend down close to the wall and their bottoms stretch out parallel to said wall. This leads to the potential between the quark and antiquark in the meson to be linear – which leads to confinement. This may be shown as follows, following the example of Zamaklar and Peeters [95]. Using the metric (4.1.1) and the parametrisation $\tau = x_0$ and $\sigma = x_1 \equiv x$ we find the Lagrangian for a string in this spacetime to be:

$$\mathcal{L} = \sqrt{g_{00}(u) g_{xx}(u) + g_{00}(u) g_{uu}(u) (u')^2}. \tag{4.1.11}$$

where

$$u' = \frac{\partial u}{\partial x}. \tag{4.1.12}$$

If we consider the string to be U shaped with its bottom at position u_B such that

$$\left.\frac{\mathrm{d}u}{\mathrm{d}x}\right|_{u=u_B} = 0 \tag{4.1.13}$$

then the Lagrangian at this point is

$$\mathcal{L}_B = \sqrt{g_{00}(u_B) g_{xx}(u_B)}. \tag{4.1.14}$$

Following the example of Kinar et al [104] we find that we can calculate the string

momentum as

$$p = \frac{\partial \mathcal{L}}{\partial u'} = \frac{g_{00}(u) g_{uu}(u)(u')}{\sqrt{g_{00}(u) g_{xx}(u) + g_{00}(u) g_{uu}(u)(u')^2}}. \tag{4.1.15}$$

We then recall the standard expression for the Hamiltonian.

$$\mathcal{H} = p\, u' - \mathcal{L} \tag{4.1.16}$$

We will see that $\mathcal{H}$ does not have an explicit time dependence so it must be a constant. If we calculate it in two different ways, we will be able to equate the results. Firstly, we will substitute in the general expressions for $\mathcal{L}$ and p from (4.1.11) and (4.1.15) into (4.1.16) to get

$$\mathcal{H} = \frac{-g_{00}(u) g_{xx}(u)}{\sqrt{g_{00}(u) g_{xx}(u) + g_{00}(u) g_{uu}(u)(u')^2}} = -\frac{g_{00}(u) g_{xx}(u)}{\mathcal{L}}. \tag{4.1.17}$$

Secondly we will also evaluate the Hamiltonian at the position u_B. Given the condition (4.1.13) and using the definition (4.1.14), we see that in this region (4.1.16) reduces to just

$$\mathcal{H} = -\mathcal{L}_B. \tag{4.1.18}$$

We therefore get

$$-\frac{g_{00}(u) g_{xx}(u)}{\mathcal{L}} = -\mathcal{L}_B. \tag{4.1.19}$$

From here we can read off

$$\begin{aligned} \mathcal{L}^2\, {\mathcal{L}_B}^2 &= \Big(g_{00}(u) g_{xx}(u)\Big)^2 \\ \Big(g_{00}(u) g_{xx}(u) + g_{00}(u) g_{uu}(u)(u')^2\Big) g_{00}(u_B) g_{xx}(u_B) &= \Big(g_{00}(u) g_{xx}(u)\Big)^2 \end{aligned} \tag{4.1.20}$$

and therefore

$$\left(\frac{\partial u}{\partial x}\right)^2 = \frac{g_{xx}(u)}{g_{uu}(u)} \frac{g_{00}(u) g_{xx}(u) - g_{00}(u_B) g_{xx}(u_B)}{g_{00}(u_B) g_{xx}(u_B)}. \tag{4.1.21}$$

Rearranging (4.1.19) we also get

$$\mathcal{L} = \frac{g_{00}(u)g_{xx}(u)}{\mathcal{L}_{\mathcal{B}}} = \frac{g_{00}(u)g_{xx}(u)}{\sqrt{g_{00}(u_B)g_{xx}(u_B)}}. \tag{4.1.22}$$

If we consider the horizontal length l of the bottom of the string, which represents the colour flux tube within the meson, and its energy E we find

$$l = \int \mathrm{d}x = \int \mathrm{d}x \frac{\partial x}{\partial u} \qquad E = \int \mathrm{d}x \mathcal{L} = \int \mathrm{d}u \frac{\partial x}{\partial u} \mathcal{L}. \tag{4.1.23}$$

Therefore, integrating E we find

$$E = \int \mathrm{d}u \sqrt{\frac{g_{00}(u)g_{xx}(u)g_{00}(u)g_{uu}(u)}{g_{00}(u)g_{xx}(u) - g_{00}(u_B)g_{xx}(u_B)}} \tag{4.1.24}$$

$$= \sqrt{g_{00}(u_B)g_{xx}(u_B)}\; l + K(u_B). \tag{4.1.25}$$

This is our desired linear relationship plus a small correction K. Something similar was not possible in AdS due to conformal invariance [95].

The Sakai-Sugimoto model has been shown to replicate the Kawarabayashi-Suzuki-Riazuddin-Fayyazuddin coupling relation [14], Regge behaviour [58], [96] and Zweig Rule [58] found in observed mesons, which supports its use for our purposes.

We may, alternatively, re-frame the model in terms of

$$z = \frac{1}{u} \qquad z_{D4} = \frac{1}{R_{D4}} \qquad z_\Lambda = \frac{1}{u_\Lambda} \tag{4.1.26}$$

in which case the metric becomes

$$\mathrm{d}s^2 = \frac{{z_{D4}}^{\frac{3}{2}}}{z^{\frac{3}{2}}} \left({\mathrm{d}x_0}^2 + \delta^{ij}\mathrm{d}x_i\mathrm{d}x_j + f(z){\mathrm{d}x_4}^2 \right) + \frac{1}{z^{\frac{5}{2}}{z_{D4}}^{\frac{3}{2}}} \left(f^{-1}(z)\mathrm{d}z^2 + z^2 \mathrm{d}{\Omega_4}^2 \right) \tag{4.1.27}$$

where

$$f(u) = 1 - \frac{z^3}{{z_\Lambda}^3}. \tag{4.1.28}$$

This parametrisation can often make calculations easier.

4.2 Finite Temperature

As discussed by Peeters and Zamaklar [95] and Aharony et al [114] for low finite temperature the metric remains the same but the direction x_0 becomes compactified as well. The period of this compactifaction is the inverse of the temperature

$$\delta x_0 \sim \frac{1}{T} \tag{4.2.1}$$

As temperature increases this period decreases – until it becomes equal to the period δx_4, at which point we get a phase transition and the metric changes.

For such high temperatures the metric becomes

$$\mathrm{d}s^2 = \frac{R^{\frac{3}{2}}}{z^{\frac{3}{2}}}\left(f(z)\mathrm{d}{x_0}^2 + \delta^{ij}\mathrm{d}x_i\mathrm{d}x_j + \mathrm{d}{x_4}^2\right) + \frac{1}{z^{\frac{5}{2}}R^{\frac{3}{2}}}\left(f^{-1}(z)\mathrm{d}z^2 + \frac{1}{z^2}\mathrm{d}{\Omega_4}^2\right) \tag{4.2.2}$$

We note that this is very similar to the previous metric (4.1.27) but with the x_0 (that is time) direction switched with the spatial x_4 direction. Both these directions remain compactified and we find the period of the x_0 direction to be:

$$\delta x_0 = \frac{4\pi}{3}\sqrt{\frac{{R_{D4}}^3}{u_\Lambda}}. \tag{4.2.3}$$

This change of geometry results in the loss of gluon confinement [12]. The temperature T represented by this set-up is given by:

$$T = \frac{1}{\delta x_0} \tag{4.2.4}$$

At very high temperatures, it becomes more energetically favourable for the $D8-\overline{D8}$ branes to separate, leading to the loss of chiral symmetry breaking.

Figure 4.1 sketches this spacetime for these different temperature regimes: in 4.1(a) we see the cigar shaped compactified x_4 direction at zero temperature, in 4.1(b) we see how time also becomes compactified at low temperature but at constant size, in 4.1(c) we see how at high temperature the geometry changes and the time direction takes on a cigar shape while the compactified x_4 direction gains a constant size, and in 4.1(d) we see how at very high temperatures – for examples in the quark-gluon

plasmas touched upon in appendix C the $D8$ and $\bar{D}8$ branes seperate. A good, detailed discussion of the phase space of the Sakai Sugimoto model may be found in [115].

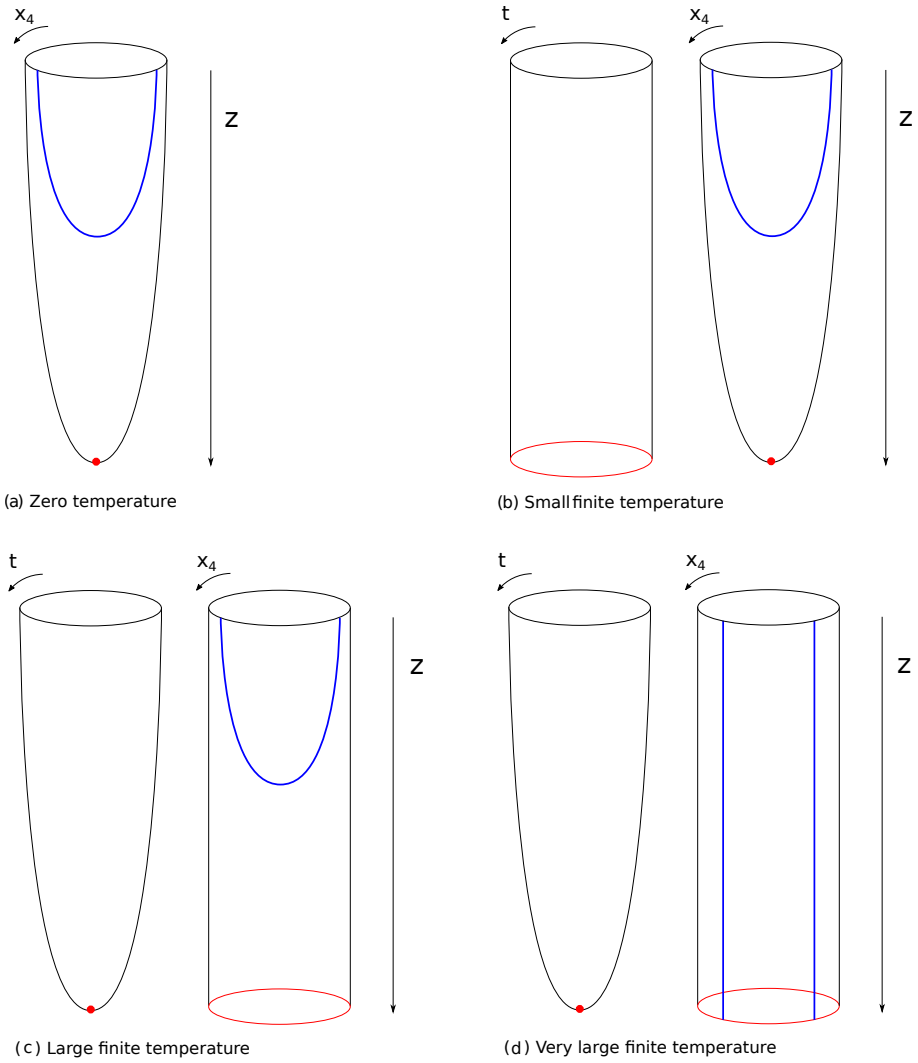

Figure 4.1: The Sakai Sugimoto spacetime for different temperature regimes. Red indicates the IR wall. Blue indicates a $D8$ or $\bar{D}8$ probe brane. Fluctuations of these results are identified with low spin massive and massless mesons. We get massless mesons when we have chiral symmetry breaking – that is when the $D8$ and $\bar{D}8$ probe branes join.

4.3 Modelling Low Spin Mesons and Baryons using Sakai Sugimoto

Mesons of low spin, that is spins of one or less, and low energy can be modelled by considering the Dirac-Born-Infield (DBI) action of small fluctuations around the solution for the probe D8 branes. Sakai and Sugimoto [14] show how this action can be simplified to

$$S_{D8} = -\int \mathrm{d}^4x \left(\frac{1}{2}\partial_\mu\varphi^{(0)}\partial^\mu\varphi^{(0)} + \sum_{n\geq 1}\left(\frac{1}{4}F_{\mu\nu}{}^{(n)}F^{\mu\nu(n)} + \frac{1}{2}m^2 B_\mu{}^{(n)}B^{\mu(n)}\right)\right) \quad (4.3.1)$$

where the field $\varphi^{(0)}$ can be interpreted as a massless scalar meson, which can be seen as equivalent to Nambu-Goto bosons in QCD [113]. Additionally

$$F_{\mu\nu}(x^\mu, z) = \sum_n \left(\partial_\mu B_\nu{}^{(n)}(x^\mu) - \partial_\nu B_\mu{}^{(n)}(x^\mu)\right)\psi_n(z) \quad (4.3.2)$$

$$F_{\mu z}(x^\mu, z) = \sum_n \left(\partial_\mu\varphi^{(n)}(x^\mu)\phi_n(z) - B_\mu{}^{(n)}(x^\mu)\dot{\psi}_n(z)\right) \quad (4.3.3)$$

where the field $\phi_n(z)$ is identified as a massive vector meson (therefore, if thinking of quarks, the mass here is the sum of the constituent masses of the quarks involved). Fluctuations of this field give masses of vector mesons given by

$$m^2_{vm\,i} = \lambda_i m^2_{KK} \quad (4.3.4)$$

where λ_i is a constant for the meson labelled by i [116]. Numerical analysis of the meson spectrum by Sakai and Sugimoto showed that the masses of mesons contained within the theory roughly agree with those found in experiment – for example, the ratio of masses of the two lightest vector mesons is 2.344 in this theory and is measured to be 2.52 experimentally. As explained previously, the theory holds up to masses of $\frac{3}{2}\sqrt{\frac{u_\Lambda}{{R_{D4}}^3}}$.

Further analysis shows that this model replicates the spontaneous chiral symmetry breaking seen in mesons. As reviewed by Erdmenger and Ammon [60] the chiral symmetry in the gauge dual picture is represented by the $U(N_f)_L \times U(N_f)_R$ symmetry

of the $D8 - \overline{D8}$ branes. As shown in figure 4.2 these branes can join together to form a single $D8$, leaving only $U(N_f)_V$ symmetry. This process corresponds to the aforementioned chiral symmetry breaking for the mesons. This is similar to the symmetry breaking observed for the $D4/D6$ model – however, since this model, unlike $D4/D6$, is not supersymmetric, it can represent non-Abelian chiral symmetry breaking. The $D4/D6$ model only includes the breaking of $U(1)_A$ symmetry.

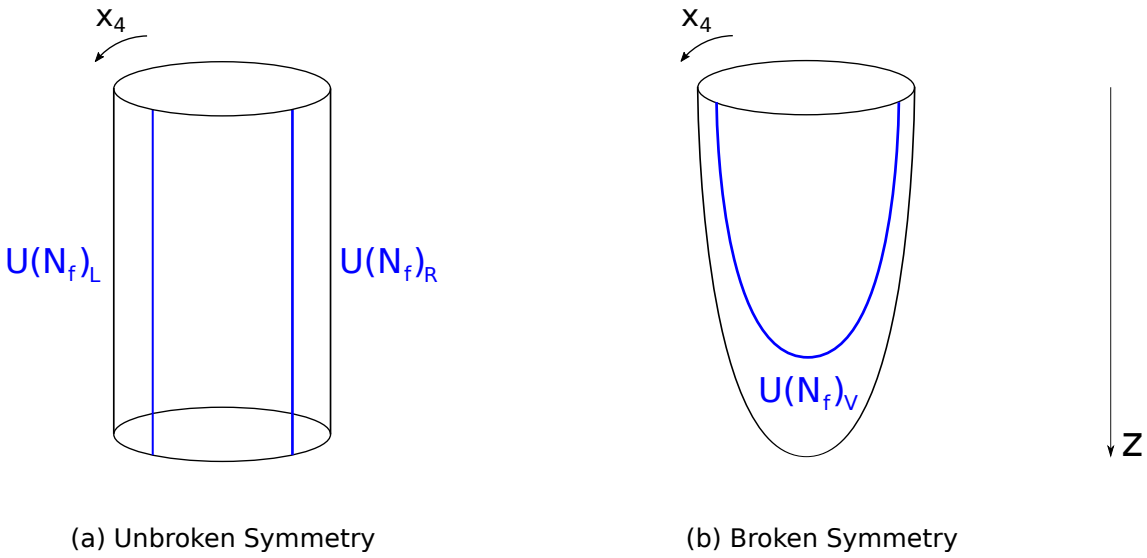

(a) Unbroken Symmetry (b) Broken Symmetry

Figure 4.2: Chiral symmetry breaking in the Sakai Sugimoto model.

We can see that the first, massless meson, term in (4.3.1) is the result of this spontaneous symmetry breaking. As described by Ammon and Erdmenger [60] we may write the action of the gauge field $A_\zeta(\zeta, x^\mu)$ (where $1+\zeta^2 = \left(\frac{z}{z_\Lambda}\right)^3$) corresponding to the fluctuations of the vacuum manifold related to the chiral symmetry breaking as

$$S \propto \int_0^\infty \mathrm{d}\zeta \int \mathrm{d}x^4 \; e^{-\phi}\sqrt{-g}g^{\zeta\zeta}g^{11}\left(-(\partial_t A_\zeta)^2 + (\partial_1 A_\zeta)^2 + (\partial_2 A_\zeta)^2 + (\partial_3 A_\zeta)^2\right). \tag{4.3.5}$$

We then consider the component of $A_\zeta(\zeta, x^\mu)$ dependent only on x^μ, that is $\varphi^{(0)}(x^\mu)$ defined as

$$A_\zeta(\zeta, x^\mu) = \frac{1}{C}\frac{1}{1+\zeta^2}\varphi^{(0)} \tag{4.3.6}$$

where C is a constant, and find that the terms of (4.3.5) that depend on $\varphi^{(0)}(x^\mu)$ become the first term of (4.3.1). Similar calculations can be used to find the spectrum of mesons at finite temperature [117].

Furthermore, Sakai and Sugimoto [14] suggest that this model also includes baryons – which are identified as D4 branes wrapped around the S^4 sphere, which may, in this set up, also be seen as Skyrmions.

In this case the baryon number may be calculated from the field by

$$n = \frac{1}{8\pi^2}\int \mathrm{tr}F^2 \tag{4.3.7}$$

where n may also be considered to be the instanton number – that is the number of times the $D4$ branes are wrapped around the S^4 sphere. The mass is proportional to the action of the $D4$ brane that models it.

$$S_{D4} = -\frac{1}{(2\pi)^4 {l_s}^5 g_s}\int_{\mathbb{R}\times S^4} \mathrm{d}x^0 \epsilon_4 \sqrt{-g_{00}g_{S^4}}e^{-\phi} \tag{4.3.8}$$

$$= -\frac{1}{27\pi} m_{KK} g_{YM}^2 {N_C}^2 \int_{\mathbb{R}} \mathrm{d}x^0 \tag{4.3.9}$$

where the mass is identified as

$$m = \frac{1}{27\pi} m_{KK} g_{YM}^2 {N_C}^2. \tag{4.3.10}$$

In a slightly different, but equivalent, picture, baryons can also be considered as four-dimensional soliton-like objects, which are referred to as 'brane-induced Skyrmions' [118], [119]. The energy and size of such a Skyrmion can then be calculated to be [118]

$$E \simeq 1.115 \times 12\pi^2 \frac{f_\pi}{2e} \tag{4.3.11}$$

$$\sqrt{\langle r^2 \rangle} = 1.268 \frac{1}{e f_\pi}, \tag{4.3.12}$$

where f_π is a constant related to the decay rate of the pion in the theory that is set by experimental data. These results, in particular the energy, give good agreement with experiment.

This model has shown promise modelling baryon decay – with particularly interesting work done on monopole catalysis of such decay [120] where monopoles are modelled, in the holographic picture, as $D6$ branes. A good discussion of baryons in this model can be found in [121].

4.4 Modelling High Spin Mesons using Sakai Sugimoto

A somewhat different approach is required when considering mesons of higher spin – which will be the focus of the next chapter. Rather than considering the dynamics of $D8-\overline{D8}$ we would want to consider static $D8$ branes acting as flavour branes and instead model mesons as macroscopic U-shaped strings with the endpoints hanging from said $D8$ flavour branes.

Such holographic methods with confining backgrounds [96] and particularly this Sakai Sugimoto background [58] have proved successful in modelling mesons. For example, as mentioned previously, they successfully replicate the Regge behaviour found in mesons. This relationship is between a meson's angular momentum M and mass J which is found to be quadratic:

$$J = \alpha + \alpha' M^2 \tag{4.4.1}$$

where α and α' are constants which are reproduced using these string models [95]. This suggests that these high spin models may be successful in other applications as well, such as calculating meson decay rates.

While previous work, particularly with the low spin mesons, has focused on the spectra of the decay products, this frameworks allows a more thorough investigation of the dynamical properties of the decay [58], [122]. This is a somewhat similar process as was discussed for high spin mesons in in section 3.4.2.

As we are modelling decays, we wish to use a holographic analogy to the worldine

instanton picture first introduced in section 2.6 to simplify our calculations. In the ideal case, we would just Wick rotate a spinning string, however, this is not a trivial task. Therefore, as a simplification, we will use a circular Euclidean Wilson Loop, of the type introduced in section 3.5 instead. We cannot say that the model represents rotating strings, but it will be shown to accurately model elements of meson decay.

This is somewhat reminiscent of the phenomenological Lund model of meson decay – which was discussed in section 2.5. However, unlike with the Lund Model or the previous work in flat spacetime in section 2.6 – we no longer have to add the masses of the mesons by hand. The curvature of the space in the holographic direction gives the constituent quarks their mass. The mass of a quark may be calculated to be the action of a straight, closed string extending from the flavour brane to the IR wall:

$$m_Q = \frac{1}{2\pi\alpha'}\int_{z_\Lambda}^{z_{m_Q}} \mathrm{d}z\,\sqrt{g_{zz}g_{00}} = \frac{1}{2\pi\alpha'}\int_{z_\Lambda}^{z_{m_Q}} \mathrm{d}z\,\frac{1}{f(z)^{1/2}z^2} \tag{4.4.2}$$

where z_{m_Q} denotes the position of the flavour brane [123]. Therefore the flavour branes the string endpoints attach to determine the mass, and therefore flavour, of the constituent quarks. The action of the horizontal segment of the string can be thought of as being proportional to the energy of the colour field flux tube of the meson. Therefore the tension of the flux – that is the energy per unit length – may be evaluated as:

$$T = \sqrt{g_{tt}g_{xx}}|_{z=z_B} = \frac{1}{{z_B}^{\frac{3}{2}}} \tag{4.4.3}$$

where z_B is the position of the bottom of the loop.

This model is particularily intuitive when considering meson decay, which is modelled by the string undergoing quantum mechanical fluctuation and oscillating up to a flavour brane and splitting. This is illustrated in figure 4.3, showing the circular loops. Mesons could also be modelled by rectangular loops – that is loops whose endpoints are straight parallel lines rather than circles, but the loss of symmetry would make calculations much more difficult.

As the two newly created string endpoints must both connect to the same flavour

brane, and one will represent a quark while the other the corresponding antiquark – this model explicitly contains flavour conservation [58]. The full probability for the decay is therefore given by the product of the probability for the string to oscillate up to the flavour brane and the probability for it to split. This is equivalent to thinking of meson decay as the production of a new quark-antiquark pair from the colour field flux tube of the meson (effectively an example of the CNN modifications to the Schwinger effect). Other work has shown similar methods to be succesful in modelling pair production from magnetic fields [113], [124], [125].

There are two other possible modes for decay [58] which will not be discussed here. Firstly, the string crossing itself and forming a new closed string loop corresponding to a glueball (such a process is suppressed by additional powers of g_s – which suppresses open to closed string amplitudes with respect to open to open string amplitudes). Secondly, fluctuations at the string endpoints can produce low spin mesons.

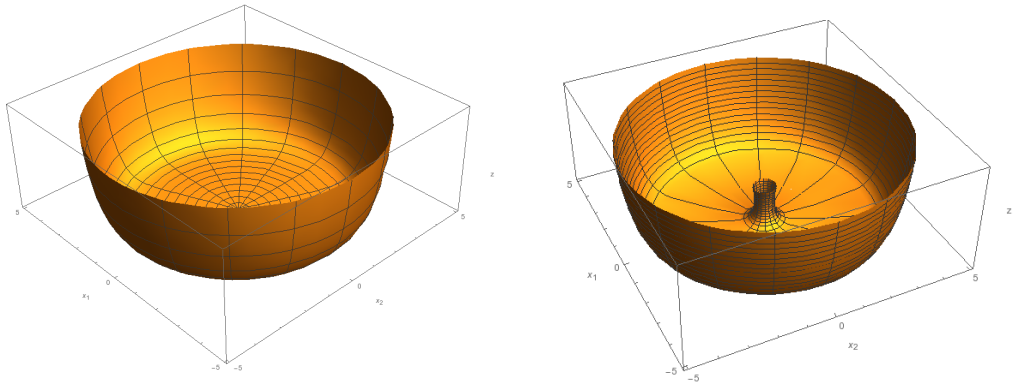

Figure 4.3: Typical single loop solution (**I**), left and a double loop solution (**II**), right.

The exact shape of the string will depend on what temperature regime and boundary conditions we are working with. This will be discussed in more detail in section 5.2.

Careful consideration of the shapes of the loops is vital due to the Gross-Ooguri phase transition [110], [126], [127]. This occurs when the action of a connected solution (that is a certain double loop) exceeds that of the corresponding disconnected solution (two single loops that each connect to a $D8$ brane at the same point as one of the

endpoints of said corresponding double loop). The double loop is therefore no longer energetically stable. We wish to consider solely the connected solution but this only exists when its action is lower than that of the disconnected solution. That is, if we want a double loop, that is a loop of type **(II)**, which ends at positions (R_1, z_{m_q}) and (R_2, z_{m_Q}), we require

$$S_{II}(R_1, z_{m_q}, R_2, z_{m_Q}) < S_I(R_1, z_{m_q}) + S_I(R_2, z_{m_Q}) \tag{4.4.4}$$

Figure 4.4 shows the relationship between connected and disconnected solutions. All results have been checked to show that they satisfy this condition.

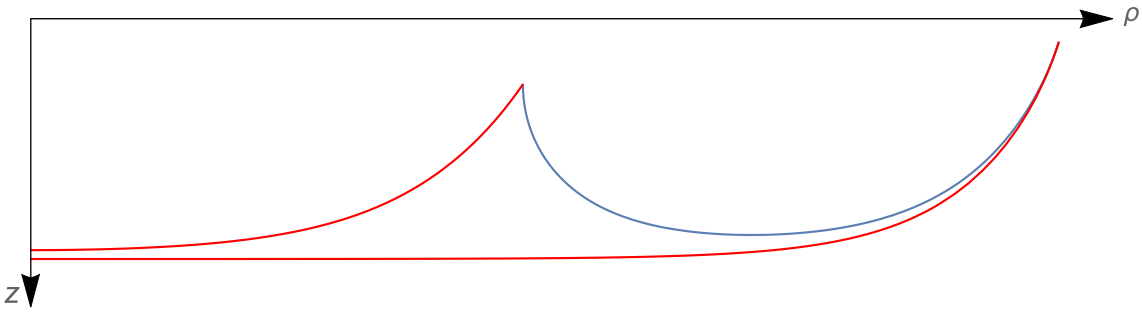

Figure 4.4: Cross section of a connected solution (blue) and the corresponding disconnected solution (red).

As explained by Peeters and Zamaklar [95] any such high spin mesons would be so unstable as to make their experimental observation, and therefore the confirmation of the effectiveness of this method, rather difficult. There exists doubt in some quarters about the existence of these mesons. However current data does not rule them out and it should be possible to analyse their decay by observing their decay products.

Chapter 5

Holographic Meson Decays

5.1 Summary of approach

The Sakai Sugimoto model was reviewed in chapter 4. D8 flavour branes are embedded in the geometry such that they fill out all directions except the cigar (u, x_4) submanifold. In the cigar submanifold, the flavour $D8$ brane has a U-shape, with the tip of the probe brane which is at some distance from the wall u_Λ, see [15].

Large spin mesons correspond to rotating strings, whose endpoints are fixed on the flavour D8-brane. The strings are prevented from collapsing by a centrifugal force [96]. As the spin of the string is increased, the distance between the string endpoints increases as well, i.e. the string becomes larger and its worldsheet becomes and more and more U-shaped. The two "vertical" parts of the string stretch almost vertically from the probe brane to the wall and the horizontal part of the string stretches almost parallel to the wall. It was shown in [96] that this string configuration is holographically equivalent to the system of two quarks which are connected by a flux tube. This is summarised in figure 5.1.

In order to model a system with different quark masses for the two quarks, one needs to introduce more than one flavour D8-brane, each hanging at different distance from the wall. The positions of these probes in the holographic direction specify

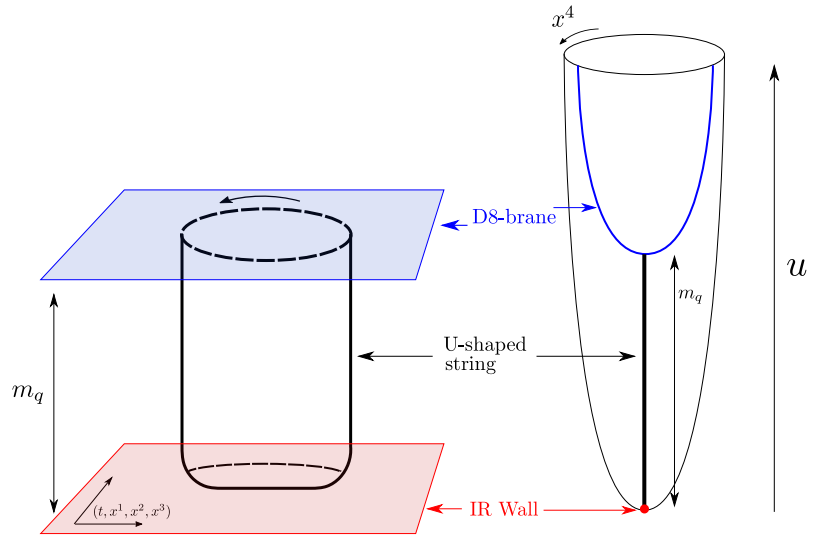

Figure 5.1: Sakai-Sugimoto background with the probe D8-brane and the U-shaped, mesonic string which hangs in the holographic direction towards the wall at $u = u_\Lambda$.

different quark masses. A meson with different quark masses is then a string with endpoints ending on these two different flavour D8-branes.

We would now like to study the decay of such a string configuration. The hanging string is subject to quantum fluctuations, and when a part of the string worldsheet touches one of the flavour branes it can split and attach new endpoints to that flavour brane. We will construct a configuration of the Euclidean worldsheet, which interpolates between the single and double U-shaped strings, that is, a worldsheet instanton. Example worldsheets were illustrated in figure 4.3.

5.2 String worldsheet instanton

The main goal is to holographically compute the probability per unit volume and time for a QCD flux tube to break. As in previous analyses [58] and as in the flat space construction from the previous section, we simplify the problem by looking at a U-shaped string with endpoints which are 'forced' to follow a circular path of some radius.

Generically the string breaking process will be sensitive to the precise boundary

conditions one imposes for the external quarks. However, one would expect that there is a limit in which the exact dynamics of the external quarks decouples from the breaking process (a sort of large volume limit), so that the quark production process in this limit can be treated as a Schwinger process in a constant external field, like in [18]. As it is a priori not clear what this limit is or whether it exists in our setup, our approach will be to first construct the general solution and compute the decay probability for an arbitrary mesonic particle, and then see if there is a limit in which this probability reduces to the Schwinger probability.

In this setup, in order to construct the instanton configuration for a splitting string, one needs to start with the string worldsheet which is "pinned" to the D8 probe at some internal worldsheet point. So we impose Dirichlet boundary conditions in u and x_4 directions both for the string endpoints and for the "pinning point". Once the string has split at the pinning point, the newly generated string endpoints are free to move in the D8 worldvolume directions (x_0, x_1, x_2, x_3 and S^4) freely, i.e. they satisfy Neumann boundary conditions.

In order to construct a worldsheet instanton, we need to solve the string equations of motion in the Wick rotated background. It will be convenient to change to background coordinates as follows,

$$z = \frac{1}{u}\,, \qquad z_{D_4} = \frac{1}{R_{D_4}}\,, \qquad z_\Lambda = \frac{1}{u_\Lambda}\,, \tag{5.2.1}$$

which turns the metric into

$$\begin{aligned} \mathrm{d}s^2 = \left(\frac{z_{D_4}}{z}\right)^{3/2} &\left(\mathrm{d}x_0^2 + \mathrm{d}\rho^2 + \rho^2\mathrm{d}\theta^2 + \rho^2\sin\theta\mathrm{d}\phi^2 + f_\Lambda(z)\mathrm{d}x_4^2\right) \\ &+ \frac{1}{z_{D_4}^{3/2} z^{5/2}}\left(f_\Lambda^{-1}(z)\mathrm{d}z^2 + z^2\mathrm{d}\Omega_4\right), \\ f_\Lambda(z) &\equiv 1 - \frac{z^3}{z_\Lambda^3} \qquad i = 1,2,3\,, \end{aligned} \tag{5.2.2}$$

and $0 \le z \le z_\Lambda$. We have Wick-rotated time and we have also introduced spherical coordinates in the (x_1, x_2, x_3) directions.

The string worldsheet extends in the radial direction z, has cylindrical symmetry

in the worldvolume directions, and hangs from a fixed position in the x_4 direction, which is at the tip of the D8-probe. A standard coordinate choice on the worldsheet is the static gauge, in which one makes the following ansatz for the string worldsheet,

$$z = \sigma\,, \qquad \rho = \rho(z)\,, \qquad \theta = \frac{\pi}{2}\,, \qquad \phi = \tau\,. \tag{5.2.3}$$

Plugging this into the string action one gets

$$\mathcal{L} = \gamma\sqrt{-(\dot{X}\cdot X')^2 + (X')^2\dot{X}^2} = \gamma\frac{\rho}{z^{3/2}}\sqrt{z_{D4}^3\rho'^2 + \frac{1}{z f_\Lambda(z)}}\,, \tag{5.2.4}$$

which leads to the equation of motion

$$\begin{aligned} &2z_\Lambda^3\left(z_\Lambda^3 + z_{D_4}^3 z(-z^3+z_\Lambda^3)\rho'^2\right)+ \\ &\quad + z_{D_4}^3\rho\left(z_\Lambda^3(z^3+2z_\Lambda^3)\rho' + 3z_{D_4}^3 z(z^3-z_\Lambda^3)^2\rho'^3 + 2zz_\Lambda^3(z^3-z_\Lambda^3)\rho''\right) = 0\,. \end{aligned} \tag{5.2.5}$$

The above choice for the worldsheet coordinate is, however, in general not very good when constructing numerical solutions. The U-shaped strings we are after have, in this system, parts in which either the z' or ρ' derivatives are large. In fact, because of the combination of almost vertical and almost horizontal segments, no single coordinate system turned out to be particularly well-suited to finding reliable solutions in all regions of the parameter space which we have explored so a number of different ones had to be used – they will be described in detail for each of the two different types of solution we found. We used built-in Mathematica numerical differential equation solving methods, using a shooting technique. We chose the endpoints of the loops and the angles at which they met the branes, and got Mathematica to calculate the shape of the rest of the loop starting from these points. Where we had to change the coordinate system while doing a calculation, we made sure that the different segments connected smoothly.

As we have seen before in other models, the equations of motion (5.2.5) admit two types of solutions which have different topologies and satisfy different boundary conditions at the string endpoints. The first solution corresponds to the single U-

shaped string and it describes the (original) quark and antiquark which are forced to "move" on a circular orbit, and are connected by a flux tube. If one was to Wick rotate this configuration to Lorentzian time, it would correspond to a quark and antiquark which accelerate away from each other, while being connected by a flux tube. We will refer to this solution as solution (**I**); see the left-hand side plot in figure 4.3.

The second solution is a string with two disconnected boundaries, which describes the process of flux tube breaking. The outer boundary of the string is forced by a Dirichlet boundary condition to be on a circle of a fixed radius R_2. The inner boundary is forced to be on a particular D8 probe (with Dirchlet boundary conditions in the x_4 and z directions), but the internal ends of this string are free to move arbitrarily along the D8 probe (Neumann boundary conditions). The physical reason why we impose "free" Neumann boundary conditions on the inner edge of the string is that this part of the worldsheet corresponds to the pair-produced quarks which move only under the influence of the flux tube, and are not coupled to any external source. We will refer to this solution as solution (**II**). We see that the cross section of this solution forms a 'banana' shape.

Solution (**II**) represents the process of meson decay and solution (**I**) represents the undecayed meson, that is the background. As in previous cases, when we consider the action, we will subtract the action of the background from the action of the decaying meson.

The inner boundary of the hanging string has to end orthogonally on the D8-brane worldvolume. Namely, in the gauge $z = \sigma$, the Neumann boundary condition in the ρ direction yields

$$\frac{\partial \mathcal{L}}{\partial \rho'} = z_{D_4}^{\frac{3}{2}} \left(z_{D_4}^3 \rho'^2 + f_\Lambda^{-1} \right)^{-\frac{1}{2}} \rho \rho' = 0 \quad \Rightarrow \quad \frac{\mathrm{d}\rho}{\mathrm{d}z} = 0 \,, \tag{5.2.6}$$

that is, the string hangs orthogonally from the D8 probe.

As discussed in chapter 4, for both string configurations, the constituent quark

masses are given by [104]

$$m_Q = \frac{1}{2\pi\alpha'}\int_{z_\Lambda}^{z_{m_Q}} \mathrm{d}z\,\sqrt{g_{zz}g_{00}} = \frac{1}{2\pi\alpha'}\int_{z_\Lambda}^{z_{m_Q}} \mathrm{d}z\,\frac{1}{f_\Lambda^{1/2}z^2}\,, \tag{5.2.7}$$

which is just the proper distance of a string hanging from the tip of the probe D8-brane, z_{m_Q} to the IR wall at z_Λ. Note that if there is more than one probe D8-brane, which each ends at a different $z_{m_{Q_i}}$, then one has a system with different quark masses m_{Q_i}.

Let us now first look at the solution of type (**I**). The equation of motion (5.2.5) is a second order differential equation, and as such has two undetermined constants of integration. In order to see which parameters characterise a solution, let us look at the $z = \sigma$ gauge, since this is the simplest and the results are independent of the gauge. In this gauge σ takes values in (z_{m_Q}, z_B) where z_B is the position of the bottom of the string loop, see figure 5.3. For the solution (**I**) we require that the tip of the loop is at the coordinate origin $\rho(z_B) = 0$. Also, as we are interested only in smooth loops, we will require that at the bottom $\frac{\mathrm{d}z}{\mathrm{d}\rho}\Big|_{z_B} = 0$. For a given position of the probe brane z_{m_Q}, these two requirements uniquely fix the solution (**I**). We are therefore only left with two parameters which specify the solution (**I**): z_B, the position of the bottom of the loop and z_{m_Q}, specifying the position of the top of the loop. In what follows we will usually work with fixed masses of the outer quarks m_Q, or equivalently we will fix z_{m_Q}. If one shifts the bottom of the string z_B, this will change the distance between the string endpoints, i.e. the distance between the outer quarks R on the probe D8. As the position of the bottom of the loop comes closer to the wall ($z_B \to z_\Lambda$) the distance between the quarks R becomes larger and larger, see figure 5.2.

In this near-wall limit, the single string loop looks more and more like a U-shaped string, see figure 5.3. Only in this limit $z_B \to z_\Lambda$ is the identification of the "vertical" parts of the loop with quark masses 5.2.7 fully justified [104]. Also, only for this kind of U-shaped string is the effective tension of the horizontal part of the string identified with $\sim \Lambda_{QCD}$, as the position of the wall specifies Λ_{QCD} in this model.

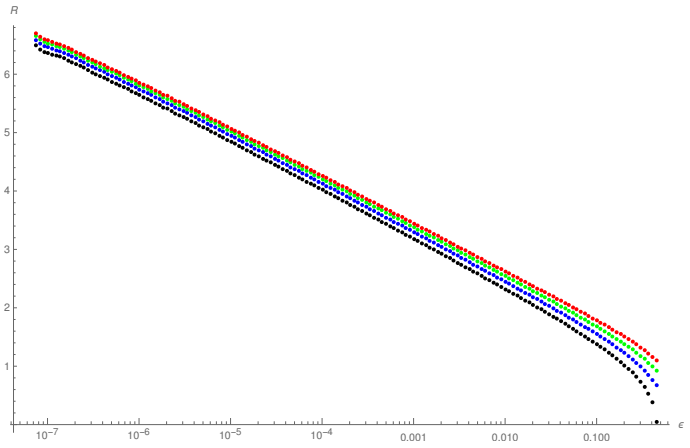

Figure 5.2: Distance between the quarks (string endpoints) for a single loop (**I**), as a function of dimensionless separation of the tip of the loop from the wall $\epsilon = (z_B - z_\Lambda)/z_\Lambda$. Plots are given for different values of the quark massess: from bottom to top, black $m = 1.31$, blue $m = 2.03$, green $m = 3.55$ and red $m = 9.5$.

As the bottom of the loop approaches the IR wall one discovers that the action scales more and more quadratically with the size of the loop, which is the expected behaviour for a single circular Wilson loop in a confining theory.

The numerical method for calculating solution (**I**) is fairly simple due to the loop's simple shape, requiring the use of the coordinate system $\sigma = \rho - z$ throughout. We used the shooting method from the bottom of the loop $\rho = 0$, $z = z_B$ with the starting angle defined by $\frac{\mathrm{d}z}{\mathrm{d}\rho}\Big|_{z_B} = 0$, stopping when we reached $z = z_{m_Q}$, as shown in figure 5.3.

For the double loop solution (**II**), one needs to introduce two probe D8-branes. The outer boundary of the string worldsheet will end on the brane with position $z = z_{m_Q}$. The position of this brane fixes the mass m_Q of the original (heavy) quark pair. Before the split, the original flux tube stretches between these two outer quarks. When the flux tube breaks, an inner boundary is formed on the string worldsheet. As argued earlier, the inner boundary of the loop ends orthogonally on the second brane which has position $z = z_{m_q}$, and this position fixes the mass of the *produced* quark-antiquark pair, m_q. When considering solutions of type (**II**), we will fix these

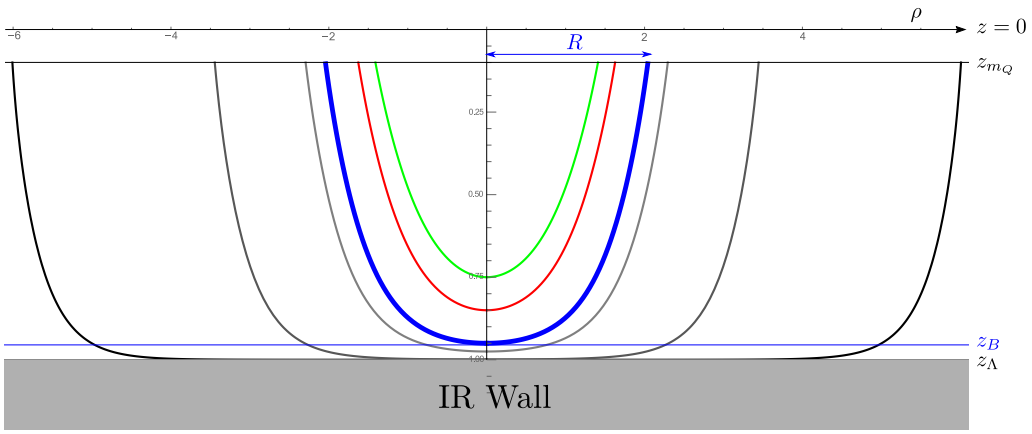

Figure 5.3: One-parameter family of solutions of type (**I**) plotted for a mass $m_Q = 9.57$ of the external quarks. Different solutions are parametrised by different distances between the quarks R, or equivalently, different distances from the bottom of the loop to the wall. For all the plots we have set $z_\Lambda = 1$.

two parameters m_Q and m_q as they are the parameters which are given in the dual gauge theory.

Note that the solution (**II**) consists of two, outer and inner branches, which are glued in a smooth way at the bottom of the loop, (z_B, R_B); these are coloured blue and red in figure 5.4. In contrast to the loop (**I**), the bottom of the loop (**II**) is no longer at the origin $\rho = 0$, but it is placed at some point $(z_B, \rho = R_B \neq 0)$. Smoothness of the solution (**II**) at the bottom, as before, implies $(dz/d\rho)|_{(z_B,R_B)} = 0$. In principle, bottom of the loop z_B can be anywhere between $0 \leq z_{m_Q} < z_{m_q} < z_B \leq z_\Lambda$. However, we will be mainly interested in the loops which have bottom near the wall $z_B \to z_\Lambda$, since newly generated flux tubes are IR objects which exist at energies $\sim \Lambda_{QCD}$. It is also useful to introduce a dimensionless parameter $\epsilon = (z_\Lambda - z_B)/z_\Lambda \ll 1$.

Once the bottom of the loop (**II**) is fixed to some $z = z_B$, for a given mass m_q, the inner (blue) branch of the solution is fully fixed by the requirement of orthogonality of the string to the m_q probe brane (see (5.2.6)) and the condition of smoothness of the loop at the bottom. Therefore, the radius of the inner loop R_1 (on the m_q brane), as well as the radius R_B of the bottom of the loop, are fixed once z_B and m_q

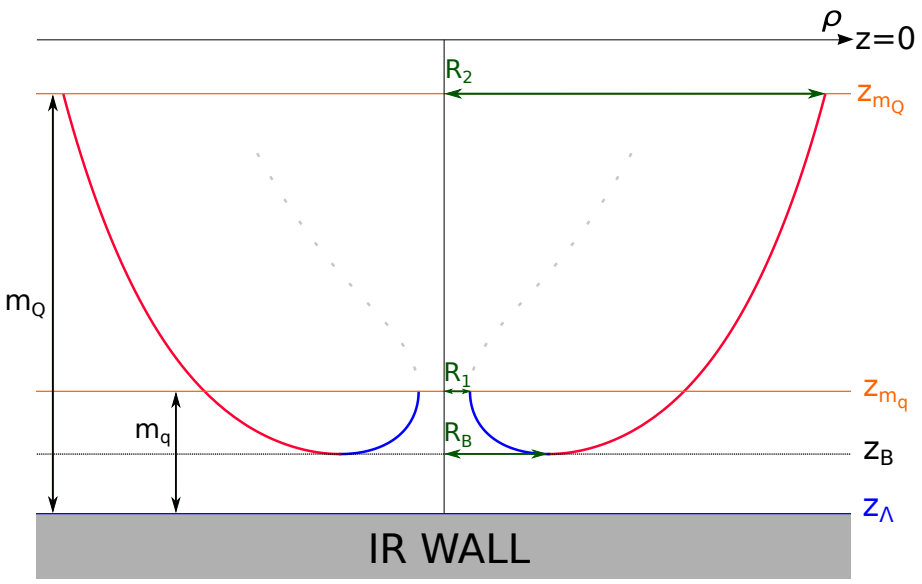

Figure 5.4: Slice of a generic double loop solution (**II**) for $\phi = \text{const}$. The labels z_{m_Q} and z_{m_q} give the positions of two D8-branes and also specify the masses of the original (outer) quarks m_Q and pair-produced (inner) quarks m_q. The dotted line shows how the inner leg of the loop would have continued had we extended the solution beyond the point specified by the Neumann condition $\frac{\mathrm{d}\rho}{\mathrm{d}z} = 0$.

are specified.

The outer (red) branch of the solution is fully fixed once the mass of the original quarks m_Q is specified and one requires that this branch is glued in a smooth way to the inner branch. Note that the outer branch of the solution (**II**) need not end orthogonally on the probe brane m_Q, as the position of the outer quarks is fixed by Dirichlet boundary conditions. So in summary, solution (**II**) is fixed by specifying the quark masses m_Q, m_q and the bottom of the loop z_B, or equivalently, m_Q, m_q and the inner radius R_1 of the loop.

The numerical method for calculating solution (**II**) was more complicated than for the single loops, requiring switching between three different coordinate systems on the worldsheet ($\sigma = z$, $\sigma = z + \rho$ and $\sigma = \rho$) when either ρ' or z' got too large. We shot from both the inner endpoint ($\rho = R_1$, $z = z_{m_q}$, and the starting angle determined by the condition (5.2.6)) and the outer endpoint ($\rho = R_2$, $z = z_{m_Q}$, being free to choose the starting angle due to the Dirichlet boundary condition on

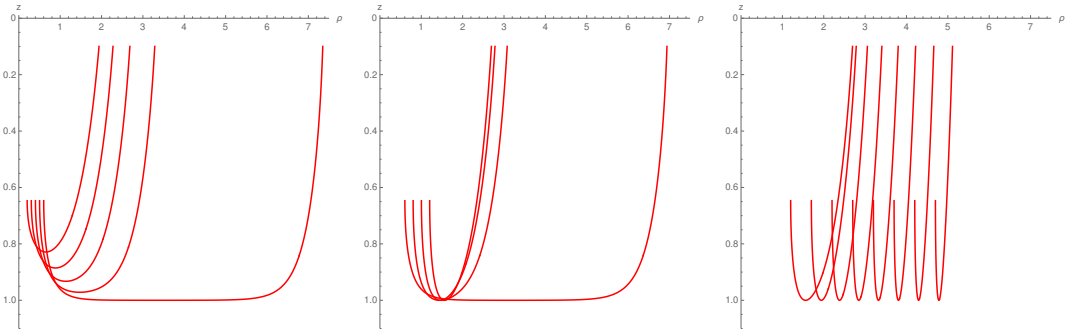

Figure 5.5: Plots of the loops of type (**II**) for increasing values of the inner radius R_1. The left panel shows region (i) until the value for which R_2 is maximal. The middle panel shows loops in region (ii), where R_2 decreases as R_1 increases, until R_2 reaches its local minimum. The right panel shows the squashed loops of region (iii) which occur beyond that.

that endpoint). We required that the two shooting solutions meet smoothly at a point, this condition reducing the free parameters back to what was described in the previous paragraph.

There are three regions of this solution, which we will refer to with lower-case Roman numerals. We observe that for fixed m_q and m_Q, as the inner radius R_1 is increased, the loop extends deeper and deeper into the bulk, towards the IR wall, or in other words, $\epsilon \equiv \frac{z_\Lambda - z_B}{z_\Lambda}$ decreases. As this happens, initially the loop becomes more and more U-shaped and wider, with increasingly longer horizontal part and with larger and larger outer radius R_2. In this region, the effective size of the system (the ratio of the outer versus the inner radius) grows. We will refer to this region as region (i). The left panel in figure 5.5 shows a series of loops in this region. When the inner radius R_1 becomes larger than a particular critical value $R_{\text{crit-1}}$ the outer radius R_2 starts to decrease as the inner radius grows, so loops become more and more *squashed*, see the middle panel in figure 5.5. Note that while the squashing happens, the bottoms of all the squashed loops stay in the region which is very close to the IR wall ($\epsilon \sim 10^{-5}$). We will refer to this region as region (ii). Finally, when the radius R_1 becomes larger than another critical value $R_{\text{crit-2}}$, both inner and outer radius start to grow, but the loop retains its squashed shape and it starts

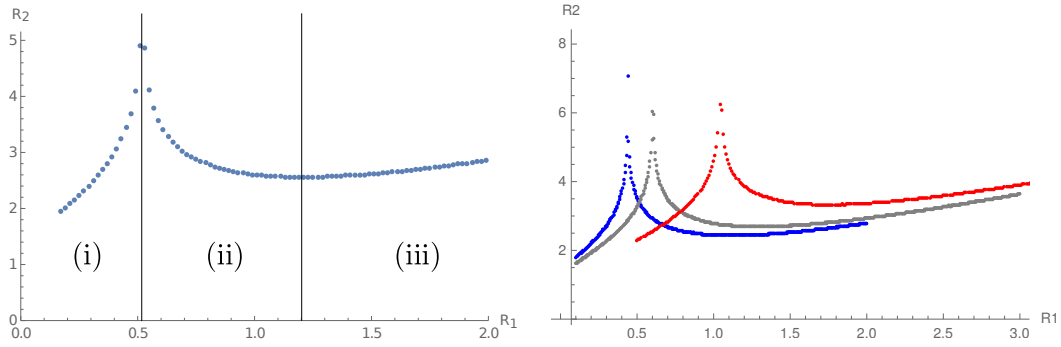

Figure 5.6: The left panel shows the behaviour of the outer radius as inner radius varies, and the three different regions. Note that there are two critical points on this graph and the "squashing" of loops takes place both in region (ii) and (iii). The right panel shows the behaviour for different masses $m_q = \{0.8, 1.0, 1.5\}$ (blue, gray, red) and fixed mass of the outer quarks $m_Q = 9.5$.

moving outwards as a whole; see the right panel in figure 5.5. We will refer to this as region (iii). Figure 5.6 shows the relation between the inner and outer radius as the inner radius varies, in all three regions. Note that as the inner quark mass is increased the position of the peak moves to the right, but in a such a way that the ratio of R_1/R_2 increases, so that the the system is effectively at smaller volume. Put differently, systems with smaller inner quark mass m_q have larger effective size in the sense discussed above, and we expect them to reproduce the Schwinger results more accurately. The peak in the R_2 vs. R_1 plot persists as $m_q \to m_Q$, but increasing the masses of outer and inner quarks to larger value reduces the height of the peak and shifts its location to larger values of R_1, so that eventually, for $m_q, m_Q \to \infty$, only region (i) remains and one is left with a simple linear relation between R_1 and R_2, as expected from, for example, [110].

In order to find the decay width of a given meson, we will need to keep R_2 and m_Q fixed and look at the decay probability for varying inner quark mass m_q. Figure 5.7 illustrates that, for strings in region (i), the radius R_1 at which the inner quarks are produced decreases as m_q is decreased. Figure 5.8 shows the dependence between m_q and R_1 quantitatively, for different values of the outer quark mass m_Q. It shows

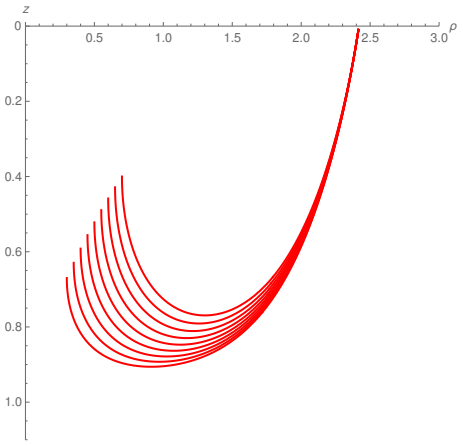

Figure 5.7: Shapes of double loops (in region (i)) for fixed outer radius $R_2 = 2.4$ and varying inner quark mass. Note that as the inner quark mass decreases, the radius at which these quarks are produced also decreases.

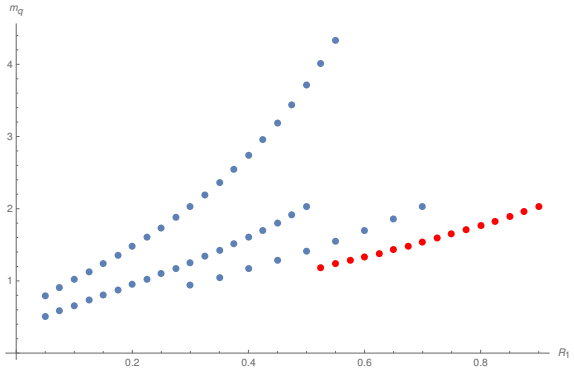

Figure 5.8: The relation between produced quark mass m_q and radius R_1 at which the pair is produced for various loops in the region (i). The plots are made for $m_Q = 9.5$ and for different outer radii $R_2 = \{1.6, 1.98, 2.37, 2.78\}$. The largest value of R_2 corresponds to the bottom (red) curve.

that when the total system is smaller (R_2 is smaller), quarks of the same mass m_q are produced at a radius R_1 which is also smaller. Figure 5.8 in addition suggests that if $R_1 \ll R_2$ the relation between R_1 and m_q becomes linear, as was the case for the Schwinger approximation (although the slopes of these lines depends on the size of the system, unlike for Schwinger). It is harder, and as we will argue below, less relevant, to produce similar plots for regions (ii) and (iii), as for the "squashed" loops in these regions the dependence of R_1 on m_q is rather weak (small variations of m_q lead to almost no change in R_1).

5.3 Extracting the probability for decay

Once the double loop solution is constructed we want to extract from it the probability for the flux tube to break. As in the case of the previous examples, in order to compute this probability, one first needs to compute the action of the solution (**II**) and then subtract from it the action of the action of the solution (**I**)

$$\Delta S(m_q, m_Q, R_2) = S_{II}(m_q, m_Q, R_2) - S_I(m_Q, R_2) \ . \tag{5.3.1}$$

Both these actions are evaluated for the loops (**I**) and (**II**) which have identical outer radius R_2, as this corresponds to the physical size of the initial system. Generically, the probability for a meson decay will depend on the size of the system R_2 and on the mass of the initial quarks m_Q, in addition to the mass of the pair produced quarks m_q. The dependence of the decay rate on the radius R_2 is something that one expects for realistic mesons, as this parameter is related to the angular momentum which the meson carries.

As noted before, for a given system of fixed and large enough R_2, generically there are three possible radia at which quarks can be pair produced, see figure 5.6. Each possible radius belongs to one of the regions (i), (ii) or (iii). Let us first analyse instantons in the region (i). Figure 5.9 shows the instanton action 5.3.1 in the region (i) as a function of quark mass. As the quark mass $m_q \to 0$, the instanton

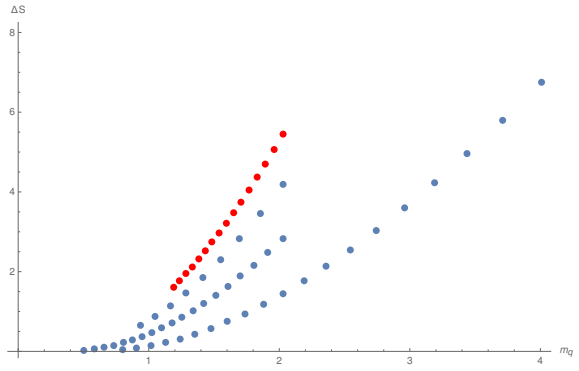

Figure 5.9: Instanton action as a function of quark mass m_q, plotted for different size systems $R_2 = \{1.6, 1.98, 2.37, 2.78\}$. The upper curve (red) with the largest action corresponds to the largest R_2. Each subsequent curve lower down corresponds to the next smallest value of R_2

action goes to zero, i.e. lighter quarks are more likely to be produced, as expected. We also see that the probability per unit time and volume depends on the size of the system, and that the probability for a larger (higher spin) meson to split is smaller than for smaller (lower spin) mesons. This may sounds unintuitive, as one may expect higher spin mesons to be more unstable. However, one should keep in mind that, when computing the lifetime of mesons, one still needs to multiply this probability with the meson volume, which is larger for higher-spin mesons.

We should also note that when evaluating the action for instantons using double loops, one always needs to make sure that the instanton action is smaller than the action of two disconnected loops which have the same radii R_1 and R_2 [126], [128]. For all the loops discussed in this paper, we have always checked that this holds so that no Gross-Ooguri-Olesen-Zarembo type phase transition takes place.

Evaluating the instanton action for radius R_1 in regions (ii) and (iii) one gets that $S(R_{1(\mathrm{i})}, R_2) < S(R_{1(\mathrm{ii})}, R_2) < S(R_{1(\mathrm{iii})}, R_2)$. We note however, that the difference between these three actions is minimal, less than a percent. Hence it seems that decay in the region (i) is the most dominant, although only marginally. Shapes of generic loops in regions (i), (ii) and (iii) which have the same R_2 are plotted in figure 5.10. At first glance it may look strange that loops in the region (ii) and (iii) have

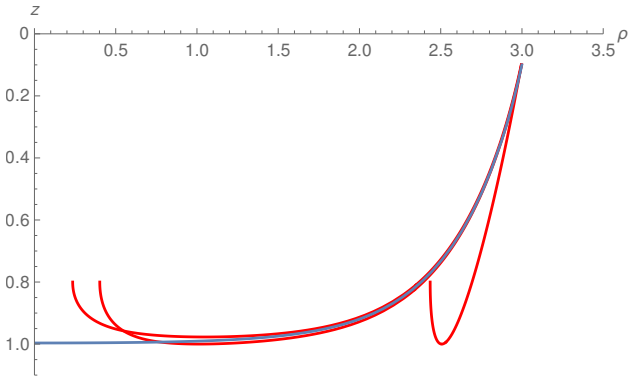

Figure 5.10: Double loops in the regions (i), (ii) and (iii) for the same outer radius $R_2 = 3.0$ and inner quark mass $m_q = 0.62$ (corresponding to $z_{m_q} = 0.8$). The blue curve extending all the way to $\rho = 0$ is a single loop with the same radius $R_2 = 3.0$.

larger action than the action of the loop (i), given that loops (ii) and (iii) look like squashed version of loop (i). However, none of these loops is strictly rectangular and for given fixed R_2 they do not have tips which are the same distance from the wall. So in order to compare actions one needs to evaluate them explicitly.

It is unclear to us at present what is the physical relevance of the squashed loops, in particular the very squashed loops in region (iii). These loops seems to suggest the existence of "exotic" decay channels for meson decay, where the pair-produced quarks remove most of the flux tube in the decay. It could be that, once the treatment of the angular momentum is taken properly into account, these decays are forbidden due to selection rules.

So in summary, the computation outlined above produces the probability for the decay of mesons of a particular size (spin). As described in the previous section, it is hard to compare our findings, even at qualitative level, with experimental data, as these are mostly not known for higher spin mesons. However, one expects that in a particular limit, the holographic computation should reproduce the computations of CNN and Schwinger which were outlined in section 2.4. Both these computations work with a constant (chromo)electric field in infinite volume and in the approximation where the produced quarks do not back-react on the field.

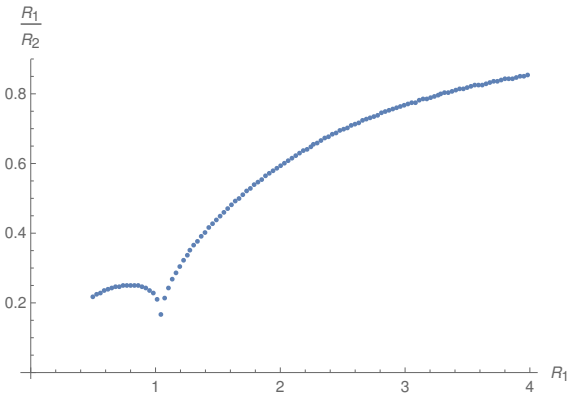

Figure 5.11: Relative radius R_1/R_2 of the system as a function of the inner radius R_1 for a fixed chosen mass $m_1 = 1.5$. The largest effective volume is achieved for configurations near the boundary between region (i) and (ii) in the notation of figure 5.6.

In order to achieve a large-volume limit in the holographic set up, one needs to look at long strings, with a horizontal part which is as large as possible in comparison to

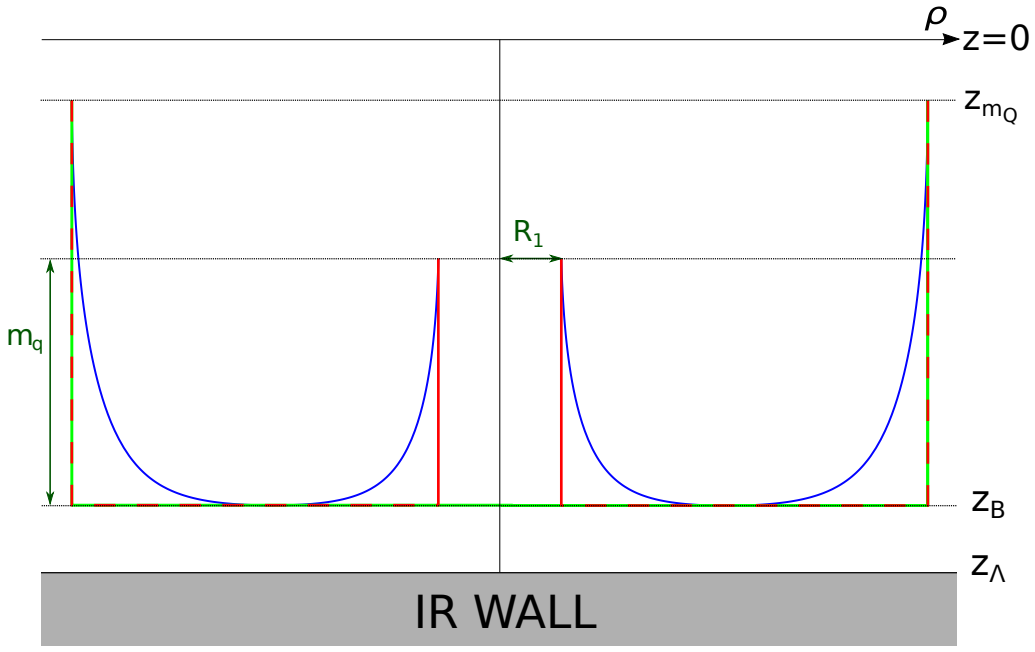

Figure 5.12: U-shaped loop approximation (red rectangular straight lines for the double loop, green straight lines for the single loop which is to be subtracted). The dashed parts are the same for the single and double loop solutions. For comparison we have also displayed an actual solution (blue curve).

the radius R_1. Figure 5.11 shows the effective size of the system, i.e. the distance R_1 at which the quarks are produced versus the full size of the system R_2 for quarks of fixed mass m_q. We see that the largest effective volume is achieved for loops at the boundary between the regions (i) and (ii). Note that having the largest effective volume does not mean that the instanton action for these loops is the smallest for a given m_q fixed. By looking at shapes of these large-volume loops, see figure 5.10, we see that they look most stretched and moreover they look most like rectangular U-shaped loops. In order to get an idea of what we should expect the action for these loops to look like in the full numerical solution, let us consider an approximation of these large-volume loops with rectangular U-shaped loops, as indicated in figure 5.12. In this approximation, the action of the outer part of the loop (the dashed red segments in the figure) is the same for single and double loops and does not contribute to the instanton action. We therefore find that

$$\Delta S_{\text{inst}} \sim S_{\text{tube}} - S_{\text{disc}} \sim 2\pi R_1 m_q - R_1^2 \pi T \,, \tag{5.3.2}$$

where we have used that m_q is proportional to the height of the tube, see (5.2.7).

Motivated by this discussion, it is interesting to consider an approximation in which we assume that the shape of the single and double loop solutions is the same everywhere from the bottom of the double loop at $\rho = R_B$ all the way to $\rho = R_2$. We will furthermore approximate the shape of the single loop solution by a straight line segment at constant $z = z_B$, reaching from $\rho = 0$ to $\rho = R_B$. This is an 'infinite volume approximation' in the sense that it holds when $R_1 \ll R_2$. As we have discussed earlier, the best way to obtain such large volume strings is to focus at double loops at the top of the peak between regions (i) and (ii) of figure 5.5, for small quark mass m_q. For these strings we find a nice linear relation between R_1 and m_q, see figure 5.13. Furthermore, when we plot the instanton action ΔS versus the produced quark mass m_q for these loops, one recovers a quadratic relation, see figure 5.14. While the best fit is quadratic, like for Schwinger, there is a nonvanishing constant present. One could remove such a term by modifying the normalisation, and it would

anyhow be cancelled in a computation of the ratio of any two probabilities, so it is irrelevant. We should also comment that the numerical factor in front of m_q^2 in this fit differs from the factor of $\pi/4$ in the Schwinger/CNN formula (2.4.18), which is what one expects. The expression (2.4.18) is valid only qualitatively in QCD and also our holographic model is not a dual of real QCD, so one should expect these kind of differences between the two results.

The probability P_{pp} for a flux tube to break, per unit length and unit time, is obtained by exponentiation of the instanton action. In the approximation of large mesons with an (infinitely long) flux tube, translation invariance implies that the total probability for a meson to split will be given by $P_{pp}L$, where L is the length of the flux tube. In finite-size systems however, P_{pp} will in general depend on the position along the flux tube a well as the size of the system. In order to evaluate the full probability we would first need to construct the non-axially symmetric instantons, and then integrate contributions of these instantons over the full length of the flux tube.

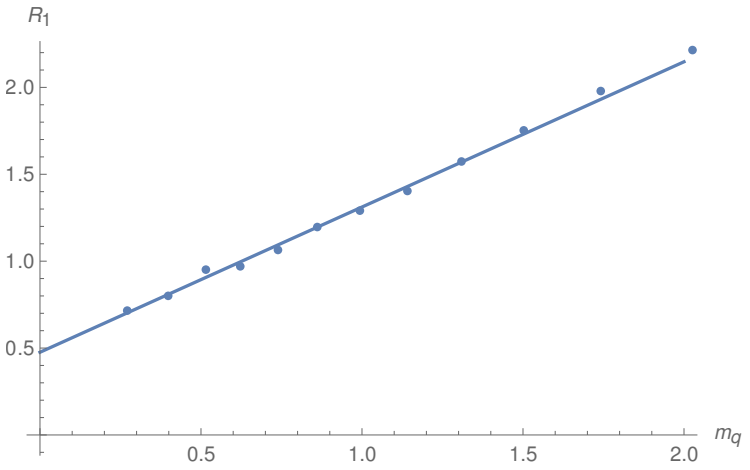

Figure 5.13: Linear relation between the radius at which quarks are produced and their mass, obtained from the series of "maximal" loops on the boundary between regions (i) and (ii).

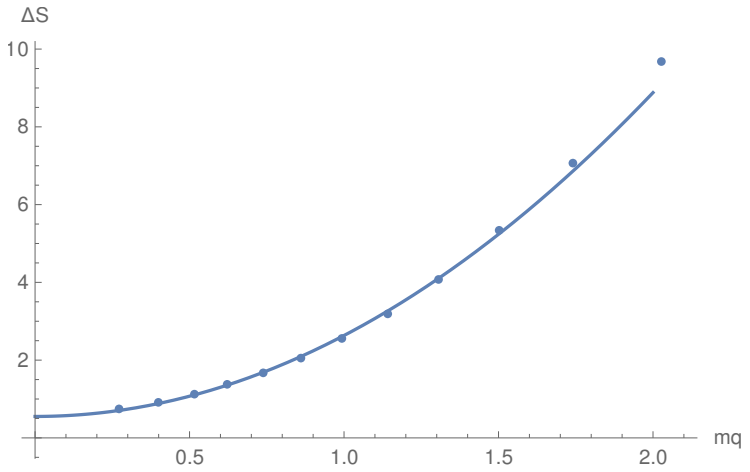

Figure 5.14: Quadratic dependence of the instanton action ΔS on the mass m_q of the pair-produced quarks in the 'infinite volume limit approximation' in which one considers only loops near the boundary between region (i) and (ii).

Chapter 6

Conclusions and Outlook

Meson decay was investigated using a toy flat space model in section 2.6 and a $D4/D8$ Sakai Sugimoto model in chapter 5.

In the first model mesons are represented by a pair of massive particles connected with a relativistic string (flux tube) in flat space. In order to study their decays, we have analytically constructed the worldsheet instanton configuration which interpolates between two mesonic particles. Using this instanton, it was possible to reproduce, up to an overall numerical factor, the formula (2.4.18) for the probability of breaking the QCD flux tube, derived a long time ago by Casher et al. [18]. They derived their formula by making a direct replacement of various quantities in the QED formula with the analogous quantities in QCD. In contrast, in this approach the connections between the theories followed naturally from our initial set up, rather than being postulated. After comparing the results for the decay probabilities it followed that the chromoelectric field had the same role as an elastic string. The derivation is very simple, yet it produces quite a non-trivial field theory result. However, it was rudimentary in the sense that only planar processes have been considered, where both in- and outgoing particles lie in the same plane. It would be interesting to generalise this derivation to allow for the presence of transverse momenta of the outgoing particles.

All of the flat space models (whether Schwinger, CNN or old string) share one

'feature': in order to incorporate (pair production of) quarks one has to introduce an extra mass term in the action by hand. In the holographic models, in contrast, there is an unified treatment of the flux tube and quarks.

In chapter 5, a holographic framework for studying the decay of large-spin mesons was developed and applied to the $D4/D8$ Sakai Sugimoto model. In the holographic approaches a family of worldsheet instanton configurations was constructed, which interpolated between an incoming large-spin meson and two outgoing large-spin mesons. The generic instanton describes the decay in which both the finite size of the system and the backreaction of the pair-produced particles is taken into account. In this sense, the set up is more powerful than either CNN or Schwinger computations which only give the probability in the large volume limit and with no backreaction taken into account. A shortcoming of the computation is that it is restricted to cylindrically symmetric decay channels. In the infinite volume limit the probability is the same for breaking at all points, but in a finite-size system we expect the probability to be different along the flux tube. It would be very important to study less symmetric decay.

When constructing instanton configurations for finite-size mesons, an interesting decay channel was discovered in which the pair-produced quarks 'eat' most of the flux tube, leading to very short outgoing mesons. At the moment it is not clear to us what is the physical significance of such a decay channel. One possibility is that once the angular momentum is properly taken into account (as it is not in our Euclidean framework) these exotic decay channels will be forbidden by a selection rule. It would be interesting to investigate this question in the future. Related to this is the question of proper treatment of angular momentum of mesons in the holographic setup. One expects that angular momentum modifies decay rates, as it provides an extra centrifugal potential for pair-produced quarks. Some of these effects have been investigated for the Schwinger process in [129].

In order to cross check our computation, the large volume limit was also investigated. As expected, the qualitative form of the Schwinger/CNN formula was rediscovered,

up to a numerical factor. The long strings which were used in this large-volume limit offer a natural playground in which one could try to set up a systematic study of finite-size effects. Namely, for large, but finite-size systems, the probability for a string to decay should have an expansion in powers of $\frac{R_1}{R_2}$, where R_1 is the radius at which quarks are produced and R_2 is the size of the system. It would be interesting to quantitatively study this expansion using the holographic set up.

It would also be interesting to extend the analysis to finite temperature field theory. By introducing a horizon in the Sakai-Sugimoto setup one could generalise the instanton configuration to this background, and obtain the thermal probability for a flux tube to split.

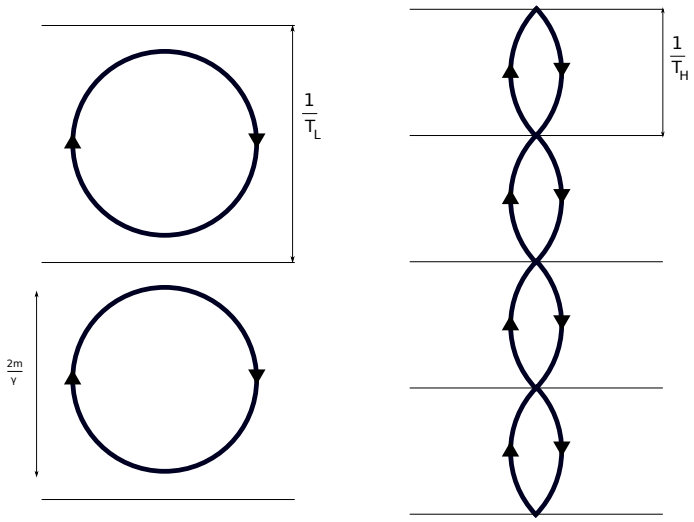

Figure 6.1: Instanton in finite tempature Sakai Sugimoto for two different temperatures $T_L < T_H$.

As discussed in section 4.2 – in the metric for finite temperature the coordinates t and x_4 effectively interchange from what they were in the zero temperature case. Therefore the time direction becomes periodic. This means that at high temperatures

$$\frac{2m_q}{\gamma} < \frac{1}{T} \tag{6.0.1}$$

we get the circular worldsheet instatons being 'cut-off' and forming 'lemon' instatons. [19]–[22]. This is shown in figure 6.1. The analysis then proceeds as before.

Worldline instanton methods for calculating meson decay rates have shown a lot

of promise and there are many interesting avenues for further developments and improvements. They do currently lag behind more phenomenological methods, such as the Lund model, when it comes to the range of systems that have been studied and the accuracy of decay calculations. However, their relative lack of need for fine tuning parameters by hand and relative ease of doing calculations indicate that this is an area worth pursuing.

Appendix A

Point Particles and String Comparison Calculations

A.1 Point Particle Action

A.1.1 Explicitly Circular Solution

We will first consider point particle pair production from a constant field. The relevant Minkowski action for a point particle of mass m in a field $A_\mu = -\frac{1}{2}F_{\mu\nu}X^\nu$ is given by

$$S_M = \int \mathrm{d}\tau \left(\frac{1}{2}\frac{\dot{X}^2}{e} - \frac{1}{2}em^2 + A_\mu \dot{X}^\mu \right). \tag{A.1.1}$$

We may then Wick rotate to Euclidean spacetime using

$$\tau \to -i\tau \tag{A.1.2}$$

$$X^0 \to -iX^0 \tag{A.1.3}$$

$$A^0 \to -iA^0. \tag{A.1.4}$$

We do this since, as explained by Semenoff and Zarembo [16], in Minkowski spacetime, there is a potential barrier that must be overcome for pair creation to happen. This

is not possible classically. However, by Wick rotating to Euclidean spacetime, we effectively flip the sign of the potential, allowing us to calculate an instanton solution.

The Wick rotation leads to

$$\begin{aligned}(X\cdot X)_M &= -(X^0)^2+(X^1)^2+(X^2)^2+(X^3)^2\\ &\downarrow\\ (X^0)^2+(X^1)^2+(X^2)^2+(X^3)^2 &= (X\cdot X)_E\end{aligned} \tag{A.1.5}$$

such that

$$\dot{X}^2 \to -\dot{X}^2 \tag{A.1.6}$$

$$A_\mu \dot{X} \to iA_\mu \dot{X}^\mu. \tag{A.1.7}$$

Rescaling such that

$$e = 2T \tag{A.1.8}$$

and finally setting the periodic boundary condition used by Semenoff and Zarembo [16]

$$X^\mu(\tau+1) = X^\mu \tag{A.1.9}$$

we recover the Euclidean action found in that paper:

$$S_E = \int_0^1 \mathrm{d}\tau \left(\frac{\dot{X}^2}{4T} + m^2 T - iA_\mu \dot{X}^\mu\right). \tag{A.1.10}$$

Taking the Euler-Lagrange equation for the einbein T we find

$$T = \frac{\sqrt{\dot{X}^2}}{2m}. \tag{A.1.11}$$

Substituting (A.1.11) back into (A.1.12) we find that we recover the Nambu-Goto form of the action:

$$S_E = \int_0^1 \mathrm{d}\tau \left(m\sqrt{\dot{X}^2} + \frac{i}{2}F_{\mu\nu}X^\nu \dot{X}^\mu\right), \tag{A.1.12}$$

where we have also expanded A_μ.

Now, taking the Euler-Lagrange equations for X_μ we find

$$\frac{i}{2}F_{\nu\mu}\dot{X}^\nu = \frac{\mathrm{d}}{\mathrm{d}\tau}\left(\frac{m}{2}\frac{2\dot{X}_\mu}{\sqrt{\dot{X}^2}} + \frac{i}{2}F_{\mu\nu}X^\nu\right) \tag{A.1.13}$$

$$iF_{\nu\mu}\dot{X}^\nu = \frac{2m\ddot{X}_\mu}{\sqrt{\dot{X}^2}} - \frac{2m\dot{X}_\mu}{\left(\dot{X}^2\right)^{\frac{3}{2}}}\dot{X}^\nu\ddot{X}_\nu + iF_{\mu\nu}\dot{X}^\nu. \tag{A.1.14}$$

As in Semenoff and Zarembo [16], we choose the field $F_{\mu\nu}$ to have non-zero components

$$F_{01} = -F_{10} = -iE \tag{A.1.15}$$

and try the ansatz

$$X_\mu = R\begin{pmatrix}\cos(2\pi n\tau)\\ \sin(2\pi n\tau)\\ 0\\ 0\end{pmatrix}. \tag{A.1.16}$$

For $\mu = 0$, (A.1.14) then becomes

$$-(2\pi n)ER\cos(2\pi n\tau) = -2(2\pi n)m\,\cos(2\pi n\tau) + (2\pi n)ER\cos(2\pi n\tau). \tag{A.1.17}$$

Which means that the equations of motion are satisfied by (A.1.16) for

$$R = \frac{m}{E}. \tag{A.1.18}$$

Substituting (A.1.16) back into (A.1.12) we find the classical Euclidean action reduces to

$$S_E = \frac{\pi m^2}{E}n, \tag{A.1.19}$$

as found by Semenoff and Zarembo [16].

A.1.2 Static Gauge Circular Solution

We may wish to consider solving the problem in the static gauge, as this is what we will do in the case of the string. Looking again at the point particle Lagranian given by Semenoff and Zarembo [16]

$$L = \frac{\dot{X}_\mu \dot{X}^\mu}{4T} + m^2 T - iA_\mu \dot{X}^\mu \tag{A.1.20}$$

$$L = m\sqrt{\dot{X}_\mu \dot{X}^\mu} - iA_\mu \dot{X}^\mu \tag{A.1.21}$$

and setting

$$X_0 = t \qquad X_1 = x \qquad A_0 = iEx \qquad A_1 = 0 \tag{A.1.22}$$

we find

$$L = m\sqrt{1+\dot{x}^2} + Ex. \tag{A.1.23}$$

The Euler-Lagrange equation for this gives

$$\frac{\mathrm{d}}{\mathrm{d}t}\left(m\frac{\dot{x}}{\sqrt{1+\dot{x}^2}}\right) = E \tag{A.1.24}$$

which gives two possible solutions

$$\dot{x} = \frac{Et}{\sqrt{m^2 - E^2t^2}} \tag{A.1.25}$$

$$x = -\frac{1}{E}\sqrt{m^2 - E^2t^2} \tag{A.1.26}$$

$$S = m\int_{-\frac{m}{E}}^{\frac{m}{E}} \left(\sqrt{\frac{1}{1-\left(\frac{E}{m}\right)^2 t^2}} - \sqrt{1-\left(\frac{E}{m}\right)^2 t^2}\right)\mathrm{d}t = \frac{\pi}{2}\frac{m^2}{E} \tag{A.1.27}$$

$$\dot{x} = -\frac{Et}{\sqrt{m^2 - E^2t^2}} \tag{A.1.28}$$

$$x = \frac{1}{E}\sqrt{m^2 - E^2t^2} \tag{A.1.29}$$

$$S = m\int_{-\frac{m}{E}}^{\frac{m}{E}} \left(\sqrt{\frac{1}{1-\left(\frac{E}{m}\right)^2 t^2}} + \sqrt{1-\left(\frac{E}{m}\right)^2 t^2}\right)\mathrm{d}t = \frac{3\pi}{2}\frac{m^2}{E} \tag{A.1.30}$$

where we have used

$$\int_{-\frac{1}{a}}^{\frac{1}{a}} \sqrt{\frac{1}{1-a^2t^2}} = \frac{1}{a}\left[\arcsin at\right]_{-\frac{1}{a}}^{0} = \frac{\pi}{a} \tag{A.1.31}$$

$$\int_{-\frac{1}{a}}^{\frac{1}{a}} \sqrt{1-a^2t^2} = \frac{1}{2a}\left[at\sqrt{1-a^2t^2} + \arcsin at\right]_{-\frac{1}{a}}^{0} = \frac{\pi}{2a} \tag{A.1.32}$$

The solution (A.1.26) is a clockwise semi-circular path, shown in figure A.1(a). The solution (A.1.29) is an anticlockwise semi-circular path, shown in figure A.1(b). In both cases, we see

$$x^2 + t^2 = \frac{m^2}{E^2}, \tag{A.1.33}$$

which agrees with Semenoff and Zarembo.

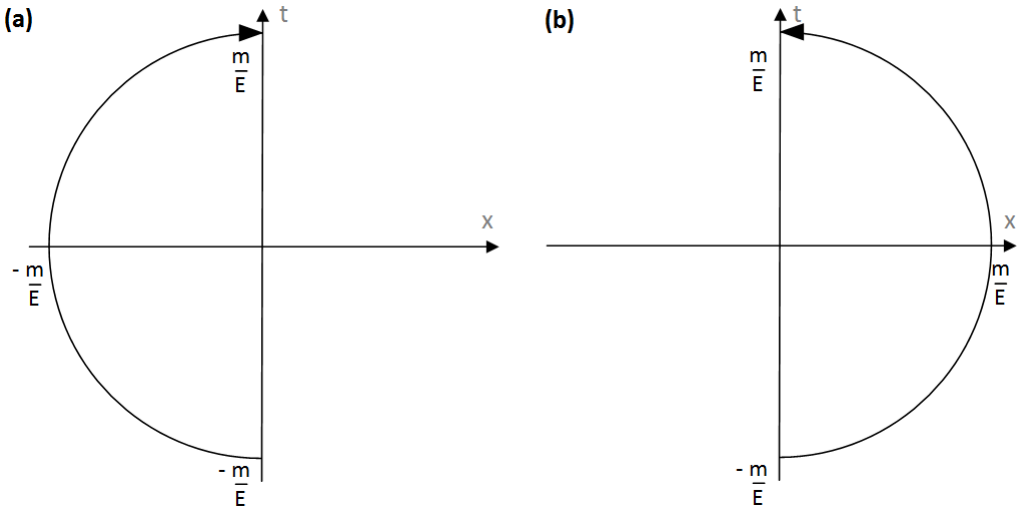

Figure A.1: Paths for the two possible solutions

Neither of the actions, however, gives Zarembo's solution of $\frac{\pi m^2}{E}$. We also need to consider the antiparticle, with Lagrangian

$$L = m\sqrt{1+\dot{x}^2} - Ex. \tag{A.1.34}$$

Similar to before, we find

$$\dot{x} = \frac{Et}{\sqrt{m^2 - E^2t^2}} \qquad \text{(A.1.35)}$$

$$x = -\frac{1}{E}\sqrt{m^2 - E^2t^2} \qquad \text{(A.1.36)}$$

$$\begin{aligned} S =& m\int_{-\frac{m}{E}}^{\frac{m}{E}} \Bigg(\sqrt{\frac{1}{1-\left(\frac{E}{m}\right)^2 t^2}} \\ &+ \sqrt{1-\left(\frac{E}{m}\right)^2 t^2} \Bigg) \mathrm{d}t \\ =& \frac{3\pi}{2}\frac{m^2}{E} \end{aligned} \qquad \text{(A.1.37)}$$

$$\dot{x} = -\frac{Et}{\sqrt{m^2 - E^2t^2}} \qquad \text{(A.1.38)}$$

$$x = \frac{1}{E}\sqrt{m^2 - E^2t^2} \qquad \text{(A.1.39)}$$

$$\begin{aligned} S =& m\int_{-\frac{m}{E}}^{\frac{m}{E}} \Bigg(\sqrt{\frac{1}{1-\left(\frac{E}{m}\right)^2 t^2}} \\ &- \sqrt{1-\left(\frac{E}{m}\right)^2 t^2} \Bigg) \mathrm{d}t \\ =& \frac{\pi}{2}\frac{m^2}{E} \end{aligned} \qquad \text{(A.1.40)}$$

The solution (A.1.36) is a clockwise semi-circular path, shown in figure A.1(a). The solution (A.1.39) is an anticlockwise semi-circular path, shown in figure A.1(b).

Looking at the paths of the solutions, we might assume that (A.1.26) goes together with (A.1.39), and (A.1.29) goes together with (A.1.36). Indeed, adding together the actions for the clockwise particle path (A.1.26) and the action for the anticlockwise anti-particle path (A.1.39) gives the action for the $n = 1$ instanton found by Semenoff and Zarembo.

We may also consider the change of momentum of the system. Considering the solution (A.1.26) we find

$$p = \frac{m\dot{x}}{\sqrt{1+\dot{x}^2}} = Et. \qquad \text{(A.1.41)}$$

Applying

$$\frac{\mathrm{d}V}{\mathrm{d}x} = \frac{\mathrm{d}p}{\mathrm{d}t} \qquad \text{(A.1.42)}$$

we find

$$V = Et, \qquad \text{(A.1.43)}$$

which is what we expected. In fact (A.1.42) is just (A.1.24) re-written in a different form. This does not immediately suggest how to determine the limits of integration.

An alternative method would be to consider when the particle comes on shell, that

is

$$p^\mu p_\mu = m^2. \tag{A.1.44}$$

We find

$$p_0 = \frac{\partial L}{\partial \dot{X}_0} = \frac{m\dot{X}_0}{\sqrt{\dot{X}_0^2 + \dot{X}_1^2}} - iA_0 = \frac{m}{\sqrt{1+\dot{x}^2}} + Ex \tag{A.1.45}$$

$$p_1 = \frac{\partial L}{\partial \dot{X}_1} = \frac{m\dot{X}_1}{\sqrt{\dot{X}_0^2 + \dot{X}_1^2}} - iA_1 = \frac{m\dot{x}}{\sqrt{1+\dot{x}^2}} \tag{A.1.46}$$

Therefore

$$p^\mu p_\mu = E^2 t^2. \tag{A.1.47}$$

The particle appears to be on shell at the initial point of the integration, $t = \frac{m}{E}$, and comes on shell again at the end point of the integration $p_\mu p^\mu$.

The result (A.1.44) may be considered unusual, as the system appears to be on shell only when the particle and anti-particle are together. Furthermore, the condition $p^\mu p_\mu = m^2$, which results from the equations of motion of a relativistic particle, appears to be broken. However, this is the consequence of the presence of the field. Considering the equation (A.1.21) we obtain

$$p_\mu = \frac{\dot{X}_\mu}{4T^2} - iA_\mu \tag{A.1.48}$$

and

$$\frac{\dot{X}_\mu \dot{X}^\mu}{4T^2} = m^2 \tag{A.1.49}$$

which, together, give

$$\left(p^0 + Ex\right)^2 + \left(p^1\right)^2 = m^2, \tag{A.1.50}$$

which is compatible with (A.1.44). However, we note that the momentum has been shifted by the field, and that (A.1.50) is the actual on shell condition, which is always obeyed.

A.2 String Action

A.2.1 Static Gauge Circular Solution

We consider a string with worldsheet parametrised by τ and σ, with σ running from 0 to π. At some $\tau = \tau^*$ the string splits at a point $\sigma = \sigma^*$.

As shown by Barbashov and Nesterenko [56], we can write the action for the unbroken string as

$$S = \int_{\tau_1}^{\tau_2} \mathrm{d}\tau \int_0^{\pi} \mathrm{d}\sigma\, \mathcal{L}_{bulk} + \int_{\tau_1}^{\tau_2} \mathrm{d}\tau\, \left(\mathcal{L}_{end,\,\sigma=0} + \mathcal{L}_{end,\,\sigma=\pi}\right) \tag{A.2.1}$$

$$= -\gamma \int_{\tau_1}^{\tau_2} \mathrm{d}\tau \int_0^{\pi} \mathrm{d}\sigma \sqrt{\left(\dot{X}\cdot X'\right)^2 - \dot{X}^2 X'^2} - m \int_{\tau_1}^{\tau_2} \mathrm{d}\tau \left(\sqrt{-\dot{X}^2(\tau,\sigma=0)} + \sqrt{-\dot{X}^2(\tau,\sigma=\pi)}\right), \tag{A.2.2}$$

where γ is a constant related to the string tension.

In Euclidean spacetime this becomes

$$S = \int_{\tau_1}^{\tau_2} \mathrm{d}\tau \int_0^{\pi} \mathrm{d}\sigma\, \mathcal{L}_{bulk} + \int_{\tau_1}^{\tau_2} \mathrm{d}\tau\, \mathcal{L}_{end} \tag{A.2.3}$$

$$= \gamma \int_{\tau_1}^{\tau_2} \mathrm{d}\tau \int_0^{\pi} \mathrm{d}\sigma \sqrt{-\left(\dot{X}\cdot X'\right)^2 + \dot{X}^2 X'^2} \; m \int_{\tau_1}^{\tau_2} \mathrm{d}\tau \left(\sqrt{\dot{X}^2(\tau,\sigma=0)} + \sqrt{\dot{X}^2(\tau,\sigma=\pi)}\right), \tag{A.2.4}$$

To find the equations of motion we require the variation of the action to be zero:

$$\begin{aligned} 0 = \delta S = &\int_{\tau_1}^{\tau_2} \mathrm{d}\tau \int_0^{\pi} \mathrm{d}\sigma \left(\frac{\partial \mathcal{L}_{bulk}}{\partial \dot{X}_\mu}\delta\dot{X}_\mu(\tau,\sigma) + \frac{\partial \mathcal{L}_{bulk}}{\partial X'_\mu}\delta X'_\mu(\tau,\sigma)\right) \\ &+ \int_{\tau_1}^{\tau_2} \mathrm{d}\tau \left(\frac{\partial \mathcal{L}_{end,\,\sigma=0}}{\partial \dot{X}_\mu}\delta\dot{X}_\mu(\tau,\sigma=0) + \frac{\partial \mathcal{L}_{end,\,\sigma=\pi}}{\partial \dot{X}_\mu}\delta\dot{X}_\mu(\tau,\sigma=\pi)\right) \qquad \text{(A.2.5)} \\ = &\int_0^{\pi} \mathrm{d}\sigma \left[\frac{\partial \mathcal{L}_{bulk}}{\partial \dot{X}_\mu}\delta X_\mu(\tau,\sigma)\right]_{\tau_1}^{\tau_2} + \int_{\tau_1}^{\tau_2} \mathrm{d}\tau \left[\frac{\partial \mathcal{L}_{bulk}}{\partial {X'}_\mu}\delta X_\mu(\tau,\sigma)\right]_0^{\pi} \\ &- \int_{\tau_1}^{\tau_2} \mathrm{d}\tau \int_0^{\pi} \mathrm{d}\sigma \left(\frac{\partial}{\partial\tau}\left(\frac{\partial \mathcal{L}_{bulk}}{\partial \dot{X}_\mu}\right) + \frac{\partial}{\partial\sigma}\left(\frac{\partial \mathcal{L}_{bulk}}{\partial X'_\mu}\right)\right)\delta X(\tau,\sigma) \\ &+ \left[\frac{\partial \mathcal{L}_{end,\,\sigma=0}}{\partial \dot{X}_\mu}\delta X_\mu(\tau,\sigma=0) + \frac{\partial \mathcal{L}_{end,\,\sigma=\pi}}{\partial \dot{X}_\mu}\delta X_\mu(\tau,\sigma=\pi)\right]_{\tau_1}^{\tau_2} \\ &- \int_{\tau_1}^{\tau_2} \mathrm{d}\tau \left(\frac{\partial}{\partial\tau}\left(\frac{\partial \mathcal{L}_{end,\,\sigma=0}}{\partial \dot{X}_\mu}\right)\delta X_\mu(\tau,\sigma=0)\right. \end{aligned}$$

$$+\frac{\partial}{\partial\tau}\left(\frac{\partial\mathcal{L}_{end,\,\sigma=\pi}}{\partial\dot{X}_\mu}\right)\delta X_\mu(\tau,\sigma=\pi)\Bigg) \tag{A.2.6}$$

$$\begin{aligned}
=&-\int_{\tau_1}^{\tau_2}\mathrm{d}\tau\int_0^{\pi}\mathrm{d}\sigma\left(\frac{\partial}{\partial\tau}\left(\frac{\partial\mathcal{L}_{bulk}}{\partial\dot{X}_\mu}\right)+\frac{\partial}{\partial\sigma}\left(\frac{\partial\mathcal{L}_{bulk}}{\partial X'_\mu}\right)\right)\delta X(\tau,\sigma)\\
&-\int_{\tau_1}^{\tau_2}\mathrm{d}\tau\left(\frac{\partial}{\partial\tau}\left(\frac{\partial\mathcal{L}_{end,\,\sigma=0}}{\partial\dot{X}_\mu}\right)+\frac{\partial\mathcal{L}_{bulk}}{\partial {X'}_\mu}\right)\Bigg|_{\sigma=0}\delta X_\mu(\tau,\sigma=0)\\
&-\int_{\tau_1}^{\tau_2}\mathrm{d}\tau\left(\frac{\partial}{\partial\tau}\left(\frac{\partial\mathcal{L}_{end,\,\sigma=\pi}}{\partial\dot{X}_\mu}\right)-\frac{\partial\mathcal{L}_{bulk}}{\partial {X'}_\mu}\right)\Bigg|_{\sigma=\pi}\delta X_\mu(\tau,\sigma=\pi),
\end{aligned} \tag{A.2.7}$$

where, to obtain (A.2.6), we integrated by parts and, to obtain (A.2.7), we used the standard assumption that $\delta X_\mu(\tau=\tau_1,\sigma)=\delta X_\mu(\tau=\tau_2,\sigma)=0$.

The first term of (A.2.7) yields the expected equation of motion for the bulk, that is for $0<\sigma<\pi$:

$$\frac{\partial}{\partial\tau}\left(\frac{\partial\mathcal{L}_{bulk}}{\partial\dot{X}_\mu}\right)+\frac{\partial}{\partial\sigma}\left(\frac{\partial\mathcal{L}_{bulk}}{\partial X'_\mu}\right)=0, \tag{A.2.8}$$

The last two terms of (A.2.7) give the boundary equations of motion:

$$\left(\frac{\partial}{\partial\tau}\left(\frac{\partial\mathcal{L}_{end,\,\sigma=0}}{\partial\dot{X}_\mu}\right)+\frac{\partial\mathcal{L}_{bulk}}{\partial {X'}_\mu}\right)\Bigg|_{\sigma=0}\delta X_\mu(\tau,\sigma=0)=0 \tag{A.2.9}$$

$$\left(\frac{\partial}{\partial\tau}\left(\frac{\partial\mathcal{L}_{end,\,\sigma=\pi}}{\partial\dot{X}_\mu}\right)-\frac{\partial\mathcal{L}_{bulk}}{\partial {X'}_\mu}\right)\Bigg|_{\sigma=\pi}\delta X_\mu(\tau,\sigma=\pi)=0. \tag{A.2.10}$$

In each case we may choose either the first part of the equation to be zero – this is the Neumann boundary condition – or the second part of the equation to be zero – this is the Dirichlet boundary condition.

Bardeen et al [57] suggest a general analytic Lorentzian solution for a string with two massive free moving endpoints:

$$X_0=\tau \tag{A.2.11}$$

$$X_1=\pm\left(\frac{2\sigma}{\pi}-1\right)\left(\sqrt{(\tau-\tau_0)^2+k^2}+\sqrt{c}\right) \tag{A.2.12}$$

where

$$k=\frac{m}{\gamma}\qquad\qquad x=\frac{\pi^2}{4}+k^2. \tag{A.2.13}$$

We may guess that the Euclidean solution for one stationary endpoint and one moving endpoint is:

$$X_0 = \tau - \tau_0 \tag{A.2.14}$$

$$X_1 = b\,\frac{\sigma}{\pi}\left(\sqrt{-(\tau-\tau_0)^2 + k^2} + x_0\right), \tag{A.2.15}$$

where b and x_0 are constants to be found

We must test whether this satisfies the bulk equations of motion (A.2.8) in the Euclidean case. Writing $X_1 = x$ we find

$$\frac{\partial \mathcal{L}_{bulk}}{\partial \dot{X}_\mu} = -\gamma \frac{-(\dot{X}\cdot X')X'^\mu + \dot{X}^\mu X'^2}{\sqrt{-(\dot{X}\cdot X')^2 + \dot{X}^2 X'^2}} \tag{A.2.16}$$

$$= -\gamma \frac{-\dot{x}x'X'^\mu + x'^2\dot{X}^\mu}{\sqrt{-\dot{x}^2x'^2 + (1+\dot{x}^2)x'^2}} \tag{A.2.17}$$

$$= -\gamma\left(x'\dot{X}^\mu - \dot{x}X'^\mu\right) \tag{A.2.18}$$

$$\frac{\partial \mathcal{L}_{bulk}}{\partial X'_\mu} = -\gamma \frac{-(\dot{X}\cdot X')\dot{X}^\mu + X'^\mu \dot{X}^2}{\sqrt{-(\dot{X}\cdot X')^2 + \dot{X}^2 X'^2}} \tag{A.2.19}$$

$$= -\gamma \frac{-\dot{x}x'\dot{X}^\mu + (1+\dot{x}^2)X'^\mu}{\sqrt{-\dot{x}^2x'^2 + (1+\dot{x}^2)x'^2}} \tag{A.2.20}$$

$$= -\gamma\left(-\dot{x}\dot{X}^\mu + \left(\frac{1+\dot{x}^2}{x'}\right)X'^\mu\right) \tag{A.2.21}$$

For $\mu = 0$ we find that

$$\frac{\partial}{\partial\tau}\left(\frac{\partial \mathcal{L}_{bulk}}{\partial \dot{X}_\mu}\right) + \frac{\partial}{\partial\sigma}\left(\frac{\partial \mathcal{L}_{bulk}}{\partial X'_\mu}\right) = -\gamma\left(\frac{\partial x'}{\partial\tau} - \frac{\partial \dot{x}}{\partial\sigma}\right) = 0 \tag{A.2.22}$$

as required. For $\mu = 1$ we find that

$$\frac{\partial}{\partial\tau}\left(\frac{\partial \mathcal{L}_{bulk}}{\partial \dot{X}_\mu}\right) + \frac{\partial}{\partial\sigma}\left(\frac{\partial \mathcal{L}_{bulk}}{\partial X'_\mu}\right) = -\gamma\left(\frac{\partial}{\partial\tau}\left(x'\dot{x} - \dot{x}x'\right) + \frac{\partial}{\partial\sigma}\left(-\dot{x}^2 + x'\frac{1+\dot{x}^2}{x'}\right)\right) = 0 \tag{A.2.23}$$

as required. It appears that the bulk equations of motion are satisfied for any $x = x(\tau,\sigma)$. We then find that the Dirichlet boundary condition for $\sigma = 0$ is trivially satisfied.

Similarly, considering the moving endpoint Neumann condition we find

$$\frac{\partial}{\partial\tau}\left(\frac{\partial\mathcal{L}_{end,\sigma=\pi}}{\partial\dot{X}_\mu}\right)-\frac{\partial\mathcal{L}_{bulk}}{\partial{X'}_\mu}=-m\frac{\partial}{\partial\tau}\left(\frac{\dot{X}^\mu}{\sqrt{\dot{X}^2}}\right)+\gamma\left(-\dot{x}\dot{X}^\mu+\left(\frac{1+\dot{x}^2}{x'}\right)X'^\mu\right)=0. \tag{A.2.24}$$

To evaluate this, we will need to find the derivatives of x, that is

$$\dot{x}=-b\frac{\sigma}{\pi}\frac{(\tau-\tau_0)}{\sqrt{-(\tau-\tau_0)^2+k^2}} \tag{A.2.25}$$

$$\ddot{x}=-b\frac{\sigma}{\pi}\frac{k^2}{(-(\tau-\tau_0)^2+k^2)^{\frac{3}{2}}} \tag{A.2.26}$$

Looking at $\mu=0$, we find

$$\begin{aligned}\frac{\partial}{\partial\tau}\left(\frac{\partial\mathcal{L}_{end,\sigma=\pi}}{\partial\dot{X}_0}\right)-\left.\frac{\partial\mathcal{L}_{bulk}}{\partial{X'}_0}\right|_{\sigma=\pi}&=\frac{\partial}{\partial\tau}\left(-\frac{m}{\sqrt{1+\dot{x}^2}}\right)-\gamma\dot{x}\\&=-m\frac{\partial}{\partial\tau}\left(\sqrt{\frac{-(\tau-\tau_0)^2+k^2}{(b^2-1)(\tau-\tau_0)^2+k^2}}\right)+\frac{\gamma b(\tau-\tau_0)}{\sqrt{-(\tau-\tau_0)^2+k^2}}\end{aligned} \tag{A.2.27}$$

We note that this only satisfies the required condition for $b=-1$, in which case we find

$$\frac{\partial}{\partial\tau}\left(\frac{\partial\mathcal{L}_{end,\sigma=\pi}}{\partial\dot{X}_0}\right)-\left.\frac{\partial\mathcal{L}_{bulk}}{\partial{X'}_0}\right|_{\sigma=\pi}=m\frac{(\tau-\tau_0)}{k^2}\sqrt{\frac{k^2}{-(\tau-\tau_0)^2+k^2}}-\frac{\gamma(\tau-\tau_0)}{\sqrt{-(\tau-\tau_0)^2+k^2}}=0. \tag{A.2.28}$$

Similarly, for $\mu=1$, we find

$$\begin{aligned}\frac{\partial}{\partial\tau}\left(\frac{\partial\mathcal{L}_{end,\sigma=\pi}}{\partial\dot{X}_1}\right)-\left.\frac{\partial\mathcal{L}_{bulk}}{\partial{X'}_1}\right|_{\sigma=\pi}&=-m\frac{\partial}{\partial\tau}\left(\frac{\dot{x}}{\sqrt{1+\dot{x}^2}}\right)+\gamma\\&=m\frac{\partial}{\partial\tau}\left(\frac{-(\tau-\tau_0)}{\sqrt{-(\tau-\tau_0)^2+k^2}}\sqrt{\frac{-(\tau-\tau_0)^2+k^2}{k^2}}\right)+\gamma=0\end{aligned} \tag{A.2.29}$$

We note that the $\sigma=\pi$ endpoint satisfies

$$(\tau-\tau_0)^2+(x-x_0)^2=\left(\frac{m}{\gamma}\right)^2. \tag{A.2.30}$$

The solution corresponds precisely to Semenoff and Zarembo's solution for a massive particle moving in an electric field [16], with the string tension γ taking the place of the electric field strenght E.

If we consider the action for this solution, we find

$$\begin{aligned} S =&\gamma \int_{-\frac{m}{\gamma}}^{\frac{m}{\gamma}} \mathrm{d}\tau \int_0^{\pi} \mathrm{d}\sigma \sqrt{-\left(\dot{X}\cdot X'\right)^2 + \dot{X}^2 X'^2} \\ &+ m \int_{-\frac{m}{\gamma}}^{\frac{m}{\gamma}} \mathrm{d}\tau \left(\sqrt{\dot{X}^2(\tau,\sigma=0)} + \sqrt{\dot{X}^2(\tau,\sigma=\pi)}\right) \\ =&\gamma \int_{-\frac{m}{\gamma}}^{\frac{m}{\gamma}} \mathrm{d}\tau \int_0^{\pi} \mathrm{d}\sigma\, x' + m \int_{-\frac{m}{\gamma}}^{\frac{m}{\gamma}} \mathrm{d}\tau \left(1 + \sqrt{1+\dot{x}^2(\tau,\sigma=\pi)}\right) \\ =&\int_{-\frac{m}{\gamma}}^{\frac{m}{\gamma}} \mathrm{d}\tau \left(m - \gamma x(\tau,\sigma=0)\right) + \int_{-\frac{m}{\gamma}}^{\frac{m}{\gamma}} \mathrm{d}\tau \left(m\sqrt{1+\dot{x}^2(\tau,\sigma=\pi)} + \gamma x(\tau,\sigma=\pi)\right). \end{aligned} \tag{A.2.31}$$

Naively, the first term of this expression is associated with the stationary, $\sigma = 0$, endpoint while the second is associated with the moving, $\sigma = \pi$, endpoint. This second term has the same form as the point particle action (A.1.23) for the problem considered by Semenoff and Zarembo [16]. Indeed writing down the solution and the Lagrangian for each of the two moving endpoints after the string splits, ignoring the contributions from the string and other endpoints, we find:

$$x_L = -\sqrt{-(\tau-\tau_0)^2 + k^2} + x_0 \tag{A.2.32}$$

$$L_L = -\left(m\sqrt{1+\dot{x}^2} + \gamma x\right) \tag{A.2.33}$$

$$x_R = +\sqrt{-(\tau-\tau_0)^2 + k^2} + x_0 \tag{A.2.34}$$

$$L_R = -\left(m\sqrt{1+\dot{x}^2} - \gamma x\right) \tag{A.2.35}$$

Therefore the two endpoints move along the same shape paths as shown in figure A.1 and, using (A.1.31) and (A.1.32), we find that the action for the two moving endpoints evaluates to $\frac{\pi m^2}{\gamma}$. This is exactly the same as the Semenoff and Zarembo [16] result, with tension γ being equivalent to field strength E.

More rigorously, however, we must first calculate the action of the full system, as shown in figure A.2(a) with both the left and right components of the string, and

subtract the 'background', as shown in figure A.2(b). That is, the correct action to use for calculating the probability of string splitting will be:

$$S = S_{sol} - S_{back} \tag{A.2.36}$$

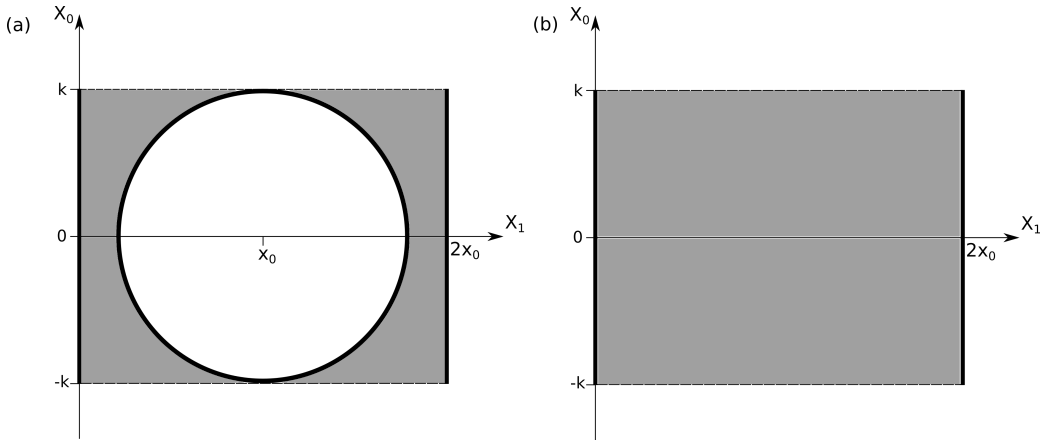

Figure A.2: Graph showing (a) motion of the string with splitting (b) motion of the string without splitting, where $k = \frac{m}{\gamma}$.

Writing the full solution for both the left and right segments of the string, and not just the endpoints, and setting $\tau_0 = 0$, we find

$$X_{L0} = X_{R0} = \tau \tag{A.2.37}$$

$$X_{L1} = x_L = -\frac{\sigma}{\pi}\left(\sqrt{-\tau^2 + k^2} - x_0\right) \tag{A.2.38}$$

$$X_{R1} = x_R = \left(1 - \frac{\sigma}{\pi}\right)\left(\sqrt{-\tau^2 + k^2} + x_0\right) + 2x_0\frac{\sigma}{\pi} \tag{A.2.39}$$

We therefore find

$$\begin{aligned}
S_{sol} =& \gamma \int_{-\frac{m}{\gamma}}^{\frac{m}{\gamma}} \mathrm{d}\tau \int_0^{\pi} \mathrm{d}\sigma \sqrt{-\left(\dot{X}_L \cdot X_L'\right)^2 + \dot{X}_L^2 {X_L'}^2} \\
&+ m \int_{-\frac{m}{\gamma}}^{\frac{m}{\gamma}} \mathrm{d}\tau \left(\sqrt{\dot{X}_L^2(\tau, \sigma = 0)} + \sqrt{\dot{X}_L^2(\tau, \sigma = \pi)}\right) \\
&+ \gamma \int_{-\frac{m}{\gamma}}^{\frac{m}{\gamma}} \mathrm{d}\tau \int_0^{\pi} \mathrm{d}\sigma \sqrt{-\left(\dot{X}_R \cdot X_R'\right)^2 + \dot{X}_R^2 {X_R'}^2} \\
&+ m \int_{-\frac{m}{\gamma}}^{\frac{m}{\gamma}} \mathrm{d}\tau \left(\sqrt{\dot{X}_R^2(\tau, \sigma = 0)} + \sqrt{\dot{X}_R^2(\tau, \sigma = \pi)}\right) \\
&+ \gamma \int_{-\frac{m}{\gamma}}^{\frac{m}{\gamma}} \mathrm{d}\tau \int_0^{\pi} \mathrm{d}\sigma\, {x_L}' + m \int_{-\frac{m}{\gamma}}^{\frac{m}{\gamma}} \mathrm{d}\tau \left(\sqrt{\dot{X}_L^2(\tau, \sigma = 0)} + \sqrt{\dot{X}_L^2(\tau, \sigma = \pi)}\right) \\
&+ \gamma \int_{-\frac{m}{\gamma}}^{\frac{m}{\gamma}} \mathrm{d}\tau \int_0^{\pi} \mathrm{d}\sigma\, {x_R}' + m \int_{-\frac{m}{\gamma}}^{\frac{m}{\gamma}} \mathrm{d}\tau \left(\sqrt{\dot{X}_R^2(\tau, \sigma = 0)} + \sqrt{\dot{X}_R^2(\tau, \sigma = \pi)}\right)
\end{aligned}$$

$$
\begin{aligned}
=&\gamma\int_{-\frac{m}{\gamma}}^{\frac{m}{\gamma}}\mathrm{d}\tau\,\Big(x_L(\tau,\sigma=\pi)-x_L(\tau,\sigma=0)\Big)+m\int_{-\frac{m}{\gamma}}^{\frac{m}{\gamma}}\mathrm{d}\tau\,\left(1+\sqrt{1+\dot{x}_L^2(\tau,\sigma=\pi)}\right)\\
&+\gamma\int_{-\frac{m}{\gamma}}^{\frac{m}{\gamma}}\mathrm{d}\tau\,\Big(x_R(\tau,\sigma=\pi)-x_R(\tau,\sigma=0)\Big)+m\int_{-\frac{m}{\gamma}}^{\frac{m}{\gamma}}\mathrm{d}\tau\,\left(\sqrt{1+\dot{x}_R^2(\tau,\sigma=0)}+1\right)\\
=&\int_{-\frac{m}{\gamma}}^{\frac{m}{\gamma}}\mathrm{d}\tau\,\left(m\sqrt{1+\dot{x}_L^2(\tau,\sigma=\pi)}+\gamma x_L(\tau,\sigma=\pi)\right)\\
&+\int_{-\frac{m}{\gamma}}^{\frac{m}{\gamma}}\mathrm{d}\tau\,\left(m\sqrt{1+\dot{x}_R^2(\tau,\sigma=0)}-\gamma x_R(\tau,\sigma=0)\right)\\
&+\int_{-\frac{m}{\gamma}}^{\frac{m}{\gamma}}\mathrm{d}\tau\,\Big(2m+2x_0\Big). \qquad \text{(A.2.40)}
\end{aligned}
$$

For the background, we find

$$X_{B0}=\tau \qquad \text{(A.2.41)}$$

$$X_{B1}=2x_0\frac{\sigma}{\pi} \qquad \text{(A.2.42)}$$

Therefore

$$
\begin{aligned}
S_{back}=&+\gamma\int_{-\frac{m}{\gamma}}^{\frac{m}{\gamma}}\mathrm{d}\tau\int_0^{\pi}\mathrm{d}\sigma\,\sqrt{-\left(\dot{X}\cdot X'\right)^2+\dot{X}^2X'^2}\\
&+m\int_{-\frac{m}{\gamma}}^{\frac{m}{\gamma}}\mathrm{d}\tau\,\left(\sqrt{\dot{X}^2(\tau,\sigma=0)}+\sqrt{\dot{X}^2(\tau,\sigma=\pi)}\right)\\
&+\gamma\int_{-\frac{m}{\gamma}}^{\frac{m}{\gamma}}\mathrm{d}\tau\int_0^{\pi}\mathrm{d}\sigma\,\frac{2_0}{\pi}\;-2m\int_{-\frac{m}{\gamma}}^{\frac{m}{\gamma}}\mathrm{d}\tau\\
=&+\int_{-\frac{m}{\gamma}}^{\frac{m}{\gamma}}\mathrm{d}\tau\,\Big(2m+2x_0\Big). \qquad \text{(A.2.43)}
\end{aligned}
$$

Therefore

$$
\begin{aligned}
S=&+\int_{-\frac{m}{\gamma}}^{\frac{m}{\gamma}}\mathrm{d}\tau\,\left(m\sqrt{1+\dot{x}_L^2(\tau,\sigma=\pi)}+\gamma x_L(\tau,\sigma=\pi)\right)\\
&+\int_{-\frac{m}{\gamma}}^{\frac{m}{\gamma}}\mathrm{d}\tau\,\left(m\sqrt{1+\dot{x}_R^2(\tau,\sigma=0)}-\gamma x_R(\tau,\sigma=0)\right) \qquad \text{(A.2.44)}\\
=&+\frac{\pi m^2}{\gamma}, \qquad \text{(A.2.45)}
\end{aligned}
$$

again using (A.1.31) and (A.1.32), finding the same answer as with our naive assumption.

It is also useful to consider the situation where the outer endpoints of the split string are constrained to move in a circle, as shown in figure A.3(a). The 'background' for

this is shown in figure A.3(b). It may appear that we need to integrate in X_0 from

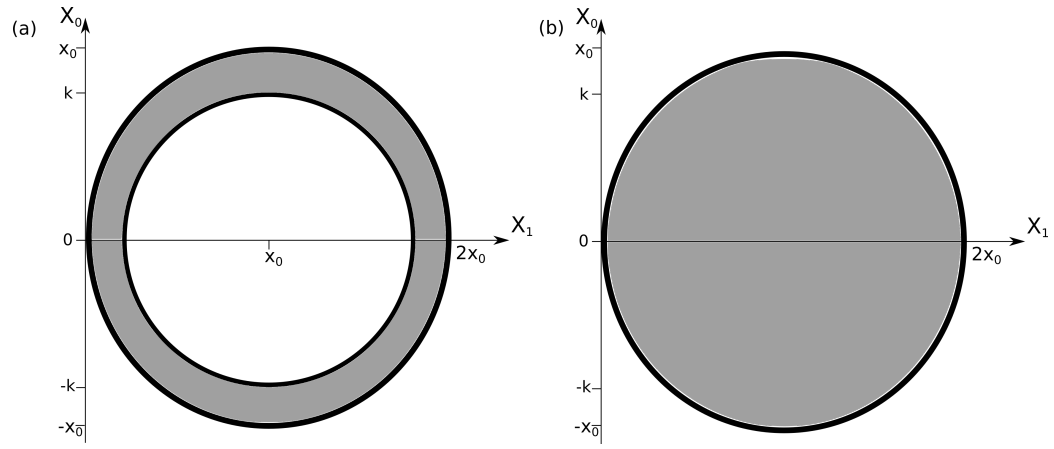

Figure A.3: Graph showing (a) motion of the string with splitting (b) motion of the string without splitting, where $k = \frac{m}{\gamma}$.

$-x_0$ to x_0. However, we find that we need only integrate from $-\frac{m}{\gamma}$ to $\frac{m}{\gamma}$. The sections that we miss out in this way are the same in the solution and the background, and therefore cancel in the final action.

We find that, for the split string, the solution is

$$X_{L0} = X_{R0} = \tau \tag{A.2.46}$$

$$X_{L1} = \ x_L \ = -\frac{\sigma}{\pi}\left(\sqrt{-\tau^2 + k^2} - x_0\right) + \left(1 - \frac{\sigma}{\pi}\right)\left(\sqrt{-\tau^2 + {x_0}^2}\right) \tag{A.2.47}$$

$$X_{R1} = \ x_R \ = \left(1 - \frac{\sigma}{\pi}\right)\left(\sqrt{-\tau^2 + k^2} + x_0\right) + \frac{\sigma}{\pi}\left(\sqrt{-\tau^2 + {x_0}^2} + x_0\right) \tag{A.2.48}$$

Therefore

$$\begin{aligned} S_{sol} = &+ \gamma \int_{-\frac{m}{\gamma}}^{\frac{m}{\gamma}} \mathrm{d}\tau \left(x_L(\tau, \sigma = \pi) - x_L(\tau, \sigma = 0)\right) \\ &+ m \int_{-\frac{m}{\gamma}}^{\frac{m}{\gamma}} \mathrm{d}\tau \left(\sqrt{1 + \dot{x}_L^2(\tau, \sigma = 0)} + \sqrt{1 + \dot{x}_L^2(\tau, \sigma = \pi)}\right) \\ &+ \gamma \int_{-\frac{m}{\gamma}}^{\frac{m}{\gamma}} \mathrm{d}\tau \left(x_R(\tau, \sigma = \pi) - x_R(\tau, \sigma = 0)\right) \\ &+ m \int_{-\frac{m}{\gamma}}^{\frac{m}{\gamma}} \mathrm{d}\tau \left(\sqrt{1 + \dot{x}_R^2(\tau, \sigma = 0)} + \sqrt{1 + \dot{x}_R^2(\tau, \sigma = \pi)}\right) \end{aligned} \tag{A.2.49}$$

For the unsplit string, we find

$$X_{B0} = \tau \tag{A.2.50}$$

$$X_{B1} = x_B = \left(1 - \frac{\sigma}{\pi}\right)\left(-\sqrt{-\tau^2 + {x_0}^2} + x_0\right) + \frac{\sigma}{\pi}\left(\sqrt{-\tau^2 + {x_0}^2} + x_0\right) \quad \text{(A.2.51)}$$

Therefore

$$\begin{aligned} S_{back} =& + \gamma \int_{-\frac{m}{\gamma}}^{\frac{m}{\gamma}} \mathrm{d}\tau \left(x_B(\tau, \sigma = \pi) - x_B(\tau, \sigma = 0)\right) \\ &+ m \int_{-\frac{m}{\gamma}}^{\frac{m}{\gamma}} \mathrm{d}\tau \left(\sqrt{1 + \dot{x}_B^2(\tau, \sigma = 0)} + \sqrt{1 + \dot{x}_B^2(\tau, \sigma = \pi)}\right) \\ &+ \gamma \int_{-\frac{m}{\gamma}}^{\frac{m}{\gamma}} \mathrm{d}\tau \left(x_R(\tau, \sigma = \pi) - x_L(\tau, \sigma = 0)\right) \\ &+ m \int_{-\frac{m}{\gamma}}^{\frac{m}{\gamma}} \mathrm{d}\tau \left(\sqrt{1 + \dot{x}_L^2(\tau, \sigma = 0)} + \sqrt{1 + \dot{x}_R^2(\tau, \sigma = \pi)}\right) \end{aligned} \quad \text{(A.2.52)}$$

which means that

$$\begin{aligned} S =& S_{sol} - S_{back} \\ =& + \int_{-\frac{m}{\gamma}}^{\frac{m}{\gamma}} \mathrm{d}\tau \left(m\sqrt{1 + \dot{x}_L^2(\tau, \sigma = \pi)} + \gamma x_L(\tau, \sigma = \pi)\right) \\ &+ \int_{-\frac{m}{\gamma}}^{\frac{m}{\gamma}} \mathrm{d}\tau \left(m\sqrt{1 + \dot{x}_R^2(\tau, \sigma = 0)} - \gamma x_R(\tau, \sigma = 0)\right) \quad \text{(A.2.53)} \\ =& + \frac{\pi m^2}{\gamma} \quad \text{(A.2.54)} \end{aligned}$$

as before.

This makes sense looking at the problem geometrically, as the action for system is effectively

$$\begin{aligned} S =& m(\text{Circumeference of circle}) - \gamma(\text{Area of circle}) \\ =& m(2\pi k) - \gamma(\pi k^2) \\ =& 2\frac{\pi m^2}{\gamma} - \frac{\pi m^2}{\gamma} = \frac{\pi m^2}{\gamma}. \end{aligned} \quad \text{(A.2.55)}$$

This is the same action as found by Semenoff and Zarembo [16], showing that we may replace an electric field with a string – with the field strength E then being equivalent to the string tension γ.

We wish to consider in more detail why the radius along which the inner endpoints move is set to $k = \frac{m}{\gamma}$. In (A.2.27) to (A.2.29) we showed that it was a result of

the interaction in the boundary equation of motion of the mass and the tension. However, it is also instructive to look at the problem at the level of the action. If we consider (A.2.44) and (A.2.53) without fixing the value of the radius k, we find

$$\begin{aligned} S =& S_{sol} - S_{back} \\ =& \int_{-k}^{k} \mathrm{d}\tau \left(m\sqrt{1+\dot{x}_L^2(\tau,\sigma=\pi)} + \gamma x_L(\tau,\sigma=\pi) \right) \\ & \int_{-k}^{k} \mathrm{d}\tau \left(m\sqrt{1+\dot{x}_R^2(\tau,\sigma=0)} - \gamma x_R(\tau,\sigma=0) \right) \\ =& 2\int_{-k}^{k} \left(\frac{mk}{\sqrt{-\tau^2+k^2}} - \gamma\sqrt{-\tau^2+k^2} \right) \\ =& \pi(-2mk+\gamma k^2) \end{aligned} \tag{A.2.56}$$

which is extremised by $k = \frac{m}{\gamma}$. We find that the term corresponding to the endpoints (proportional to m) has the opposite sign to the term corresponding to the bulk (proportional to γ).

It may seem surprising, however, that when the outer endpoints are constrained to move in a circle, the motion of the inner endpoints does not change. Let's examine the left hand string in this set up in more detail. This is described by equations (A.2.47) and (A.2.48). From (A.2.22) and (A.2.23) we see that the bulk equations of motion are trivially satisfied since $X_0 = \tau$ and $X_1 = x(\tau,\sigma)$.

Let us therefore consider the Neumann boundary condition (A.2.24). As before, we note that at $\mu = 0$ this evaluates to

$$-m\frac{\partial}{\partial\tau}\left(\frac{1}{\sqrt{1+\dot{x}_L^2}}\right) + \gamma\dot{x_L} = 0 \tag{A.2.57}$$

and that at $\mu = 1$ this evaluates to

$$-m\frac{\partial}{\partial\tau}\left(\frac{\dot{x}_L}{\sqrt{1+\dot{x}_L^2}}\right) - \gamma = 0 \tag{A.2.58}$$

We note that these expressions are only in terms of $\dot{x}_L$, evaluated at $\sigma = \pi$. However, we find from (A.2.47):

$$\dot{x}_L(\tau,\sigma=\pi) = \frac{\tau}{\sqrt{-\tau^2+k^2}}. \tag{A.2.59}$$

This is precisely the same form as (A.2.25). That is, $\dot{x}_L(\tau, \sigma = \pi)$ is the same whether the outer endpoints move in a circle or in a straight line. The difference between the two different forms of $\dot{x}_L(\tau, \sigma = \pi)$ in these two scenarios, which evaluates to $\left(1 - \frac{\sigma}{\pi}\right) \frac{-\tau}{\sqrt{-\tau^2 + x_0^2}}$, goes to zero at $\sigma = \pi$. Therefore the moving endpoint condition is satisfied.

It may also be instructive, however, to consider minimising the action with the background not subtracted. This is action (A.2.40):

$$\begin{aligned} S = &\int_{-k}^{k} \mathrm{d}\tau \, \left(m\sqrt{1 + \dot{x}_L^2(\tau, \sigma = \pi)} + \gamma x_L(\tau, \sigma = \pi) \right) \\ &\int_{-k}^{k} \mathrm{d}\tau \, \left(m\sqrt{1 + \dot{x}_R^2(\tau, \sigma = 0)} - \gamma x_R(\tau, \sigma = 0) \right) \\ &\int_{-k}^{k} \mathrm{d}\tau \, \left(2m + 2x_0 \right) \\ = &- 2mk\pi + \gamma k^2 + 2k(m + 2x_0). \end{aligned} \tag{A.2.60}$$

Extremising this yields

$$k = \frac{m\pi - 2(m + x_0)}{\gamma\pi} \tag{A.2.61}$$

which is does not agree with the value of the radius k calculated from the endpoint equation of motion.

We have, however, been using $\pm k$ as the τ limits of integration. It seems more valid to use the same limits each time, say arbitrary $\pm T$ such that $T > k$. This is shown in figure A.4.

In this case, we find

$$\begin{aligned} S = &+ \int_{-T}^{T} \mathrm{d}\tau \, \left(m\sqrt{1 + \dot{x}_L^2(\tau, \sigma = \pi)} + \gamma x_L(\tau, \sigma = \pi) \right) \\ &+ \int_{-T}^{T} \mathrm{d}\tau \, \left(m\sqrt{1 + \dot{x}_R^2(\tau, \sigma = 0)} - \gamma x_R(\tau, \sigma = 0) \right) \\ &+ \int_{-T}^{T} \mathrm{d}\tau \, \left(2m + 2x_0 \right) \\ = &+ \gamma(\text{Area of String Worldsheet}) + m(\text{Length of Endpoint Worldline}) \\ = &+ \gamma(2.2x_0(T - k) + (4kx_0 - \pi k^2)) + m(2.2T + 2\pi k) \end{aligned}$$

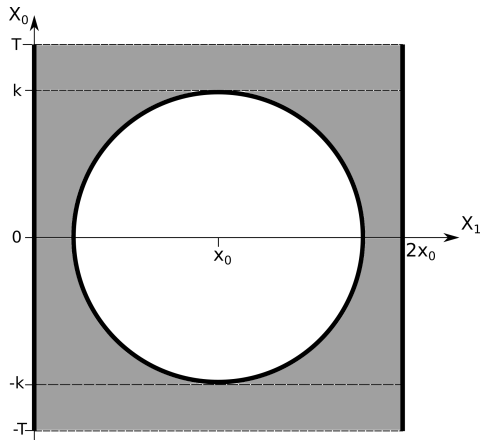

Figure A.4: Graph showing (a) motion of the string with splitting (b) motion of the string without splitting, where $k = \frac{m}{\gamma}$.

$$= -\gamma\pi k^2 + 2m\pi\gamma + 4Tm + 4\gamma x_0 T. \tag{A.2.62}$$

Extremising this gives,

$$k = \frac{m}{\gamma} \tag{A.2.63}$$

which agrees with the result from the equations of motion.

A.2.2 Generic Outer Path

Indeed we find that we can constrain the outer endpoints to move in any shape, that is, we can re-write the solutions as:

$$x_L \to \tilde{x}_L = x_L + f_L(\tau)\,(\sigma - \pi) \tag{A.2.64}$$

$$x_R \to \tilde{x}_R = x_R + f_R(\tau)\,\sigma \tag{A.2.65}$$

where $f_L(\tau)$ and $f_R(\tau)$ are generic functions of τ. As before, the Neumann boundary conditions (as shown in (A.2.27)) are satisfied as they are evaluated at $\sigma = \pi$ for x_L and $\sigma = 0$ for x_R, so the new terms do not contribute.

Similarly, the action evaluates to

$$S_{sol} = +\gamma \int_{-T}^{T} \mathrm{d}\tau \left(\tilde{x}_L(\tau, \sigma = \pi) - \tilde{x}_L(\tau, \sigma = 0)\right)$$

$$
\begin{aligned}
&+ m\int_{-T}^{T} \mathrm{d}\tau \left(\sqrt{1+\dot{\tilde{x}}_L{}^2(\tau,\sigma=0)} + \sqrt{1+\dot{\tilde{x}}_L{}^2(\tau,\sigma=\pi)}\right) \\
&+ \gamma\int_{-T}^{T} \mathrm{d}\tau \left(\tilde{x}_R(\tau,\sigma=\pi) - \tilde{x}_R(\tau,\sigma=0)\right) \\
&+ m\int_{-T}^{T} \mathrm{d}\tau \left(\sqrt{1+\dot{\tilde{x}}_R{}^2(\tau,\sigma=0)} + \sqrt{1+\dot{\tilde{x}}_R{}^2(\tau,\sigma=\pi)}\right) \qquad \text{(A.2.66)} \\
=&+ \int_{-k}^{k} \mathrm{d}\tau \left(m\sqrt{1+\dot{x}_L^2(\tau,\sigma=\pi)} + \gamma x_L(\tau,\sigma=\pi)\right) \\
&+ \int_{-k}^{k} \mathrm{d}\tau \left(m\sqrt{1+\dot{x}_R^2(\tau,\sigma=0)} - \gamma x_R(\tau,\sigma=0)\right) \\
&+ \int_{-T}^{T} \mathrm{d}\tau \left(m\sqrt{1+\left(\dot{x}_L(\tau,\sigma=0) - \pi\dot{f}_L(\tau)\right)^2} - \gamma\Big(x_L(\tau,\sigma=0) - \pi f_L(\tau)\Big)\right) \\
&+ \int_{-T}^{T} \mathrm{d}\tau \left(m\sqrt{1+\left(\dot{x}_R(\tau,\sigma=\pi) + \pi\dot{f}_R(\tau)\right)^2} + \gamma\Big(x_R(\tau,\sigma=\pi) + \pi f_R(\tau)\Big)\right) \\
& \qquad\qquad\qquad\qquad\qquad\qquad\qquad\qquad\qquad\qquad\qquad\qquad\qquad\qquad \text{(A.2.67)} \\
=&- \gamma\pi k^2 + 2m\pi\gamma + C \qquad\qquad\qquad\qquad\qquad\qquad\qquad\qquad\qquad\qquad\qquad\qquad \text{(A.2.68)}
\end{aligned}
$$

where, as before, we start and end at arbitrary constant times $\pm T$ and we have

$$
\begin{aligned}
C =& \int_{-T}^{T} \mathrm{d}\tau \left(m\sqrt{1+\left(\dot{x}_L(\tau,\sigma=0) - \pi\dot{f}_L(\tau)\right)^2} - \gamma\Big(x_L(\tau,\sigma=0) - \pi f_L(\tau)\Big)\right) \\
& \int_{-T}^{T} \mathrm{d}\tau \left(m\sqrt{1+\left(\dot{x}_R(\tau,\sigma=\pi) + \pi\dot{f}_R(\tau)\right)^2} + \gamma\Big(x_R(\tau,\sigma=\pi) + \pi f_R(\tau)\Big)\right)
\end{aligned}
\qquad \text{(A.2.69)}
$$

C depends on the outer path but not the inner radius k – the k dependence only coming in at $x_L(\tau,\sigma=\pi)$ and $x_R(\tau,\sigma=0)$, which is described by the first two terms of the equation. Therefore, extremising for k, we get the same solution.

A.2.3 Lorentzian Solution

If we look at the Lorentzian solution presented by Bardeen [57] (again bisected to give the Dirichlet boundary condition $X_1(\tau,\sigma=0)=0$)

$$
\begin{aligned}
X_0 =& \tau \qquad\qquad\qquad\qquad\qquad\qquad\qquad\qquad\qquad\qquad\qquad\qquad\qquad\qquad \text{(A.2.70)} \\
X_1 =& x = \frac{\sigma}{\pi}\left(-\sqrt{(\tau-\tau_0)^2+k^2} + x_0\right) \qquad\qquad\qquad\qquad\qquad\qquad \text{(A.2.71)}
\end{aligned}
$$

and consider the Neumann boundary condition at $\sigma = \pi$ we find

$$\frac{\partial}{\partial\tau}\left(\frac{\partial\mathcal{L}_{end,\sigma=\pi}}{\partial\dot{X}_\mu}\right) - \frac{\partial\mathcal{L}_{bulk}}{\partial{X'}_\mu}\bigg|_{\sigma=\pi} = -m\frac{\partial}{\partial\tau}\left(\frac{\dot{X}^\mu}{\sqrt{\dot{X}^2}}\right) - \gamma\left(\dot{x}\dot{X}^\mu + \left(\frac{1-\dot{x}^2}{x'}\right)X'^\mu\right)\bigg|_{\sigma=\pi} = 0. \tag{A.2.72}$$

For $\mu = 1$ this gives

$$\frac{m}{k} - \gamma = 0 \tag{A.2.73}$$

again setting $k = \frac{m}{\gamma}$. Unlike in the Euclidean case, however, the motion of endpoint at $\sigma = \pi$ does depend on x_0, it's initial starting position. While the curvature parameter, k does not change based on x_0, the moving endpoint will take longer to reach $x = 0$ if the x_0 is larger. This is not the case in the Euclidean spacetime as the term $\sqrt{-\tau^2 + k^2}$, sets at what value of τ the motion of the moving endpoint starts and finishes.

In Bardeen's paper x_0 is set to $x_0 = \sqrt{\frac{\pi^2}{4} + \frac{m^2}{\gamma^2}}$. However this does not appear to be a consequence of the equations of motion, and rather a means to ensure that $x\left(\tau = \frac{\pi}{2}, \sigma = \pi\right) = 0$. Bardeen glues together solutions with different τ_0 wherever $x(\tau, \sigma = \pi) = 0$ in order to give a periodic solution, and the choice of $x_0 = \sqrt{\frac{\pi^2}{4} + \frac{m^2}{\gamma^2}}$ ensures a period of 2π.

A.2.4 Summary

The Euclidean action for the system is:

$$\begin{aligned} S =& \int_{\tau_1}^{\tau_2} \mathrm{d}\tau \int_0^\pi \mathrm{d}\sigma\, \mathcal{L}_{bulk} + \int_{\tau_1}^{\tau_2} \mathrm{d}\tau\, \mathcal{L}_{end} && \text{(A.2.74)} \\ =& \gamma \int_{\tau_1}^{\tau_2} \mathrm{d}\tau \int_0^\pi \mathrm{d}\sigma \sqrt{-\left(\dot{X}\cdot X'\right)^2 + \dot{X}^2 X'^2} \\ & m\int_{\tau_1}^{\tau_2} \mathrm{d}\tau \left(\sqrt{\dot{X}^2(\tau, \sigma = 0)} + \sqrt{\dot{X}^2(\tau, \sigma = \pi)}\right), && \text{(A.2.75)} \end{aligned}$$

We find the following concentric string solution:

$$X_{L0} = X_{R0} = \tau \tag{A.2.76}$$

$$X_{L1} = x_L = -\frac{\sigma}{\pi}\left(\sqrt{-\tau^2+k^2} - x_0\right) + \left(1-\frac{\sigma}{\pi}\right)\left(\sqrt{-\tau^2+{x_0}^2}\right) \tag{A.2.77}$$

$$X_{R1} = x_R = \left(1-\frac{\sigma}{\pi}\right)\left(\sqrt{-\tau^2+k^2} + x_0\right) + \frac{\sigma}{\pi}\left(\sqrt{-\tau^2+{x_0}^2} + x_0\right) \tag{A.2.78}$$

We consider the Neumann boundary condition at $\sigma = \pi$. We find

$$\begin{aligned}
\frac{\partial}{\partial\tau}\left(\frac{\partial\mathcal{L}_{end,\sigma=\pi}}{\partial\dot{X}_\mu}\right) - \left.\frac{\partial\mathcal{L}_{bulk}}{\partial{X'}_\mu}\right|_{\sigma=\pi} &= 0 \\
-m\frac{\partial}{\partial\tau}\left(\frac{\dot{X}^\mu}{\sqrt{\dot{X}^2}}\right) + \gamma\left.\frac{-(\dot{X}\cdot X')\dot{X}^\mu + X'^\mu\dot{X}^2}{\sqrt{-(\dot{X}\cdot X')^2+\dot{X}^2X'^2}}\right|_{\sigma=\pi} &= 0 \\
-m\frac{\partial}{\partial\tau}\left(\frac{\dot{X}^\mu}{\sqrt{1+\dot{x}^2}}\right) + \gamma\left.\frac{-\dot{x}x'\dot{X}^\mu + (1+\dot{x}^2)X'^\mu}{\sqrt{-\dot{x}^2x'^2+(1+\dot{x}^2)x'^2}}\right|_{\sigma=\pi} &= 0 \\
-m\frac{\partial}{\partial\tau}\left(\frac{\dot{X}^\mu}{\sqrt{1+\dot{x}^2}}\right) + \gamma\left(-\dot{x}\dot{X}^\mu + \left(\frac{1+\dot{x}^2}{x'}\right)X'^\mu\right)\Bigg|_{\sigma=\pi} &= 0.
\end{aligned} \tag{A.2.79}$$

For $\mu = 1$ this gives

$$-m\frac{\partial}{\partial\tau}\left(\frac{\dot{x}^\mu}{\sqrt{1+\dot{x}^2}}\right) + \gamma = 0 \tag{A.2.80}$$

All the σ derivatives vanish because we only have two dimensions. If we were working in higher dimensions, we would have terms $\frac{X'^\mu}{\sqrt{X'^\mu X'_\mu}}$, which would not cancel.

Concentrating now, for clarity, just the left hand sided string segment, X_L we we find that

$$-m\frac{\partial}{\partial\tau}\left(\frac{\tau}{\sqrt{-\tau^2+k^2}}\frac{\sqrt{-\tau^2+k^2}}{k}\right) + \gamma = 0 \tag{A.2.81}$$

$$-\frac{m}{k} + \gamma = 0 \tag{A.2.82}$$

which fixes $k = \frac{m}{\gamma}$. We get the same value of k from setting $\mu = 0$

If we consider the action we find

$$\begin{aligned}
S =& \gamma(\text{Area of String Worldsheet}) + m(\text{Length of Endpoint Worldline}) \\
=& \gamma(\pi x_0^2 - \pi k^2) + m(2\pi x_0 + 2\pi k).
\end{aligned} \tag{A.2.83}$$

Extremising this for k also yields $k = \frac{m}{\gamma}$. Throughout, we find that the action for the system evaluates to $\frac{\pi m^2}{\gamma}$, the same factor we encountered in previous sections.

Appendix B

Potential Analysis

It is instructive to consider the potentials in the case of pair produced particles more carefully as this can help to give a more intuitive understanding of how the process works. We may consider the potential between two pair produced particles of mass m and separation x to be

$$V(x) = 2m - Ex - \frac{\alpha_s}{x} \tag{B.0.1}$$

where E is the field between the particles and α represents the coupling [16]. This is demonstrated in figure B.1. We may therefore consider the process of the particles coming on shell to be equivalent to tunnelling. In the rest of this work the field has been seen as being equivalent to string tension in the holographic picture, and the matter of the tunnelling has been dealt with by doing a Wick rotation, thereby reversing the potential. However, a lot of interesting work, including by Semenoff and Zarembo [16], Bolognesi et al [124] and Sato and Yoshida [130], has been done in a different picture, where we have strings in an external field and with no Wick rotation.

A crucial interesting feature of this picture is the existence of a critical field (which was previously explored in [131], [132] – which is indicated by the central plot, mid grey, plot in figure B.1. Above this critical field strength the potential is always negative, which means that the pair production is no longer exponentially suppressed.

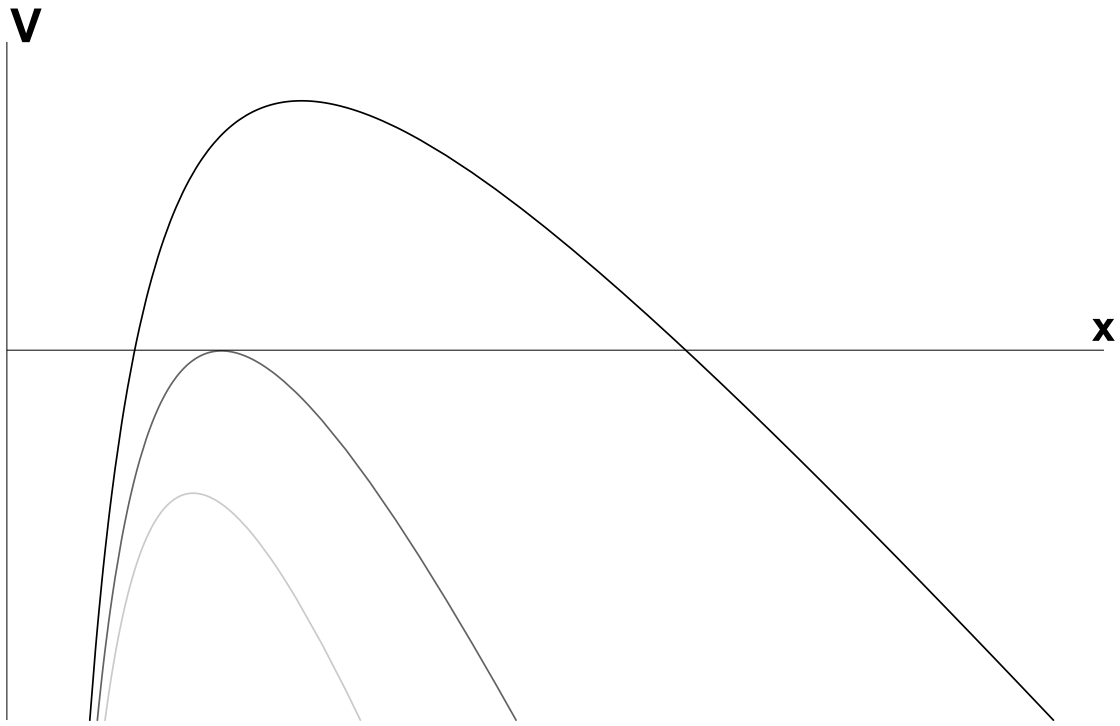

Figure B.1: The potential of the pair produced quarks as a function of their separation. The darker the lines represent weaker field strengths E and the lighter lines represent stronger field strengths E

Therefore, if the 'external' field is being used to represent the field within a composite particle such as a meson, if said field strength is too high, the mesons decay instantly.

As discussed by Semenoff and Zarembo [16], the coupling may be calculated to be

$$\alpha = \frac{4\pi g_{YM}\sqrt{N}}{\Gamma^4(\frac{1}{4})} \tag{B.0.2}$$

and therefore the critical field may be evaluated as

$$E_c \sim \frac{m^2}{\alpha} = \frac{\Gamma^4(\frac{1}{4})m^2}{4\pi^2\sqrt{\lambda}}. \tag{B.0.3}$$

Sato and Yoshida [130] calculated the total potential for a background $D3$ brane system which may be expressed as

$$V = 2\gamma \int_0^{\frac{x}{2}} \mathrm{d}\sigma \mathcal{L} \; - Ex \tag{B.0.4}$$

$$= 2\gamma u_0 \int_1^{\frac{1}{a}} \mathrm{d}y \sqrt{\frac{y^4 - \frac{b^4}{a^4}}{y^4 - 1}} \; - Ex \tag{B.0.5}$$

where γ is the string tension, u_0 is the position of the probe flavour brane and u_b is the position of the bottom of the string loop such that

$$y \equiv \frac{u}{u_b} \qquad a \equiv \frac{u_b}{u_0} \qquad b \equiv \frac{u_\Lambda}{u_0} \tag{B.0.6}$$

The equation (B.0.4) may be evaluated numerically to find a critical field strength, as expected. A similar DBI calculation yields the same result. This indicates that this effect shows up in holographic calculations and is therefore worthy of future study by those researching holographic methods of meson decay.

Appendix C

Holographic models of quark-gluon fluids

The existence of strongly coupled quark gluon plasma was first confirmed at the Relativistic Heavy Ion Collider (RHIC), sparking a great deal of interest [133]. This is another area which merits further investigation using holography [12], [95], [134].

For example, early research has shown that holographic method successfully model the dependence of the mass of mesons in a quark-gluon plasma on the temperature [12]. As temperature increases meson mass decreases. This is because for higher temperatures probe branes get closer to the IR wall. It can be seen from (4.4.2) that the distance between the probe brane and the IR wall is roughly proportional to the quark mass. Similarly, holographic models [12] successfully predict that as the angular momentum of mesons increases their spin increases, and so does the separation of quarks within the mesons.

A different phenomenon of particular interest is jet quenching [135]–[137]. When a quark-antiquark pair is produced near the edge of a quark gluon fluid it is possible that one of the pair will have a far shorter distance to travel before it escapes said fluid. Therefore, the particle with the shorter path through the fluid will retain most of its energy and any observer will note a standard jet. The jet for the particle with the longer path will be quenched – it will either be observed to be more 'smeared-out'

and lower energy, or not be observed at all. It is possible to model the energy lost holographically, with each quark modelled individually as an open string with only one endpoint attached to the flavour brane.

We may do so following the example of [138]. We consider the action

$$S = \int \mathrm{d}\tau \mathcal{L} = \int \mathrm{d}\tau \sqrt{g_{\mu\nu} \frac{\mathrm{d}X^\mu}{\mathrm{d}\tau} \frac{\mathrm{d}X^\nu}{\mathrm{d}\tau}} \tag{C.0.1}$$

but, with a more general metric

$$\mathrm{d}s^2 = b^2(z) \left(\frac{1}{f_1(z)} \mathrm{d}z^2 - f_2(z) \mathrm{d}t^2 + \mathrm{d}x^2 \right). \tag{C.0.2}$$

We calculate the equations of motion for t and x_i:

$$\frac{1}{\mathcal{L}} b^2(z) f_2(z) \dot{t} = C \tag{C.0.3}$$

$$\frac{1}{\mathcal{L}} b^2(z) \dot{x} = D, \tag{C.0.4}$$

where the dot indicates a derivative with respect to τ and C and D are constants. Combining these, we find

$$\frac{\mathrm{d}x}{\mathrm{d}t} = A f_2(z), \tag{C.0.5}$$

where $A = \frac{D}{C}$.

Now, imposing the null geodesic condition

$$\frac{1}{f_1(z)} \left(\frac{\mathrm{d}z}{\mathrm{d}t} \right)^2 - f_2(z) + \sum_{i=1}^{3} \left(\frac{\mathrm{d}x}{\mathrm{d}t} \right)^2 = 0 \tag{C.0.6}$$

and combining with (C.0.5), we find

$$\frac{\mathrm{d}z}{\mathrm{d}t} = \sqrt{f_1(z) f_2(z) (1 - 3A^2 f_2(z))}. \tag{C.0.7}$$

Applying the condition

$$\left. \frac{\mathrm{d}z}{\mathrm{d}t} \right|_{z=z_0} = 0 \tag{C.0.8}$$

we find

$$A^2 = \frac{1}{3 f_2(z_0)} \tag{C.0.9}$$

giving the result:

$$\frac{\mathrm{d}z}{\mathrm{d}t} = \sqrt{f_1(z)f_2(z)\left(1 - \frac{f_2(z)}{f_2(z_0)}\right)} \tag{C.0.10}$$

$$\Rightarrow \frac{\mathrm{d}z}{\mathrm{d}x_i} = \sqrt{3\frac{f_1(z)}{f_2(z)}\Big(f_2(z_0) - f_2(z)\Big)}. \tag{C.0.11}$$

We then consider the energy:

$$\dot{E} = -\frac{1}{2\pi\alpha'} g_{00}\dot{t} \tag{C.0.12}$$

$$\frac{\mathrm{d}E}{\mathrm{d}t} = \frac{b^2(z)\, f_2(z)}{2\pi\alpha'}. \tag{C.0.13}$$

Using (C.0.10) and (C.0.11) we then find:

$$\frac{\mathrm{d}E}{\mathrm{d}z} = \frac{b^2(z)}{2\pi\alpha'}\sqrt{\frac{f_2(z)}{f_1(z)}\,\frac{f_2(z_0)}{f_2(z_0) - f_2(z)}} \tag{C.0.14}$$

$$\frac{\mathrm{d}E}{\mathrm{d}x} = \frac{b^2(z)}{2\pi\alpha'}\sqrt{3f_2(z_0)} \tag{C.0.15}$$

One may therefore find the energy and motion of the quark by integrating this.

For the specific example of

$$f(z) = 1 - \frac{z^4}{{z_t}^4}, \tag{C.0.16}$$

that is the Sakai-Sugimoto background with confining $D3$ branes as discussed by Sato and Yoshida [113], we find the quark's stopping distance

$$\Delta x_{stop} = {z_t}^2\left(\frac{\sqrt{\pi}\Gamma\left[\frac{5}{4}\right]}{z_0\Gamma\left[\frac{3}{4}\right]} - \frac{{}_2F_1\left[\frac{1}{4},\frac{1}{2},\frac{5}{4},\frac{{z_0}^4}{{z_t}^4}\right]}{z_t}\right) \tag{C.0.17}$$

and initial energy

$$E_{initial} = \frac{\sqrt{\lambda}}{2\pi}\sqrt{{z_t}^4 - {z_0}^4}\left(\frac{\sqrt{\pi}\Gamma\left[\frac{5}{4}\right]}{z_0\Gamma\left[\frac{3}{4}\right]} - \frac{{}_2F_1\left[\frac{1}{4},\frac{1}{2},\frac{5}{4},\frac{{z_0}^4}{{z_t}^4}\right]}{z_t} + \frac{\sqrt{\pi}\Gamma\left[\frac{3}{4}\right]}{{z_0}^3\Gamma\left[\frac{1}{4}\right]} - \frac{{}_2F_1\left[\frac{1}{2},\frac{3}{4},\frac{7}{4},\frac{{z_0}^4}{{z_t}^4}\right]}{z_t}\right). \tag{C.0.18}$$

Taking the limit $\frac{z_0}{z_t} \to 0$ equation (C.0.17) becomes

$$\Delta x_{stop} = \frac{{z_H}^2\sqrt{\pi}\Gamma\left[\frac{5}{4}\right]}{z_0\Gamma\left[\frac{3}{4}\right]} \tag{C.0.19}$$

and equation (C.0.18) becomes

$$E_{initial} = \frac{{z_H}^2 \sqrt{\lambda} \Gamma\left[\frac{3}{4}\right]}{2\sqrt{\pi} {z_0}^3 \Gamma\left[\frac{1}{4}\right]}. \tag{C.0.20}$$

Combining (C.0.19) and (C.0.20) we get:

$$\Delta x_{stop} = \frac{2^{\frac{1}{3}} \left(\Gamma\left[\frac{1}{4}\right]\right)^{\frac{1}{3}} \Gamma\left[\frac{5}{4}\right]}{\pi^{\frac{2}{3}} \lambda^{\frac{1}{6}} \left(\Gamma\left[\frac{3}{4}\right]\right)^{\frac{4}{3}}} \left(\frac{E_{initial}}{T^4}\right)^{\frac{1}{3}}. \tag{C.0.21}$$

We have therefore shown it is possible to calculate the energy and stopping distance of quark jets through a quark-gluon plasma using this framework.

Bibliography

[1] L. H. Ryder. *QUANTUM FIELD THEORY*. Cambridge University Press, 1996. ISBN: 9780521478144, 9781139632393, 9780521237642.

[2] Rajan Gupta. 'Introduction to lattice QCD: Course'. In: *Probing the standard model of particle interactions. Proceedings, Summer School in Theoretical Physics, NATO Advanced Study Institute, 68th session, Les Houches, France, July 28-September 5, 1997. Pt. 1, 2.* 1997, pp. 83–219. arXiv: hep-lat/9807028 [hep-lat].

[3] Kenneth G. Wilson. 'Confinement of quarks'. In: *Phys. Rev. D* 10 (8 1974), pp. 2445–2459. DOI: 10.1103/PhysRevD.10.2445. URL: https://link.aps.org/doi/10.1103/PhysRevD.10.2445.

[4] B. Andersson. *The Lund Model*. Vol. 7. Cambridge Monographs on Particle Physics, Nuclear Physics and Cosmology. Cambridge University Press, 1998.

[5] B. Andersson, G. Gustafson, G. Ingelman et al. 'Parton fragmentation and string dynamics'. In: *Physics Reports* 97.2 (1983), pp. 31 –145. ISSN: 0370-1573. DOI: 10.1016/0370-1573(83)90080-7. URL: http://www.sciencedirect.com/science/article/pii/0370157383900807.

[6] Torbjörn Sjöstrand, Stefan Ask, Jesper R. Christiansen et al. 'An Introduction to PYTHIA 8.2'. In: *Comput. Phys. Commun.* 191 (2015), pp. 159–177. DOI: 10.1016/j.cpc.2015.01.024. arXiv: 1410.3012 [hep-ph].

[7] Sebastian De Haro, Daniel R. Mayerson and Jeremy N. Butterfield. 'Conceptual Aspects of Gauge/Gravity Duality'. In: *Found. Phys.* 46.11 (2016), pp. 1381–1425. DOI: 10.1007/s10701-016-0037-4. arXiv: 1509.09231 [physics.hist-ph].

[8] Juan Martin Maldacena. 'TASI 2003 lectures on AdS / CFT'. In: *Progress in string theory. Proceedings, Summer School, TASI 2003, Boulder, USA, June 2-27, 2003*. 2003, pp. 155–203. arXiv: hep-th/0309246 [hep-th].

[9] Juan Martin Maldacena. 'The Large N limit of superconformal field theories and supergravity'. In: *Int. J. Theor. Phys.* 38 (1999). [Adv. Theor. Math. Phys.2,231(1998)], pp. 1113–1133. DOI: 10.1023/A:1026654312961,10.4310/ATMP.1998.v2.n2.a1. arXiv: hep-th/9711200 [hep-th].

[10] Johanna Erdmenger, Nick Evans, Ingo Kirsch et al. 'Mesons in Gauge/Gravity Duals - A Review'. In: *Eur. Phys. J.* A35 (2008), pp. 81–133. DOI: 10.1140/epja/i2007-10540-1. arXiv: 0711.4467 [hep-th].

[11] Martin Kruczenski, David Mateos, Robert C. Myers et al. 'Towards a holographic dual of large N(c) QCD'. In: *JHEP* 05 (2004), p. 041. DOI: 10.1088/1126-6708/2004/05/041. arXiv: hep-th/0311270 [hep-th].

[12] Kasper Peeters, Jacob Sonnenschein and Marija Zamaklar. 'Holographic melting and related properties of mesons in a quark gluon plasma'. In: *Phys. Rev.* D74 (2006), p. 106008. DOI: 10.1103/PhysRevD.74.106008. arXiv: hep-th/0606195 [hep-th].

[13] Edward Witten. 'Anti-de Sitter space, thermal phase transition, and confinement in gauge theories'. In: *Adv. Theor. Math. Phys.* 2 (1998), pp. 505–532. DOI: 10.4310/ATMP.1998.v2.n3.a3. arXiv: hep-th/9803131 [hep-th].

[14] Tadakatsu Sakai and Shigeki Sugimoto. 'Low energy hadron physics in holographic QCD'. In: *Prog. Theor. Phys.* 113 (2005), pp. 843–882. DOI: 10.1143/PTP.113.843. arXiv: hep-th/0412141 [hep-th].

[15] Tadakatsu Sakai and Shigeki Sugimoto. 'More on a holographic dual of QCD'. In: *Prog. Theor. Phys.* 114 (2005), pp. 1083–1118. DOI: 10.1143/PTP.114.1083. arXiv: hep-th/0507073 [hep-th].

[16] Gordon W. Semenoff and Konstantin Zarembo. 'Holographic Schwinger Effect'. In: *Phys. Rev. Lett.* 107 (2011), p. 171601. DOI: 10.1103/PhysRevLett.107.171601. arXiv: 1109.2920 [hep-th].

[17] Julian Schwinger. 'On Gauge Invariance and Vacuum Polarization'. In: *Physical Review* 82.5 (1951), p. 664.

[18] A. Casher, H. Neuberger and S. Nussinov. 'Chromoelectric-flux-tube model of particle production'. In: *Phys. Rev. D* 20 (1 1979), pp. 179–188. DOI: 10.1103/PhysRevD.20.179. URL: https://link.aps.org/doi/10.1103/PhysRevD.20.179.

[19] Leandro Medina and Michael C. Ogilvie. 'Schwinger Pair Production at Finite Temperature'. In: *Phys. Rev.* D95.5 (2017), p. 056006. DOI: 10.1103/PhysRevD.95.056006. arXiv: 1511.09459 [hep-th].

[20] K. B. Selivanov and M. B. Voloshin. 'DESTRUCTION OF FALSE VACUUM BY MASSIVE PARTICLES'. In: *JETP Lett.* 42 (1985), p. 422.

[21] Adam R. Brown. 'Schwinger pair production at nonzero temperatures or in compact directions'. In: *Phys. Rev.* D98.3 (2018), p. 036008. DOI: 10.1103/PhysRevD.98.036008. arXiv: 1512.05716 [hep-th].

[22] Jaume Garriga. 'Instantons for vacuum decay at finite temperature in the thin wall limit'. In: *Phys. Rev.* D49 (1994), pp. 5497–5506. DOI: 10.1103/PhysRevD.49.5497. arXiv: hep-th/9401020 [hep-th].

[23] John Lawson, Steven Charlton and Imran M. *Thesis Template*. Durham Mathematical Sciences Department. URL: http://www.maths.dur.ac.uk/PG/latextemplates.html.

[24] Michael E. Peskin and Daniel V. Schroeder. *An Introduction to quantum field theory*. Reading, USA: Addison-Wesley, 1995. ISBN: 9780201503975, 0201503972. URL: http://www.slac.stanford.edu/~mpeskin/QFT.html.

[25] Leonard Susskind. 'Coarse Grained Quantum Chromodynamics'. In: *Weak and Electromagnetic Interactions at High Energy*. Ed. by Roger Balian and Christopher H. Llewellyn Smith. Vol. 29. Les Houches - Ecole d'Ete de Physique Theorique. North-Holland, 1976. Chap. 3.

[26] Richard Feynman. 'Gauge Theories'. In: *Weak and Electromagnetic Interactions at High Energy*. Ed. by Roger Balian and Christopher H. Llewellyn Smith. Vol. 29. Les Houches - Ecole d'Ete de Physique Theorique. North-Holland, 1976. Chap. 2.

[27] Michael H. Seymour. 'Quantum chromodynamics'. In: *2004 European School of High-Energy Physics, Sant Feliu de Guixols, Spain, 30 May - 12 June 2004*. 2005, pp. 49–94. arXiv: hep-ph/0505192 [hep-ph]. URL: http://doc.cern.ch/yellowrep/CERN-PH-TH-2005-083.

[28] H. Sazdjian. 'Introduction to chiral symmetry in QCD'. In: *EPJ Web Conf.* 137 (2017), p. 02001. DOI: 10.1051/epjconf/201713702001. arXiv: 1612.04078 [hep-ph].

[29] Juan Rojo. *The Strong Interaction and LHC phenomenology*. University of Oxford. 2014. URL: https://www2.physics.ox.ac.uk/sites/default/files/2014-03-31/qcdgrad_rojo_oxford_tt14_2_basics_pdf_40958.pdf.

[30] David Tong. *Chiral Symmetry Breaking*. DAMTP. URL: http://www.damtp.cam.ac.uk/user/tong/gaugetheory/5chisb.pdf.

[31] Yuya Tanizaki. 'Anomaly constraint on massless QCD and the role of Skyrmions in chiral symmetry breaking'. In: *JHEP* 08 (2018), p. 171. DOI: 10.1007/JHEP08(2018)171. arXiv: 1807.07666 [hep-th].

[32] J. Goldstone. 'Field theories with « Superconductor » solutions'. In: *Il Nuovo Cimento (1955-1965)* 19.1 (1961), pp. 154–164. ISSN: 1827-6121. DOI: 10.1007/BF02812722. URL: 10.1007/BF02812722.

[33] David J. Gross and Frank Wilczek. 'Asymptotically Free Gauge Theories. I'. In: *Phys. Rev. D* 8 (10 1973), pp. 3633–3652. DOI: 10.1103/PhysRevD.8.3633. URL: https://link.aps.org/doi/10.1103/PhysRevD.8.3633.

[34] H. David Politzer. 'Reliable Perturbative Results for Strong Interactions?' In: *Phys. Rev. Lett.* 30 (26 1973), pp. 1346–1349. DOI: 10.1103/PhysRevLett.30.1346. URL: https://link.aps.org/doi/10.1103/PhysRevLett.30.1346.

[35] Michaelangelo L Mangano. 'Introduction to QCD'. In: *European School on High-Energy Physics*. Ed. by Nick Ellis and John David March-Russell. 1998, pp. 53–97. DOI: 10.5170/CERN-1999-004. URL: https://cds.cern.ch/record/454171/files/p41.pdf.

[36] *Introduction to Renormalization – QCD*. University of Southampton High Energy Physics Department. URL: http://www.personal.soton.ac.uk/ab1u06/teaching/qft/qft3/lit/2007-04-20-chen.pdf.

[37] F Hautmann. 'An Introduction to QED & QCD'. In: *RAL High Energy Physics Summer School*. 2012. URL: https://stfc.ukri.org/files/introduction-to-qed-and-qcd/.

[38] Joshua P. Ellis. 'TikZ-Feynman: Feynman diagrams with TikZ'. In: *Computer Physics Communications* 210 (2017), pp. 103 –123. ISSN: 0010-4655. DOI: 10.1016/j.cpc.2016.08.019. URL: http://www.sciencedirect.com/science/article/pii/S0010465516302521.

[39] Michiel Botje. Nikhef. 2013. URL: https://www.nikhef.nl/~h24/qcdcourse/section-6.pdf.

[40] Hideo Matsufuru. *Introduction to lattice QCD simulations*. High Energy Accelerator Research Organization (KEK). 2007. URL: http://research.kek.jp/

people/matufuru/Research/Docs/Lattice/Introduction/note_lattice.pdf.

[41] Roger Horsley. 'Lattice QCD with dynamical quarks'. In: *Journal of Physics: Conference Series* 287.1 (2011), p. 012014. URL: http://stacks.iop.org/1742-6596/287/i=1/a=012014.

[42] Marco Panero. 'Recent results in large-N lattice gauge theories'. In: *PoS* LATTICE2012 (2012), p. 010. DOI: 10.22323/1.164.0010. arXiv: 1210.5510 [hep-lat].

[43] C. A. Ballon Bayona, Kasper Peeters and Marija Zamaklar. 'A Non-homogeneous ground state of the low-temperature Sakai-Sugimoto model'. In: *JHEP* 06 (2011), p. 092. DOI: 10.1007/JHEP06(2011)092. arXiv: 1104.2291 [hep-th].

[44] Frithjof Karsch. 'Lattice QCD at nonzero chemical potential and the resonance gas mode'. In: *rog. Theor. Phys. Suppl.* 153 (2004). DOI: 10.1143/PTPS.153.106.

[45] H.B. Nielsen and M. Ninomiya. 'Absence of neutrinos on a lattice: (I). Proof by homotopy theory'. In: *Nuclear Physics B* 185.1 (1981), pp. 20 –40. ISSN: 0550-3213. DOI: 10.1016/0550-3213(81)90361-8. URL: http://www.sciencedirect.com/science/article/pii/0550321381903618.

[46] Prasant Samantray and Suprit Singh. 'Schwinger Pair Production in Hot Anti-de Sitter Space'. In: (2018). arXiv: 1804.04140 [hep-th].

[47] Silvia Ferreres-Solé and Torbjörn Sjöstrand. 'The Space-Time Structure of Hadronization in the Lund Model'. In: (2018). arXiv: 1808.04619 [hep-ph].

[48] C. D. Buchanan and S. B. Chun. 'Simple predictive model for flavor production in hadronization'. In: *Phys. Rev. Lett.* 59 (18 1987), pp. 1997–2000. DOI: 10.1103/PhysRevLett.59.1997. URL: https://link.aps.org/doi/10.1103/PhysRevLett.59.1997.

[49] B Andersson, G Gustafson and T Sjostrand. 'Baryon Production in Jet Fragmentation and Gamma-Decay'. In: *Physica Scripta* 32.6 (1985), p. 574.

[50] Patrik Eden and Gosta Gustafson. 'Baryon production in the string fragmentation picture'. In: *Z. Phys.* C75 (1997), pp. 41–49. DOI: 10.1007/s002880050445. arXiv: hep-ph/9606454 [hep-ph].

[51] Bo Andersson, G. Gustafson and J. Samuelsson. 'Discrete QCD: A New approximation for QCD cascades'. In: *Nucl. Phys.* B463 (1996), pp. 217–237. DOI: 10.1016/0550-3213(96)00022-3.

[52] Alan D. Martin. 'Proton structure, Partons, QCD, DGLAP and beyond'. In: *Acta Phys. Polon.* B39 (2008), pp. 2025–2062. arXiv: 0802.0161 [hep-ph].

[53] A I Vaĭnshteĭn, Valentin I Zakharov, Viktor A Novikov et al. 'ABC of instantons'. In: *Soviet Physics Uspekhi* 25.4 (1982), p. 195. URL: http://stacks.iop.org/0038-5670/25/i=4/a=R01.

[54] Ian K Affleck, Orlando Alvarez and Nicholas S Manton. 'Pair Production at Strong Coupling in Weak External Field'. In: *Nuclear Physics B* 197 (1982), p. 509.

[55] Ian K. Affleck and Nicholas S. Manton. 'Monopole pair production in a magnetic field'. In: *Nuclear Physics B* 194.1 (1982), pp. 38 –64. ISSN: 0550-3213. DOI: 10.1016/0550-3213(82)90511-9. URL: http://www.sciencedirect.com/science/article/pii/0550321382905119.

[56] B.M. Barbashov and V.V. Nesterenko. *Introduction to the Relativistic String Theory*. World Scientific, 1990.

[57] W.A. Bardeen, Itzhak Bars, Andrew J. Hanson et al. 'Study of the longitudinal kink modes of the string'. In: *Physical Review D: Particles and Fields* 13.8 (1976), pp. 2364–2382.

[58] Kasper Peeters, Jacob Sonnenschein and Marija Zamaklar. 'Holographic decays of large-spin mesons'. In: *JHEP* 02 (2006), p. 009. DOI: 10.1088/1126-6708/2006/02/009. arXiv: hep-th/0511044 [hep-th].

[59] Gerard 't Hooft. 'A Planar Diagram Theory for Strong Interactions'. In: *Nuclear Physics B* 73 (1974), p. 461.

[60] J. Erdmenger and M. Ammon. *Gauge/Gravity Duality: Foundations and Applications*. Ed. by Cambridge University Press. Cambridge University Press, 2015.

[61] Johanna Erdmenger. 'Introduction to Gauge/Gravity Duality (TASI Lectures 2017)'. In: *PoS* TASI2017 (2017), p. 001. arXiv: 1807.09872 [hep-th].

[62] Gary T. Horowitz and Joseph Polchinski. *Gauge/gravity duality*. arXiv:gr-qc/0602037.

[63] Veronika E. Hubeny. 'The AdS/CFT Correspondence'. In: *Class. Quant. Grav.* 32.12 (2015), p. 124010. DOI: 10.1088/0264-9381/32/12/124010. arXiv: 1501.00007 [gr-qc].

[64] Edward Witten. 'Anti-de Sitter space and holography'. In: *Adv. Theor. Math. Phys.* 2 (1998), pp. 253–291. DOI: 10.4310/ATMP.1998.v2.n2.a2. arXiv: hep-th/9802150 [hep-th].

[65] A. Zee. *Einstein Gravity In a Nutshell*. Princeton University Press, 2013.

[66] Joseph Polchinski. 'Dirichlet Branes and Ramond-Ramond charges'. In: *Phys. Rev. Lett.* 75 (1995), pp. 4724–4727. DOI: 10.1103/PhysRevLett.75.4724. arXiv: hep-th/9510017 [hep-th].

[67] Carlos Alfonso Bayona and Nelson R. F. Braga. 'Anti-de Sitter boundary in Poincare coordinates'. In: *Gen. Rel. Grav.* 39 (2007), pp. 1367–1379. DOI: 10.1007/s10714-007-0446-y. arXiv: hep-th/0512182 [hep-th].

[68] Steven Weinberg and Edward Witten. 'Limits on massless particles'. In: *Physics Letters B* 96.1 (1980), pp. 59 –62. ISSN: 0370-2693. DOI: 10.1016/0370-2693(80)90212-9. URL: http://www.sciencedirect.com/science/article/pii/0370269380902129.

[69] Oliver DeWolfe. 'TASI Lectures on Applications of Gauge/Gravity Duality'. In: *Theoretical Advanced Study Institute in Elementary Particle Physics: Physics at the Fundamental Frontier (TASI 2017) Boulder, CO, USA, June*

5-30, 2017. 2018. arXiv: 1802.08267 [hep-th]. URL: https://inspirehep.net/record/1657199/files/1802.08267.pdf.

[70] Tatsuma Nishioka, Shinsei Ryu and Tadashi Takayanagi. 'Holographic Entanglement Entropy: An Overview'. In: *J. Phys.* A42 (2009), p. 504008. DOI: 10.1088/1751-8113/42/50/504008. arXiv: 0905.0932 [hep-th].

[71] Sean A. Hartnoll, Christopher P. Herzog and Gary T. Horowitz. 'Building a Holographic Superconductor'. In: *Phys. Rev. Lett.* 101 (2008), p. 031601. DOI: 10.1103/PhysRevLett.101.031601. arXiv: 0803.3295 [hep-th].

[72] Subir Sachdev. 'Condensed Matter and AdS/CFT'. In: (2010). [Lect. Notes Phys.828,273(2011)]. DOI: 10.1007/978-3-642-04864-7_9. arXiv: 1002.2947 [hep-th].

[73] Markus Greiner and Simon Fölling. 'Condensed-matter physics: Optical lattices'. In: *Nature* 453 (2008), pp. 763–738. DOI: 10.1038/453736a.

[74] Sean A. Hartnoll. 'Lectures on holographic methods for condensed matter physics'. In: *Class. Quant. Grav.* 26 (2009), p. 224002. DOI: 10.1088/0264-9381/26/22/224002. arXiv: 0903.3246 [hep-th].

[75] John McGreevy. 'Holographic duality with a view toward many-body physics'. In: *Adv. High Energy Phys.* 2010 (2010), p. 723105. DOI: 10.1155/2010/723105. arXiv: 0909.0518 [hep-th].

[76] Peter Breitenlohner and Daniel Z. Freedman. 'Positive Energy in anti-De Sitter Backgrounds and Gauged Extended Supergravity'. In: *Phys. Lett.* 115B (1982), pp. 197–201. DOI: 10.1016/0370-2693(82)90643-8.

[77] Peter Breitenlohner and Daniel Z. Freedman. 'Stability in Gauged Extended Supergravity'. In: *Annals Phys.* 144 (1982), p. 249. DOI: 10.1016/0003-4916(82)90116-6.

[78] J L F Barbón. 'Black holes, information and holography'. In: *Journal of Physics: Conference Series* 171.1 (2009), p. 012009. URL: http://stacks.iop.org/1742-6596/171/i=1/a=012009.

[79] P. Kovtun, Dan T. Son and Andrei O. Starinets. 'Viscosity in strongly interacting quantum field theories from black hole physics'. In: *Phys. Rev. Lett.* 94 (2005), p. 111601. DOI: 10.1103/PhysRevLett.94.111601. arXiv: hep-th/0405231 [hep-th].

[80] David Mateos. 'String Theory and Quantum Chromodynamics'. In: *Class. Quant. Grav.* 24 (2007), S713–S740. DOI: 10.1088/0264-9381/24/21/S01. arXiv: 0709.1523 [hep-th].

[81] Dam T. Son and Andrei O. Starinets. 'Minkowski space correlators in AdS / CFT correspondence: Recipe and applications'. In: *JHEP* 09 (2002), p. 042. DOI: 10.1088/1126-6708/2002/09/042. arXiv: hep-th/0205051 [hep-th].

[82] Nick Evans, Jonathan P. Shock and Tom Waterson. 'Towards a perfect QCD gravity dual'. In: *Phys. Lett.* B622 (2005), pp. 165–171. DOI: 10.1016/j.physletb.2005.07.014. arXiv: hep-th/0505250 [hep-th].

[83] S. S. Gubser, Igor R. Klebanov and Alexander M. Polyakov. 'Gauge theory correlators from noncritical string theory'. In: *Phys. Lett.* B428 (1998), pp. 105–114. DOI: 10.1016/S0370-2693(98)00377-3. arXiv: hep-th/9802109 [hep-th].

[84] Jacob Sonnenschein and Dorin Weissman. 'The decay width of stringy hadrons'. In: *Nuclear Physics B* 927 (2018), pp. 368 –454. ISSN: 0550-3213. DOI: 10.1016/j.nuclphysb.2017.12.017. URL: http://www.sciencedirect.com/science/article/pii/S0550321317304029.

[85] Andreas Karch and Emanuel Katz. 'Adding flavor to AdS / CFT'. In: *JHEP* 06 (2002), p. 043. DOI: 10.1088/1126-6708/2002/06/043. arXiv: hep-th/0205236 [hep-th].

[86] Martin Cederwall, Alexander von Gussich, Aleksandar R. Mikovic et al. 'On the Dirac-Born-Infeld action for d-branes'. In: *Phys. Lett.* B390 (1997), pp. 148–152. DOI: 10.1016/S0370-2693(96)01367-6. arXiv: hep-th/9606173 [hep-th].

[87] J. Babington, J. Erdmenger, Nick J. Evans et al. 'Chiral symmetry breaking and pions in nonsupersymmetric gauge / gravity duals'. In: *Phys. Rev.* D69 (2004), p. 066007. DOI: 10.1103/PhysRevD.69.066007. arXiv: hep-th/0306018 [hep-th].

[88] Riccardo Apreda, Johanna Erdmenger and Nick Evans. 'Scalar effective potential for D7 brane probes which break chiral symmetry'. In: *JHEP* 05 (2006), p. 011. DOI: 10.1088/1126-6708/2006/05/011. arXiv: hep-th/0509219 [hep-th].

[89] J. Babington, J. Erdmenger, Nick J. Evans et al. 'A Gravity dual of chiral symmetry breaking'. In: *Fortsch. Phys.* 52 (2004), pp. 578–582. DOI: 10.1002/prop.200310147. arXiv: hep-th/0312263 [hep-th].

[90] Johanna Erdmenger, Nick Evans and Johannes Grosse. 'Heavy-light mesons from the AdS/CFT correspondence'. In: *JHEP* 01 (2007), p. 098. DOI: 10.1088/1126-6708/2007/01/098. arXiv: hep-th/0605241 [hep-th].

[91] Nick J. Evans and Jonathan P. Shock. 'Chiral dynamics from AdS space'. In: *Phys. Rev.* D70 (2004), p. 046002. DOI: 10.1103/PhysRevD.70.046002. arXiv: hep-th/0403279 [hep-th].

[92] Neil R. Constable and Robert C. Myers. 'Exotic scalar states in the AdS / CFT correspondence'. In: *JHEP* 11 (1999), p. 020. DOI: 10.1088/1126-6708/1999/11/020. arXiv: hep-th/9905081 [hep-th].

[93] J. Babington, J. Erdmenger, Nick J. Evans et al. 'Chiral symmetry breaking and pions in nonsupersymmetric gauge / gravity duals'. In: *Phys. Rev.* D69 (2004), p. 066007. DOI: 10.1103/PhysRevD.69.066007. arXiv: hep-th/0306018 [hep-th].

[94] Richard C. Brower, Samir D. Mathur and Chung-I Tan. 'Glueball spectrum for QCD from AdS supergravity duality'. In: *Nucl. Phys.* B587 (2000), pp. 249–276. DOI: 10.1016/S0550-3213(00)00435-1. arXiv: hep-th/0003115 [hep-th].

[95] Kasper Peeters and Marija Zamaklar. 'The String/gauge theory correspondence in QCD'. In: *Eur. Phys. J. ST* 152 (2007), pp. 113–138. DOI: 10.1140/epjst/e2007-00379-0. arXiv: 0708.1502 [hep-ph].

[96] Martin Kruczenski, Leopoldo A. Pando Zayas, Jacob Sonnenschein et al. 'Regge trajectories for mesons in the holographic dual of large-N(c) QCD'. In: *JHEP* 06 (2005), p. 046. DOI: 10.1088/1126-6708/2005/06/046. arXiv: hep-th/0410035 [hep-th].

[97] Martin Kruczenski, David Mateos, Robert C. Myers et al. 'Meson spectroscopy in AdS / CFT with flavor'. In: *JHEP* 07 (2003), p. 049. DOI: 10.1088/1126-6708/2003/07/049. arXiv: hep-th/0304032 [hep-th].

[98] Sungho Hong, Sukjin Yoon and Matthew J. Strassler. 'Quarkonium from the fifth-dimension'. In: *JHEP* 04 (2004), p. 046. DOI: 10.1088/1126-6708/2004/04/046. arXiv: hep-th/0312071 [hep-th].

[99] Sungho Hong, Sukjin Yoon and Matthew J. Strassler. 'On the couplings of vector mesons in AdS / QCD'. In: *JHEP* 04 (2006), p. 003. DOI: 10.1088/1126-6708/2006/04/003. arXiv: hep-th/0409118 [hep-th].

[100] Angel Paredes and P. Talavera. 'Multiflavor excited mesons from the fifth dimension'. In: *Nucl. Phys.* B713 (2005), pp. 438–464. DOI: 10.1016/j.nuclphysb.2005.02.021. arXiv: hep-th/0412260 [hep-th].

[101] Jin Dai and Joseph Polchinski. 'The decay of macroscopic fundamental strings'. In: *Physics Letters B* 220.3 (1989), pp. 387 –390. ISSN: 0370-2693. DOI: 10.1016/0370-2693(89)90892-7. URL: http://www.sciencedirect.com/science/article/pii/0370269389908927.

[102] R.B. Wilkinson, N. Turok and D. Mitchell. 'The decay of highly excited closed strings'. In: *Nuclear Physics B* 332.1 (1990), pp. 131 –145. ISSN: 0550-3213. DOI: 10.1016/0550-3213(90)90032-9. URL: http://www.sciencedirect.com/science/article/pii/0550321390900329.

[103] D. Mitchell, N. Turok, R. Wilkinson et al. 'The decay of highly excited open strings'. In: *Nuclear Physics B* 315.1 (1989), pp. 1 –24. ISSN: 0550-3213. DOI: 10.1016/0550-3213(89)90446-X. URL: http://www.sciencedirect.com/science/article/pii/055032138990446X.

[104] Y. Kinar, E. Schreiber and J. Sonnenschein. '$Q\bar{Q}$ potential from strings in curved space-time: Classical results'. In: *Nucl. Phys. B* 566 (2000), pp. 103–125. DOI: 10.1016/S0550-3213(99)00652-5. eprint: hep-th/9811192.

[105] Juan Martin Maldacena. 'Wilson loops in large N field theories'. In: *Phys. Rev. Lett.* 80 (1998), pp. 4859–4862. DOI: 10.1103/PhysRevLett.80.4859. arXiv: hep-th/9803002 [hep-th].

[106] J. Sonnenschein. 'What does the string / gauge correspondence teach us about Wilson loops?' In: *Supersymmetry in the theories of fields, strings and branes. Proceedings, Advanced School, Santiago de Compostela, Spain, July 26-31, 1999.* 1999, pp. 219–269. arXiv: hep-th/0003032 [hep-th].

[107] Jacob Sonnenschein. 'Stringy confining Wilson loops'. In: *PoS* tmr2000 (2000), p. 008. DOI: 10.22323/1.006.0008. arXiv: hep-th/0009146 [hep-th].

[108] Nissan Itzhaki, Juan Martin Maldacena, Jacob Sonnenschein et al. 'Supergravity and the large N limit of theories with sixteen supercharges'. In: *Phys. Rev.* D58 (1998), p. 046004. DOI: 10.1103/PhysRevD.58.046004. arXiv: hep-th/9802042 [hep-th].

[109] K. Zarembo. 'Wilson loop correlator in the AdS / CFT correspondence'. In: *Phys. Lett.* B459 (1999), pp. 527–534. DOI: 10.1016/S0370-2693(99)00717-0. arXiv: hep-th/9904149 [hep-th].

[110] Adi Armoni, Maurizio Piai and Ali Teimouri. 'Correlators of Circular Wilson Loops from Holography'. In: *Phys. Rev.* D88.6 (2013), p. 066008. DOI: 10.1103/PhysRevD.88.066008. arXiv: 1307.7773 [hep-th].

[111] Umut Gursoy, Elias Kiritsis, Liuba Mazzanti et al. 'Improved Holographic QCD'. In: *Lect. Notes Phys.* 828 (2011), pp. 79–146. DOI: 10.1007/978-3-642-04864-7_4. arXiv: 1006.5461 [hep-th].

[112] Adi Armoni. 'Beyond The Quenched (or Probe Brane) Approximation in Lattice (or Holographic) QCD'. In: *Phys. Rev.* D78 (2008), p. 065017. DOI: 10.1103/PhysRevD.78.065017. arXiv: 0805.1339 [hep-th].

[113] Yoshiki Sato and Kentaroh Yoshida. 'Holographic Schwinger effect in confining phase'. In: *JHEP* 09 (2013), p. 134. DOI: 10.1007/JHEP09(2013)134. arXiv: 1306.5512 [hep-th].

[114] Ofer Aharony, Steven S. Gubser, Juan Martin Maldacena et al. 'Large N field theories, string theory and gravity'. In: *Phys. Rept.* 323 (2000), pp. 183–386. DOI: 10.1016/S0370-1573(99)00083-6. arXiv: hep-th/9905111 [hep-th].

[115] Oren Bergman, Gilad Lifschytz and Matthew Lippert. 'Holographic Nuclear Physics'. In: *JHEP* 11 (2007), p. 056. DOI: 10.1088/1126-6708/2007/11/056. arXiv: 0708.0326 [hep-th].

[116] Anton Rebhan. 'The Witten-Sakai-Sugimoto model: A brief review and some recent results'. In: *EPJ Web Conf.* 95 (2015), p. 02005. DOI: 10.1051/epjconf/20159502005. arXiv: 1410.8858 [hep-th].

[117] Nick Evans and Ed Threlfall. 'Mesonic quasinormal modes of the Sakai-Sugimoto model at high temperature'. In: *Phys. Rev.* D77 (2008), p. 126008. DOI: 10.1103/PhysRevD.77.126008. arXiv: 0802.0775 [hep-th].

[118] Kanabu Nawa, Hideo Suganuma and Toru Kojo. 'Brane-induced skyrmions: Baryons in holographic QCD'. In: *Prog. Theor. Phys. Suppl.* 168 (2007), pp. 231–236. DOI: 10.1143/PTPS.168.231. arXiv: hep-th/0701007 [hep-th].

[119] Kanabu Nawa, Hideo Suganuma and Toru Kojo. 'Baryons in holographic QCD'. In: *Phys. Rev. D* 75 (8 2007), p. 086003. DOI: 10.1103/PhysRevD.75.086003. URL: https://link.aps.org/doi/10.1103/PhysRevD.75.086003.

[120] Deog Ki Hong, Ki-Myeong Lee, Cheonsoo Park et al. 'Holographic Monopole Catalysis of Baryon Decay'. In: *JHEP* 08 (2008), p. 018. DOI: 10.1088/1126-6708/2008/08/018. arXiv: 0804.1326 [hep-th].

[121] Hiroyuki Hata, Tadakatsu Sakai, Shigeki Sugimoto et al. 'Baryons from instantons in holographic QCD'. In: *Prog. Theor. Phys.* 117 (2007), p. 1157. DOI: 10.1143/PTP.117.1157. arXiv: hep-th/0701280 [HEP-TH].

[122] Oliver Gould and Arttu Rajantie. 'Thermal Schwinger pair production at arbitrary coupling'. In: *Phys. Rev.* D96.7 (2017), p. 076002. DOI: 10.1103/PhysRevD.96.076002. arXiv: 1704.04801 [hep-th].

[123] Y. Kinar, E. Schreiber, J. Sonnenschein et al. 'Quantum fluctuations of Wilson loops from string models'. In: *Nucl. Phys.* B583 (2000), pp. 76–104. DOI: 10.1016/S0550-3213(00)00238-8. arXiv: hep-th/9911123 [hep-th].

[124] S. Bolognesi, F. Kiefer and E. Rabinovici. 'Comments on critical electric and magnetic fields from holography'. In: *Journal of High Energy Physics* 2013.1 (2013), p. 174. ISSN: 1029-8479. DOI: 10.1007/JHEP01(2013)174. URL: https://doi.org/10.1007/JHEP01(2013)174.

[125] Yoshiki Sato and Kentaroh Yoshida. 'Holographic description of the Schwinger effect in electric and magnetic field'. In: *Journal of High Energy Physics* 2013.4 (2013), p. 111. ISSN: 1029-8479. DOI: 10.1007/JHEP04(2013)111. URL: 10.1007/JHEP04(2013)111.

[126] David J. Gross and Hirosi Ooguri. 'Aspects of large N gauge theory dynamics as seen by string theory'. In: *Phys. Rev.* D58 (1998), p. 106002. DOI: 10.1103/PhysRevD.58.106002. arXiv: hep-th/9805129 [hep-th].

[127] Hungsoo Kim, DaeKil Park, Sayat Tamaryan et al. 'Gross-Ooguri phase transition at zero and finite temperature: two circular Wilson loop case'. In: *Journal of High Energy Physics* 2001.03 (2001), p. 003. URL: http://stacks.iop.org/1126-6708/2001/i=03/a=003.

[128] P. Olesen and L. Zarembo. *Phase transition in Wilson loop correlator from AdS/CFT correspondence'*. 2000. eprint: arXiv:hep-th/0009210.

[129] K. S. Gupta and C. Rosenzweig. 'Semiclassical decay of excited string states on leading Regge trajectories'. In: *Phys. Rev.* D50 (1994), pp. 3368–3376. DOI: 10.1103/PhysRevD.50.3368. arXiv: hep-ph/9402263 [hep-ph].

[130] Yoshiki Sato and Kentaroh Yoshida. 'Potential analysis in holographic Schwinger effect'. In: *Journal of High Energy Physics* 2013.8 (2013), p. 2. ISSN: 1029-8479. DOI: 10.1007/JHEP08(2013)002. URL: 10.1007/JHEP08(2013)002.

[131] C. Bachas and M. Porrati. 'Pair creation of open strings in an electric field'. In: *Phys. Lett.* B296 (1992), pp. 77–84. DOI: 10.1016/0370-2693(92)90806-F. arXiv: hep-th/9209032 [hep-th].

[132] E.S. Fradkin and A.A. Tseytlin. 'Quantum string theory effective action'. In: *Nuclear Physics B* 261 (1985), pp. 1 –27. ISSN: 0550-3213. DOI: 10.1016/0550-3213(85)90559-0. URL: http://www.sciencedirect.com/science/article/pii/0550321385905590.

[133] Edward Shuryak. 'What RHIC experiments and theory tell us about properties of quark–gluon plasma?' In: *Nuclear Physics A* 750.1 (2005). Quark-Gluon Plasma. New Discoveries at RHIC: Case for the Strongly Interacting Quark-Gluon Plasma. Contributions from the RBRC Workshop held May 14-15, 2004, pp. 64 –83. ISSN: 0375-9474. DOI: 10.1016/j.nuclphysa.2004.10.022. URL: http://www.sciencedirect.com/science/article/pii/S0375947404011340.

[134] Jorge Casalderrey-Solana, Hong Liu, David Mateos et al. 'Gauge/String Duality, Hot QCD and Heavy Ion Collisions'. In: (2011). DOI: 10.1017/CBO9781139136747. arXiv: 1101.0618 [hep-th].

[135] Nestor Armesto, Carlos A. Salgado and Urs Achim Wiedemann. 'Gluon radiation off massive quarks in a QCD medium'. In: *QCD and high energy hadronic interactions. Proceedings, 39th Rencontres de Moriond, La Thuile,*

Italy, March 28-April 2, 2004. 2004, pp. 325–328. arXiv: hep-ph/0405184 [hep-ph]. URL: http://weblib.cern.ch/abstract?CERN-PH-TH-2004-093.

[136] Hong Liu, Krishna Rajagopal and Urs Achim Wiedemann. 'Calculating the jet quenching parameter from AdS/CFT'. In: *Phys. Rev. Lett.* 97 (2006), p. 182301. DOI: 10.1103/PhysRevLett.97.182301. arXiv: hep-ph/0605178 [hep-ph].

[137] Urs Achim Wiedemann. 'Jet Quenching in Heavy Ion Collisions'. In: (2010). [Landolt-Bornstein23,521(2010)], pp. 521–562. DOI: 10.1007/978-3-642-01539-7_17. arXiv: 0908.2306 [hep-ph].

[138] Andrej Ficnar and Steven S. Gubser. 'Finite momentum at string endpoints'. In: *Phys. Rev.* D89.2 (2014), p. 026002. DOI: 10.1103/PhysRevD.89.026002. arXiv: 1306.6648 [hep-th].